

Strongly coupled phases of $\mathcal{N} = 1$ S-duality

Iñaki García-Etxebarria^a and Ben Heidenreich^b

^a*Max Planck Institute for Physics, Föhringer Ring 6, 80805 Munich, Germany*

^b*Department of Physics, Harvard University, Cambridge, MA 02138, USA*

E-mail: inaki@mpp.mpg.de, bjheiden@physics.harvard.edu

ABSTRACT: We analyze S-duality of orientifolds of the Calabi-Yau cone over the first del Pezzo surface (dP_1). The S-duals of known phases, described by quiver gauge theories, contain intrinsically strongly-coupled sectors. These sectors are realized by a higher multiplicity intersection of NS5 branes and D5 branes atop an O5 plane, and can be thought of as stuck at the infinite coupling point between two Seiberg-dual gauge theories. We argue that such sectors appear generically in orientifolds of non-orbifold singularities, where in many examples every orientifold phase contains such a sector. Understanding such sectors is therefore key to understanding orientifolds of Calabi-Yau singularities. We construct the strongly-coupled sectors for dP_1 orientifolds using deconfinement, and show that they have interesting, non-trivial properties. Using this construction, we verify the predictions of S-duality for dP_1 .

Contents

1	Introduction	2
2	Del Pezzo orientifolds	4
2.1	The orientifold geometry	4
2.2	Known gauge theory constructions	5
2.3	Discrete torsion in del Pezzo orientifolds	11
2.4	Counting orientifolds of del Pezzo singularities	13
3	Phases of the dP_1 orientifold	15
3.1	Discrete torsion for the classical phases	16
3.2	Brane tilings and orientifolds	19
3.3	Quad CFTs	25
4	Deconfinement and strong coupling	27
4.1	Deconfinement in the gauge theory	27
4.2	Deconfinement in the brane tiling	29
4.3	Deconfining phase II	34
4.4	Deconfining phase III	39
4.5	On symmetric tensor deconfinement	43
5	S-duality for all phases of dP_1	45
5.1	Matching the superconformal index	49
6	Conclusions	53
A	Del Pezzo orientifold singularities	54
B	Exceptional collections and brane charges	55
C	Results for the superconformal index of dP_1	58
C.1	$\text{II}^+_+ = \text{III}_+, Q_{\text{D3}} = 8$	59
C.2	$\text{I}^-_A = \text{I}^-_B = \text{III}_-, Q_{\text{D3}} = 8$	60
C.3	$\text{I}^+_A = \text{II}^-_-, Q_{\text{D3}} = 9$	61
C.4	$\text{I}^+_B = \text{II}^-_+, Q_{\text{D3}} = 9$	62

1 Introduction

S-duality, where two dual theories are related by an exactly marginal deformation, is a ubiquitous phenomenon in theories with extended supersymmetry. Perhaps the most elegant example is Montonen-Olive duality in $\mathcal{N} = 4$ gauge theories, which exchanges electric and magnetic fields and replaces the gauge group with its Langlands dual. A subclass of these dualities admit a simple embedding in string theory as the self-duality of the world-volume gauge theory on D3 branes induced by S-duality in type IIB string theory, as well as the various dualities which arise when the D3 branes are coincident with an O3 plane. The latter case was concisely described by [1], where it was shown that the O3 plane type is characterized in the gravity dual by a pair of discrete holonomies (hereafter referred to as discrete torsion) for the RR and NSNS two-form potentials, and that the S-dualities between the corresponding gauge theories are explained by the well-known action of type IIB S-duality on these potentials.

There are a number of ways that S-duality can be realized in $\mathcal{N} = 1$ gauge theories. It occurs in mass deformations of S-dual theories with extended supersymmetry [2, 3] as well as in $\mathcal{N} = 1$ gaugings of Gaiotto dualities [4]. The distinct phenomenon of universality, where two theories are related by renormalization group flow, is ubiquitous in $\mathcal{N} = 1$ gauge theories [5, 6], and bears some relation to S-dualities in theories with extended supersymmetry [2].

Another manifestation of $\mathcal{N} = 1$ S-duality occurs in the chiral world-volume gauge theory on D3 branes probing a Calabi-Yau singularity [7–9], analogous the realization of Montonen-Olive duality on D3 branes in a flat background.¹ As in the $\mathcal{N} = 4$ case, the dual theories correspond to different weakly-coupled “cusps” along the same fixed line, where $g_s \rightarrow 0$ in some dual description of the parent string theory. The addition of orientifold planes leads to non-zero beta functions near the cusp, hence the infrared fixed point is interacting and there is a non-trivial relationship between the dynamics at distinct dual cusps.²

These S-dualities are distinguished by their chiral, intrinsically $\mathcal{N} = 1$ nature³ and their rich infrared dynamics near the cusp, with examples exhibiting confinement, chiral symmetry breaking, and a dynamically generated superpotential. Moreover, they provide an important cross-check on the physics of Calabi-Yau orientifold singularities — where the S-dualities originate from the $SL(2, \mathbb{Z})$ self-duality of type IIB string theory — a role which will prove to be crucial in the present paper.

In [9], a systematic understanding of S-dualities arising in orientifolds of isolated orbifold singularities was obtained by repeating the analysis of discrete torsion in [1] for these geometries. In this class of theories, the pattern of S-dualities predicted by string theory is reproduced perfectly in the dual gauge theories, passing all available checks.

¹ $\mathcal{N} = 0$ generalizations of these dualities have also been argued to exist [10–12].

²Even in the infrared of these orientifold gauge theories, the $g_s = 0$ cusp is a distinguished point along the fixed line, where (depending on the theory) there are enhanced global symmetries and/or free vector multiplets.

³See also [13–15] for some recent work on chiral $\mathcal{N} = 1$ S-dualities arising from compactifications of 6d $(1, 0)$ theories.

However, applying the same arguments to more general isolated singularities immediately gives rise to a conundrum. The geometry allows for additional discrete torsions, yet the number of known dual gauge theories is insufficient to fill out all the possible choices of torsion, and moreover these gauge theories do not fill out complete $SL(2, \mathbb{Z})$ multiplets, a problem which was recognized in [7] for perhaps the simplest non-orbifold example, the Calabi-Yau cone over the first del Pezzo surface (dP_1). The problem is worse still for the higher del Pezzo singularities, where for most orientifold involutions no dual gauge theory is known [16], despite the rapidly growing set of discrete torsions. Other non-orbifold singularities exhibit similar problems.

In this paper, we resolve this puzzle for the dP_1 singularity, developing techniques which will generalize to other cases. We find that there are more orientifold phases than previously known, with the new phases precisely filling out the allowed discrete torsions. The new phases consist of a quiver gauge theory coupled to an intrinsically strongly-coupled sector, dual to a higher multiplicity intersection of NS5 and D5 branes atop an O5 plane. We describe this strongly-coupled sector via deconfinement [17, 18], which produces a large collection of quiver gauge theories in the same universality class as it. This sector exhibits novel behavior, such as baryons transforming in the spinor representation of an $SO(2N)$ flavor symmetry which emerges accidentally in the gauge theory description.

These new sectors can be thought of as arising at the midpoint of a Seiberg duality, where the presence of an orientifold plane prevents a deformation to one or the other of the Seiberg-dual descriptions, trapping the theory at strong coupling. We argue that these sectors occur in certain orientifold phases of every toric non-orbifold singularity, including those with trivial discrete torsion. For most orientifold involutions of more complicated isolated singularities such as cones over the higher del Pezzo surfaces, every phase includes a strongly coupled sector, explaining the lack of known gauge theory duals.

Combining the strongly-coupled sector with known ingredients, we obtain a list of theories describing the dP_1 orientifold which is in complete agreement with the discrete torsion classification, and which exhibits the S-dualities predicted by that classification, including but generalizing the dP_1 duality found in [7]. We test these dualities by computing the superconformal index for all the phases, including those involving the strongly-coupled sector. We find that the theories predicted to be S-dual have indices which match for a large number of low-lying states (limited only by computational power), whereas theories not predicted to be S-dual have distinct indices.

Our paper is organized as follows. In §2, we describe a class of del Pezzo orientifolds, including our main focus, the dP_1 orientifold. We then summarize the known gauge theory duals and classify the available discrete torsions, highlighting the mismatch between the two. In §3, we determine the discrete torsions of the known dP_1 orientifold gauge theories by partially resolving to the dP_0 orientifold singularity studied in [7, 9] plus an O3 plane. We compare this torsion classification with a brane tiling construction of the orientifold, suggesting that the missing theories contain a sector dual to a higher-multiplicity intersection

of NS5 branes atop a stack of D5 branes, frozen in place by an O5 plane. We then comment on the expected properties of these strongly-coupled “quad CFT” sectors. In §4, we obtain a gauge-theory description of the quad-CFTs by engineering deconfinement in the brane tiling, resolving the higher-multiplicity intersection. In the process, extra information is uncovered (in the form of flavor branes in the deconfined theory) which is crucial to reproducing the RR discrete torsion in the gravity dual. We describe some novel properties of the quad CFTs and compare their behavior with our expectations, providing non-trivial evidence that our description is correct. Finally, in §5 we apply the deconfinement construction of the quad CFTs to describe the missing phases of the dP_1 orientifold. We verify that the new theories neatly fill out the missing discrete torsions, and provide highly non-trivial evidence that the predicted S-dualities are realized in these theories, based on comparing the superconformal indices between the various phases. We conclude in §6.

Appendix A contains a brief review of the geometry of del Pezzo singularities, appendix B gives a microscopic description of the previously-known phases of dP_1 in terms of exceptional collections, useful for determining the brane charges, and appendix C summarizes some of our explicit results for the superconformal indices of all phases of the dP_1 orientifold.

2 Del Pezzo orientifolds

In this section, we construct a simple class of orientifold singularities and explore their properties.

2.1 The orientifold geometry

The Calabi-Yau cone over the first del Pezzo surface (dP_1) is the toric variety described by the following gauged linear sigma model (GLSM, see [19] for an introduction):

$$\begin{array}{c|ccccc} & z_1 & z_2 & z_3 & z_4 & t \\ \hline U(1)_a & 1 & 0 & 1 & 1 & -3 \\ U(1)_b & 0 & 1 & 0 & 1 & -2 \end{array} \quad (2.1)$$

subject to the D-term conditions

$$|z_1|^2 + |z_3|^2 + |z_4|^2 - 3|t|^2 = \xi_a \quad , \quad |z_2|^2 + |z_4|^2 - 2|t|^2 = \xi_b \quad , \quad (2.2)$$

where the Fayet-Iliopoulos (FI) parameters ξ_a and ξ_b control the resolutions of the singularity. For $\xi_a > \xi_b > 0$ the exceptional divisor $t = 0$ is dP_1 , and the O3/O7 involution $t \rightarrow -t$ describes an O7 plane wrapping this divisor.

We now generalize this construction to the other del Pezzo surfaces. Let K_Σ denote the canonical bundle of a smooth divisor Σ embedded in a smooth Calabi-Yau threefold Y . We have [20]

$$K_\Sigma = K_Y|_\Sigma \otimes N_\Sigma \quad (2.3)$$

where N_Σ is the normal bundle of $\Sigma \subset Y$, and K_Y is the canonical bundle of Y . The Calabi-Yau condition implies that K_Y is trivial, hence $K_\Sigma = N_\Sigma$. Thus, the local embedding of Σ in

Y is isomorphic to the canonical bundle K_Σ on Σ , and is independent of the global structure of Y .

Locally, we can always construct an involution $\sigma : Y \rightarrow Y$ by reflecting the fibers of N_Σ ($\mathbb{C} \rightarrow -\mathbb{C}$). σ is holomorphic by construction with an isolated fixed plane Σ , and corresponds to wrapping an O7 plane on Σ .⁴ As above, the local geometry is independent of the global structure of Y , though σ may or may not extend to a globally defined holomorphic involution, depending on Y .

Let $[\Sigma] \in H^{(1,1)}(Y)$ denote the divisor class of Σ . If $-[\Sigma]$ is a positive class then there is a corresponding Kähler modulus of Y with Σ as the exceptional divisor. In this case, the adjunction formula implies that $-K_\Sigma = -N_\Sigma$ is ample, hence Σ is a del Pezzo surface: either \mathbb{P}^2 blown up at k generic points ($0 \leq k \leq 8$) — denoted dP_k — or the zeroth Hirzebruch surface, $\mathbb{F}_0 \cong \mathbb{P}^1 \times \mathbb{P}^1$.

For each of these ten cases, we can construct an affine cone by setting the corresponding Kähler modulus of Y to zero and reading off the local geometry $Y_p \subset Y$ near the singular point p . An orientifold $X_p = Y_p/\sigma$ can be constructed using the involution described above, where p is an isolated fixed point of σ .⁵ For completeness, concrete geometric realizations of all ten varieties and their orientifolds are presented in appendix A.

2.2 Known gauge theory constructions

We now present the known gauge theory duals of D3 branes probing the orientifold singularities described in the previous subsection. These are only known for the dP_0 , dP_1 and \mathbb{F}_0 orientifold singularities, and we later argue that this list is incomplete even in the dP_1 and \mathbb{F}_0 cases.

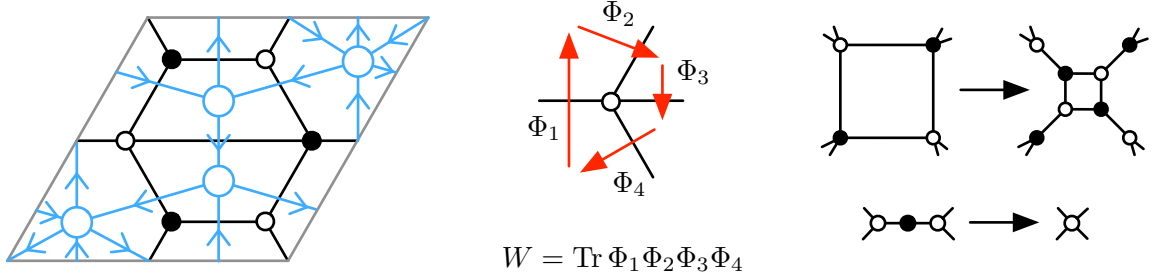
We begin with the toric cases: dP_k for $k \leq 3$ and \mathbb{F}_0 . In these cases, we can use the dimer model technology developed in [22, 23] and the orientifold rules laid out in [24] to derive the gauge theories corresponding to these orientifold singularities. We briefly review the required tools, referring the interested reader to the extensive literature (see e.g. [25, 26] and references therein) for further details.

As illustrated in figure 1, a dimer model is a bipartite graph embedded on the torus such that the surface of the torus is divided into contractible faces by the edges of the graph.⁶ A dimer model corresponds to a quiver gauge theory by graph dualization: each face of the dimer model corresponds to a node in the quiver, and each edge to an arrow in the quiver, oriented so that the arrows circulate clockwise (counterclockwise) around the white

⁴Unless Σ is a K3 surface or T^4 , N_Σ must be non-trivial, hence tadpole cancellation requires the presence of D7 branes intersecting or wrapping Σ . To avoid “flavor” D7 branes, we assume that four D7 branes wrap Σ , cancelling the C_0 charge of the O7 plane.

⁵The affine varieties Y_p and X_p depend only on the choice of del Pezzo surface — and on the $2k - 8$ complex structure moduli of dP_k for $k \geq 5$ — and not on the global details of Y . However, all ten singularities admit global embeddings, see e.g. [21], where σ can be defined globally by $w \rightarrow -w$ in the notation of that paper.

⁶More technically, we are only interested in “non-degenerate” dimers, in the sense of [27]. Other “consistency” conditions are often imposed (see e.g. [28]), but we will not do so for reasons which become clear in §4.



(a) A dimer model and its dual quiver. (b) Reading off W . (c) Seiberg duality in the dimer.

Figure 1: (a) A dimer model (black) and its dual quiver (blue). This dimer corresponds to the dP_1 singularity. (b) Each vertex in the dimer represents a superpotential term. (c) Seiberg duality (top) and integrating out (bottom) have a graphical interpretation in the dimer.

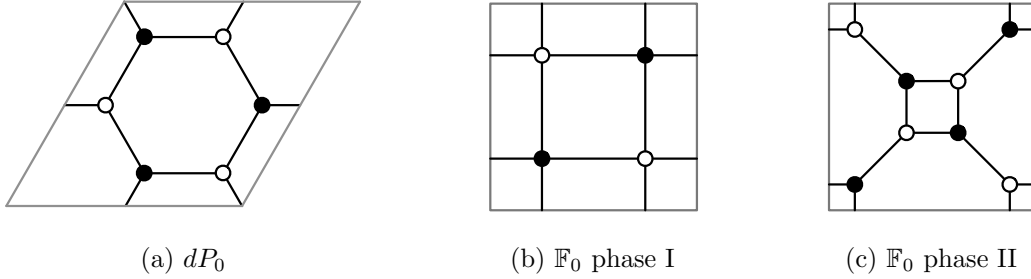


Figure 2: Dimer models for (a) dP_0 , (b) \mathbb{F}_0 phase I, and (c) \mathbb{F}_0 phase II. The dimer for dP_1 is shown in figure 1(a).

(black) vertices of the bipartite graph. The vertices encode the superpotential: the loop in the quiver surrounding each white (black) vertex corresponds to a term in the superpotential with coefficient $+1$ (-1).

The mesonic moduli space of this quiver gauge theory is a toric Calabi-Yau singularity which can be read off using the forward algorithm [23, 29]. Conversely, for each toric Calabi-Yau singularity, one or more dimer models can be constructed using the inverse algorithm [28, 29]. When more than one dimer model is obtainable using the inverse algorithm, these *toric phases* are related to each other by Seiberg duality [30], which takes the form of “urban renewal” in the dimer [23], see figure 1(c).

The quiver gauge theories obtained by the inverse algorithm describe the infrared of the worldvolume gauge theory on D3 branes probing the toric singularity in question. dP_0 (figure 2(a)) and dP_1 (figure 1(a)) each have a single toric phase, whereas \mathbb{F}_0 (figures 2(b)-2(c)) and dP_2 (figure 3(a)) have two phases each, and dP_3 (figure 3(b)) has four phases.

Following [24], we can construct the worldvolume gauge theory on D3 branes probing an orientifold of a toric singularity by orientifolding the dimer model itself. The geometric

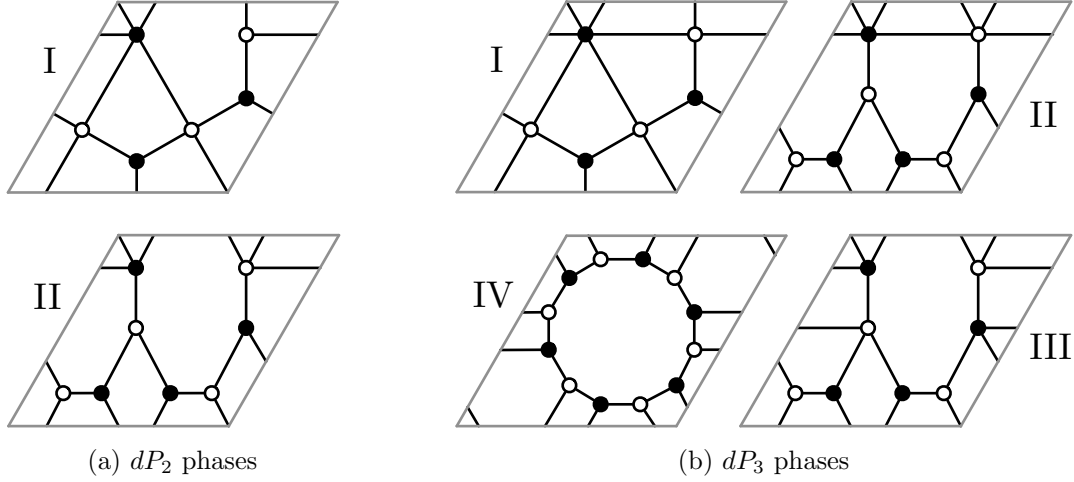


Figure 3: Dimer models for (a) dP_2 and (b) dP_3 .

involution considered above preserves all the isometries of the toric singularity, so that the quotient space is also toric. Geometric involutions of this type correspond to involutions of the dimer model with four isolated fixed points mapping white nodes to black nodes and vice versa. Each fixed point has an associated sign, or “T-parity” [31], subject to the requirement that the product of all four T-parities is positive (negative) when the number of white vertices in the dimer is even (odd). A (generalized) quiver gauge theory can be read off as before, where now each face and its image corresponds to a single $SU(n)$ gauge group, each edge and its image to a single matter multiplet, and each vertex and its image to a single superpotential term.⁷ When a face is mapped to itself, it corresponds to an SO (USp) gauge group if the enclosed fixed point is positive (negative), whereas an edge mapped to itself corresponds to symmetric (antisymmetric) tensor matter if the fixed point it crosses is positive (negative), see figure 4(a).

We consider dP_1 first.⁸ The corresponding dimer model is shown in figure 1(a). Up to the choice of fixed point signs, a single fixed-point involution is possible. The relative signs of the fixed points can be fixed by the requirement that the $SU(2) \times U(1)$ isometry of dP_1 is unbroken, giving two distinct orientifolds, which we call I_A and I_B . The orientifolded dimer model is shown in figure 4(a), and the resulting quivers and superpotential are displayed in figure 4(b) using the generalized quiver notation defined in figure 5. The dP_0 orientifold studied in [7, 9] can be obtained from here by Higgsing the tensor Z .

For \mathbb{F}_0 , there are two toric phases to consider. In phase I, two different involutions are possible, but they are related to each other by rotating the dimer model by 90° , exchanging the two \mathbb{P}^1 factors. As above, the relative signs of the fixed points can be fixed by requiring that

⁷The sign of the coefficient is no longer important.

⁸The dP_1 and \mathbb{F}_0 orientifold gauge theories derived below were first written down in [7]. The dP_0 orientifold theories have been known much longer [32–34].

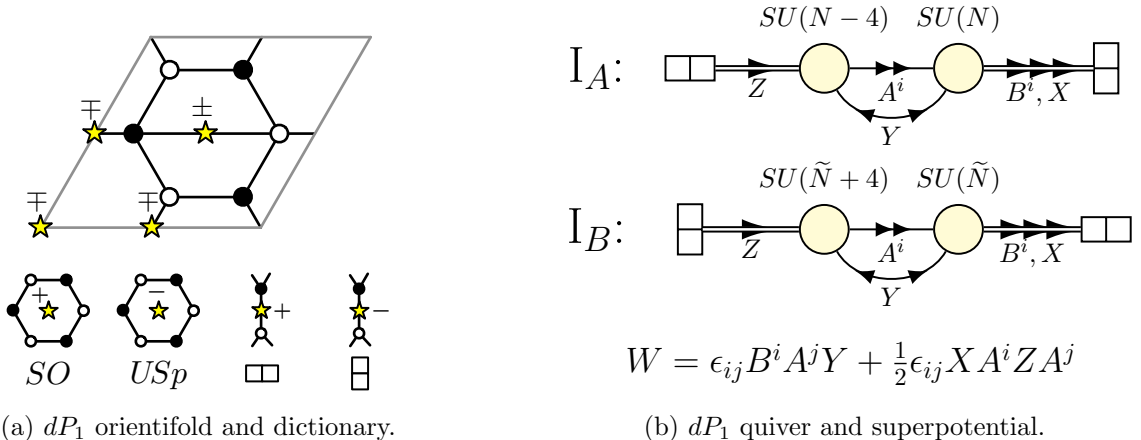


Figure 4: (a) (top) Orientifolds of the dP_1 dimer model which preserve the $SU(2) \times U(1)$ isometry of dP_1 . (bottom) The orientifold gauge theory can be read off from the dimer using this dictionary. (b) Quivers for the dP_1 orientifolds, where A (B) corresponds to the upper (lower) choice of fixed point signs in (a). Our notation for quivers is explained in figure 5.

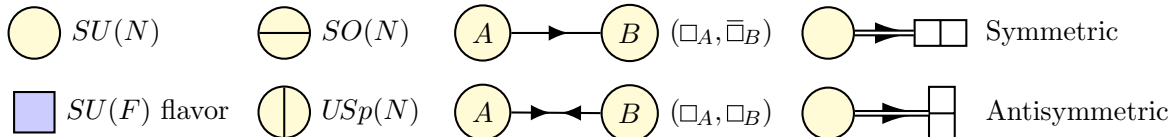
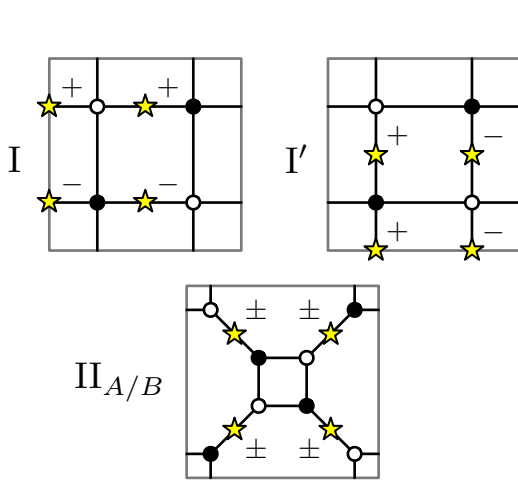


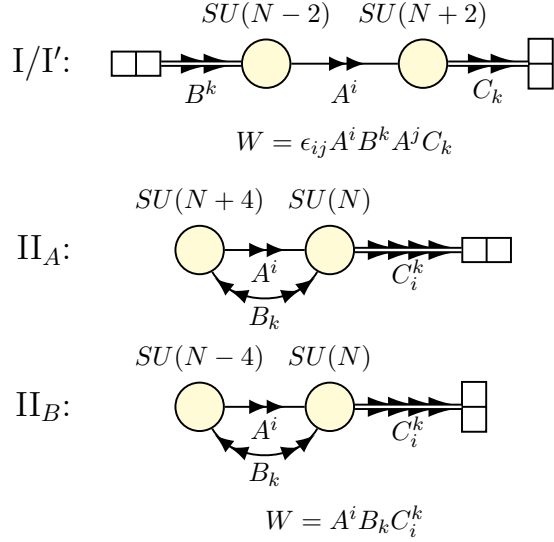
Figure 5: Summary of our quiver notation. Reversing the directions of the arrows corresponds to taking the charge conjugate of the representation, and multiple arrowheads in the same direction indicate multiple fields in the same representation.

the $SU(2) \times SU(2)$ isometry of $\mathbb{F}_0 \cong \mathbb{P}^1 \times \mathbb{P}^1$ is unbroken, whereas the two remaining choices are related by translating the torus by half a period, hence they are equivalent. In phase II, only one involution is possible, but the two sign choices consistent with the $SU(2) \times SU(2)$ isometry are not equivalent, giving two distinct orientifold theories, II_A and II_B . However, unlike phases I_A and I_B of dP_1 or dP_0 , II_A and II_B are related by Seiberg duality, and therefore lie in the same universality class. The orientifolded dimers are shown in figure 6(a) and the resulting quiverfolds and superpotentials in figure 6(b).

The higher del Pezzos dP_2 and dP_3 are strikingly different. In these cases, no fixed-point involutions are possible in any toric phase [16]! For instance, dP_2 phase II and dP_3 phases III and IV each have a unique largest face with either 8 or 12 sides. The involution must map this face to itself, but this is incompatible with the rule that white vertices are mapped to black vertices, so no fixed-point involution exists for these phases. Likewise, dP_2 phase I and dP_3 phase I each have a black vertex with valence 5 or 6 and no white vertices with valence greater than four, once again violating the rule that white vertices are mapped to



(a) \mathbb{F}_0 orientifolds.



(b) Orientifold quivers and superpotentials.

Figure 6: (a) Orientifolds of \mathbb{F}_0 phase I and phase II, where II_A (II_B) corresponds to the upper (lower) choice of fixed point signs. The orientifolds I and I' are related by a rotation of the dimer model, which generates an outer automorphism of the global symmetry group of the corresponding gauge theory. (b) Quivers for the \mathbb{F}_0 orientifolds. The orientifolds I and I' give identical gauge theories up to the labeling of the global symmetries. The orientifolds II_A and II_B are Seiberg duals.

black vertices. By contrast, dP_3 phase II admits a unique involution that exchanges white and black vertices, but this involution — a horizontal translation by half a period — has no fixed points and breaks the toric isometries, hence it cannot correspond to one of the orientifolds considered above. In fact, as shown in §3.2, the absence of fixed-point involutions for these theories generalizes to a broad class of isolated toric singularities, and is one of the central mysteries that we aim to address in this work.

We comment briefly on the non-toric cases, dP_k for $4 \leq k \leq 8$. In these cases, the toric technology of [23, 24] is unavailable, though quivers and superpotentials for the parent gauge theory are known [35], and — following [36] (see also [7]) — we can in principle orientifold these quivers to obtain the orientifold gauge theories of interest.⁹ However, since there are an infinite number of Seiberg-dual quivers to orientifold, a systematic approach may not be possible.¹⁰ Instead, we consider a few examples to illustrate the difficulties which arise.

The dP_k for $k \geq 5$ have $2k - 8$ complex structure moduli, none of which are projected out

⁹One can show that in the toric case the approaches of [36] and [24] are equivalent [37].

¹⁰It may be that only a finite number of quivers admit an involution. It would be interesting to explore this further.

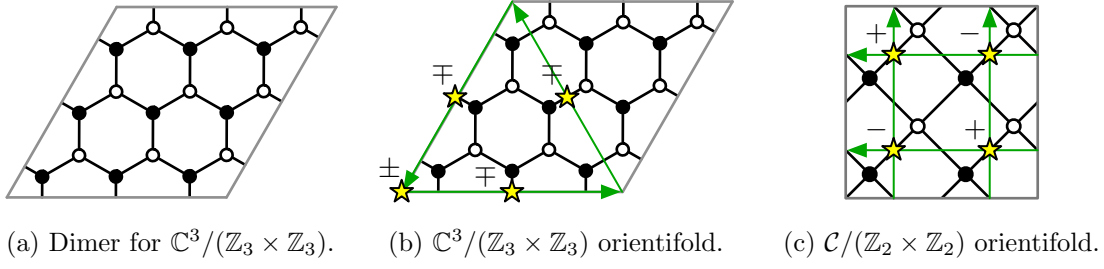


Figure 7: (a) The dimer model for $\mathbb{C}^3/\mathbb{Z}_3 \times \mathbb{Z}_3$, which is a toric degeneration of the dP_6 singularity. (b) An orientifold of $\mathbb{C}^3/\mathbb{Z}_3 \times \mathbb{Z}_3$ with fixed-point signs chosen to correspond to the del Pezzo orientifolds considered in the text. The green arrows represent cubic mesons which are projected out in the orientifold theory, obstructing the superpotential deformation required for generic complex structure moduli. (c) One toric phase of the $\mathbb{Z}_2 \times \mathbb{Z}_2$ orbifold of the conifold (which is a toric degeneration of the dP_5 singularity) and its orientifold. The green arrows represent quartic mesons which are projected out in the orientifold theory, obstructing deformation of the superpotential as above. The other toric phases are similar.

by the orientifold considered above, and we expect that the correct gauge theory dual will have corresponding exactly marginal deformations. (These appear as superpotential deformations in the unorientifolded quivers of [35].) For dP_5 and dP_6 there are points in complex structure moduli space where the del Pezzo surface degenerates and the del Pezzo singularity becomes a non-isolated toric singularity. For instance, the cubic $XYZ - W^3 = 0$ — equivalent to the orbifold singularity $\mathbb{C}^3/(\mathbb{Z}_3 \times \mathbb{Z}_3)$ via the embedding $X = x^3, Y = y^3, Z = z^3, W = xyz$ — is a degeneration of the dP_6 singularity and the complete intersection of quadrics $Z^2 = XY = UV$ — equivalent to a $\mathbb{Z}_2 \times \mathbb{Z}_2$ orbifold of the conifold via the embedding $X = x^2, Y = y^2, U = u^2, V = v^2$ and $Z = xyuv$ — is a degeneration of the dP_5 singularity. There is also a degeneration of the dP_5 singularity which is a partial resolution of $\mathbb{C}^3/(\mathbb{Z}_3 \times \mathbb{Z}_3)$.

Since there are points in moduli space where the Calabi-Yau is toric, it may be possible to construct the gauge theory dual of the orientifold at these points using dimer models, and then to generalize the result by deforming it. For instance, the dimer model for $\mathbb{C}^3/(\mathbb{Z}_3 \times \mathbb{Z}_3)$ is shown in figure 7(a). The entire complex structure moduli space of dP_6 can be reproduced in the parent theory with a general superpotential, whereas the toric superpotential encoded by the dimer corresponds to one point in that moduli space (the degeneration given above). There is a unique involution of the dimer, with two possible choices of fixed-point signs which correspond to the desired geometric involution,¹¹ see figure 7(b).

To deform these candidate orientifold theories, we modify the superpotential as in the parent theory. At a generic point in the moduli space of the parent theory, all 27 possible cubic superpotential terms are present [35]. However, not all of these terms can be switched on in the orientifold theory described above, as some mesons vanish identically, see figure 7(b).

¹¹Up to an overall sign, the fixed point signs are determined by the meson sign rules of [24].

Thus, these gauge theories fail to describe the dP_6 singularity at a generic point in moduli space.¹²

A similar story applies to the toric degenerations of dP_5 , see e.g. figure 7(c). While this does not rule out the possibility of obtaining the correct gauge theory dual by orientifolding one of the many Seiberg dual quivers describing these singularities, it does imply that this cannot be done for the “toric” phases of dP_5 and dP_6 (phases with equal rank nodes regardless of the superpotential), and the failure of the approach of [24] for dP_2 and dP_3 already suggests that the solution to these problems lies elsewhere.

2.3 Discrete torsion in del Pezzo orientifolds

So far, we have made no distinction between different supersymmetric orientifolds with the same geometric involution. This is too naive — even in a flat background — because orientifold planes carry RR charges, and typically come in at least two variants (Op^+ and Op^- planes). In a curved background, orientifold planes may carry additional charges, and more than one orientifold plane can be hidden at a singularity, potentially leading to a large number of distinct orientifolds with the same geometric involution.

Fortunately, the AdS/CFT correspondence allows us to translate the difficult problem of classifying BPS orientifold planes at a singularity into the much easier one of classifying closed-string charges in the near-horizon geometry of the singularity, which is smooth if the singularity is isolated.

The idea, as in [1, 7, 9], is that distinct BPS O3/O7 orientifolds are distinguished by their RR and NSNS three-form charges, classified by $H^3(X_5, \tilde{\mathbb{Z}})$ where $X_5 = Y_5/\sigma$ is the orientifolded horizon and $\tilde{\mathbb{Z}}$ denotes local coefficients, twisted by σ due to the projection $\sigma^* F_3 = -F_3$, $\sigma^* H_3 = -H_3$.¹³

For instance, O3 planes in a flat background are classified by $[F], [H] \in \mathbb{Z}_2$ [1], where $H^3(S^5/\mathbb{Z}_2, \tilde{\mathbb{Z}}) \cong \mathbb{Z}_2$ for the O3 involution $z^i \rightarrow -z^i$ of \mathbb{C}^3 , see figure 8. In this case, the NSNS torsion $[H]$ is trivial (nontrivial) for O3[−] (O3⁺) planes, whereas the RR torsion $[F]$ is trivial (nontrivial) for the O3[−] ($\widetilde{O3}^- = O3^- + \frac{1}{2}$ D3) variants, and likewise for the variants O3⁺ and $\widetilde{O3}^+$. (The latter are perturbatively equivalent, being related by $\tau \rightarrow \tau + 1$ in the $SL(2, \mathbb{Z})$ self-duality group of type IIB string theory, but they differ in their nonperturbative spectra in the presence of D3 branes.) Orientifold planes of other codimensions can be classified in an analogous manner, see e.g. [39].

In the remainder of this section, we compute the twisted homology groups $H_i(X_5, \tilde{\mathbb{Z}})$ for the del Pezzo orientifolds considered above. This determines $H^3(X_5, \tilde{\mathbb{Z}})$ by Poincaré duality, and will help to clarify where the gaps in the collection of known field theory duals enumerated in the previous section lie.

¹²It would be interesting to understand the string-theoretic interpretation of these orientifold theories, if any.

¹³A cohomology classification is sufficient for our present purposes [38], and is able to reproduce the observed S-duality structure of the orientifold theories. A K-theoretic approach is difficult due in part to its unequal treatment of the RR and NSNS two-forms.

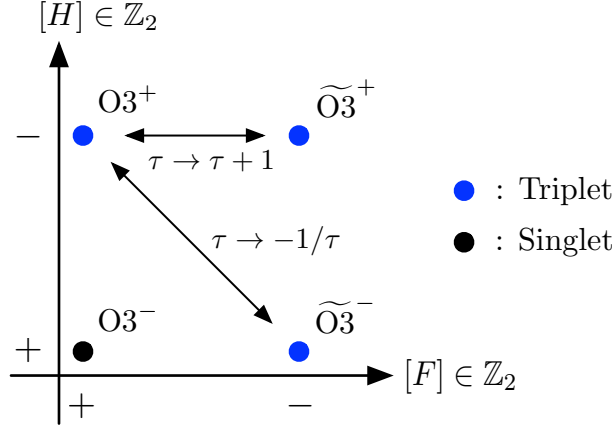


Figure 8: O3 planes are classified by the RR and NSNS torsion classes $[F]$ and $[H]$ in $H^3(S^5/\mathbb{Z}_2, \tilde{\mathbb{Z}}) \cong \mathbb{Z}_2$. The known action of $SL(2, \mathbb{Z})$ on the RR and NSNS three-forms F_3 and H_3 dictates its action on the O3 plane variants.

Our calculation is based upon the long exact sequence [40]:

$$\dots \longrightarrow H_i(X, \tilde{\mathbb{Z}}) \longrightarrow H_i(Y, \mathbb{Z}) \xrightarrow{p_*^i} H_i(X, \mathbb{Z}) \longrightarrow H_{i-1}(X, \tilde{\mathbb{Z}}) \longrightarrow \dots \quad (2.4)$$

where $X = Y/\sigma$, and p_*^i is induced by the projection $p : Y \rightarrow X$. In our case, it will turn out that p_*^i is injective for every i , hence the long exact sequence breaks into short exact sequences

$$0 \longrightarrow H_i(Y, \mathbb{Z}) \xrightarrow{p_*^i} H_i(X, \mathbb{Z}) \longrightarrow H_{i-1}(X, \tilde{\mathbb{Z}}) \longrightarrow 0 \quad (2.5)$$

and we can compute the twisted homology groups given the homology groups of X and Y and the maps p_*^i .

We begin by describing the (co)homology of dP_k (see e.g. [41]), which is a complex manifold with the Hodge numbers $h^{0,0} = h^{2,2} = 1$, $h^{1,1} = k + 1$ and $h^{i,j} = 0$ for $i \neq j$, formed by blowing up \mathbb{P}^2 at k generic points. There are $k + 1$ two cycles, which we denote by H for the hyperplane section of \mathbb{P}^2 and E_i , $i = 1, \dots, k$, for the exceptional divisors of the k blow-ups. The canonical class is $[K] = -3H + \sum_i E_i$. The intersection form is $H \cdot H = 1$, $E_i \cdot E_j = -\delta_{ij}$ and $H \cdot E_i = 0$.

The upstairs horizon Y_5 is the principal $U(1)$ bundle associated to the normal bundle N of the del Pezzo embedded in the Calabi-Yau threefold, where $N \cong K$ by (2.3). A two-cycle A on the del Pezzo lifts to a two-cycle of Y_5 iff the $U(1)$ bundle is trivial restricted to A (and hence admits a global section). This occurs iff $\int_A [N] = \int_{dP_k} A \wedge [N] = A \cdot [N] = 0$. Thus,

$$H_2(Y_5, \mathbb{Z}) \cong \{A \in H_2(dP_k, \mathbb{Z}) \mid A \cdot [K] = 0\} \cong \mathbb{Z}^k \quad (2.6)$$

since the resulting two-cycle is homologically trivial iff A is. By contrast, any two cycle B on the del Pezzo lifts to a three-cycle on Y_5 (the $U(1)$ bundle over B), but the resulting

three-cycle may be trivial even for non-trivial B . This can only happen if the intersection form on Y_5 vanishes for this three-cycle, hence if $B \propto [N]$ (since the intersection form on dP_k is non-degenerate). Given that $\pi_1(Y_5) = \mathbb{Z}_3$ for $k = 0$ (generated by a loop once around the fiber) and $\pi_1(Y_5) = 0$ for $k > 0$, compatibility with Poincaré duality and the universal coefficient theorem implies that the three cycle is trivial iff $B = n[N]$ for $n \in \mathbb{Z}$, hence

$$H_3(Y_5, \mathbb{Z}) \cong H_2(dP_k, \mathbb{Z}) / \{n[K] \mid n \in \mathbb{Z}\} \cong \begin{cases} \mathbb{Z}^k, & k > 0, \\ \mathbb{Z}_3, & k = 0. \end{cases} \quad (2.7)$$

We conclude that

$$H_\bullet(Y_5, \mathbb{Z}) \cong \begin{cases} \{\mathbb{Z}, 0, \mathbb{Z}^k, \mathbb{Z}^k, 0, \mathbb{Z}\}, & k > 0, \\ \{\mathbb{Z}, \mathbb{Z}_3, 0, \mathbb{Z}_3, 0, \mathbb{Z}\}, & k = 0, \end{cases} \quad (2.8)$$

which is well-known (see e.g. [41]).

The downstairs horizon X_5 is obtained by orbifolding the fiber $U(1) \rightarrow U(1)/\mathbb{Z}_2$. Equivalently, we replace $N \rightarrow 2K$. Following the same steps as before, we find:

$$H_\bullet(X_5, \mathbb{Z}) \cong \begin{cases} \{\mathbb{Z}, \mathbb{Z}_2, \mathbb{Z}^k, \mathbb{Z}^k \oplus \mathbb{Z}_2, 0, \mathbb{Z}\}, & k > 0, \\ \{\mathbb{Z}, \mathbb{Z}_6, 0, \mathbb{Z}_6, 0, \mathbb{Z}\}, & k = 0, \end{cases} \quad (2.9)$$

where the generators of $H_2(X_5)$ are the same as before, $H_3(X_5, \mathbb{Z}) \cong H_2(dP_k, \mathbb{Z}) / \{2n[K] \mid n \in \mathbb{Z}\}$, and $H_1(X_5) \cong \pi_1(X_5)$ is generated by a loop once around the orientifolded fiber.

With an explicit description of the generators of $H_i(X_5)$ and $H_i(Y_5)$, the projection map p_*^i is readily described. We find that p_*^{2j} is an isomorphism and p_*^{2j+1} maps $\mathbb{Z} \rightarrow 2\mathbb{Z}$ and $\mathbb{Z}_3 \rightarrow \mathbb{Z}_3 \subset \mathbb{Z}_6$. Thus, p_*^i is injective and using (2.5), we obtain:

$$H_\bullet(X_5, \tilde{\mathbb{Z}}) \cong \{\mathbb{Z}_2, 0, \mathbb{Z}_2^{k+1}, 0, \mathbb{Z}_2, 0\}. \quad (2.10)$$

The calculation for $\mathbb{F}_0 \cong \mathbb{P}^1 \times \mathbb{P}^1$ is similar. In this case, $h^{1,1} = 2$, generated by the two hyperplane classes H_1, H_2 with the intersection form $H_i \cdot H_j = 1 - \delta_{ij}$ and $[K] = -2H_1 - 2H_2$. We find

$$H_\bullet(Y_5, \mathbb{Z}) \cong \{\mathbb{Z}, \mathbb{Z}_2, \mathbb{Z}, \mathbb{Z} \oplus \mathbb{Z}_2, 0, \mathbb{Z}\}, \quad H_\bullet(X_5, \mathbb{Z}) \cong \{\mathbb{Z}, \mathbb{Z}_4, \mathbb{Z}, \mathbb{Z} \oplus \mathbb{Z}_4, 0, \mathbb{Z}\}, \quad (2.11)$$

where the twisted homology groups are the same as those of dP_1 .

2.4 Counting orientifolds of del Pezzo singularities

With the twisted homology groups (2.10) in hand, we can now classify the possible orientifolds of del Pezzo singularities with the geometric involution considered in §2.1. For dP_k , these are classified by $[F], [H] \in H^3(X_5, \tilde{\mathbb{Z}}) \cong \mathbb{Z}_2^{k+1}$, for a total of 2^{2k+2} choices of discrete torsion. We divide these into five classes with $([F], [H]) = (1, 1)$, $([F], [H]) = (\alpha, 1)$, $([F], [H]) = (1, \alpha)$, $([F], [H]) = (\alpha, \alpha)$, and $([F], [H]) = (\alpha, \beta)$, where α and β are distinct non-trivial elements of \mathbb{Z}_2^{k+1} . The first class has a single member, the lone $SL(2, \mathbb{Z})$ singlet. The second, third, and fourth classes each have $2^{k+1} - 1$ members, which together

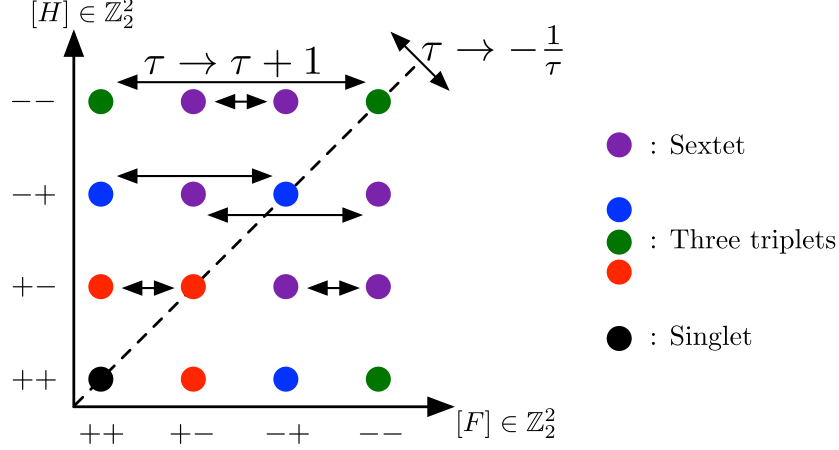


Figure 9: Choices of discrete torsion for the dP_1 orientifold considered in the text. The 16 torsions arrange themselves into five irreducible representations — one singlet, three triplets, and one sextet — under the $SL(2, \mathbb{Z})$ symmetry of type IIB string theory. The generator $\tau \rightarrow \tau + 1$ maps the $g_s \rightarrow 0$ cusps to themselves, hence the torsions connected by horizontal arrows correspond to the same cusp at different values of axion $C_0 = \text{Re } \tau$.

form $2^{k+1} - 1$ $SL(2, \mathbb{Z})$ triplets, with orbits of the form $(\alpha, 1), (1, \alpha), (\alpha, \alpha)$. The last class has $2(2^{k+1} - 1)(2^k - 1)$ members, which form $\frac{(2^{k+1}-1)(2^k-1)}{3}$ $SL(2, \mathbb{Z})$ sextets, with orbits of the form $(\alpha, \beta), (\beta, \alpha), (\gamma, \beta), (\beta, \gamma), (\gamma, \alpha), (\alpha, \gamma)$ where $\gamma = \alpha\beta$. The $SL(2, \mathbb{Z})$ orbits of the various multiplets are illustrated in figure 9 for the case of dP_1 .

Not all of the 2^{2k+2} choices of discrete torsion will lead to distinct $g_s \rightarrow 0$ limits of the string theory background. Torsions related by $[F] \rightarrow [F] + [H]$ differ by a shift of the type IIB axion $\tau \rightarrow \tau + 1$, and correspond to the same “cusp” on the modular curve parameterized by τ . The number of distinct cusps depends on the $SL(2, \mathbb{Z})$ multiplet: for singlets, there is only one, whereas for triplets there are two, and for sextets there are three. Adding up the results of the previous paragraph, we expect $2^k(2^{k+1} + 1)$ cusps for the dP_k orientifold.

As in the well-understood $\mathcal{N} = 4$ and orbifold cases [7, 9], we expect each cusp to correspond to a distinct $\mathcal{N} = 1$ gauge theory, some of which are related by S-duality. However, as shown in table 1, the number of cusps grows rapidly with k , whereas the number of known field theory duals is extremely limited, as discussed in §2.2. For dP_0 , the gauge theory duals are in precise agreement with the discrete torsion classification [7, 9]. Conversely, for dP_k , $k > 1$, no CFT duals are known, despite the large and rapidly growing number of cusps! Moreover, for dP_1 , only four distinct theories are known, two of which are S-dual, despite the expectation of five different $SL(2, \mathbb{Z})$ orbits and ten different cusps!¹⁴

¹⁴The situation for \mathbb{F}_0 is similar, except that we need to account for the \mathbb{Z}_2 discrete symmetry which exchanges the two \mathbb{P}^1 factors and likewise the two generators of the twisted homology group $H^3(\frac{S^3 \times S^2}{\mathbb{Z}_4}, \tilde{\mathbb{Z}}) \cong \mathbb{Z}_2^2$. Up to \mathbb{Z}_2 -induced isomorphisms, we expect four different $SL(2, \mathbb{Z})$ multiplets and seven different cusps, in contrast to the six known gauge theories, which occupy four different universality classes, two of which are S-dual [7].

	Singlets	Triplets	Sextets	$SL(2, \mathbb{Z})$ multiplets	Cusps
dP_0	1	1	0	2	3
dP_1, \mathbb{F}_0	1	3	1	5	10
dP_2	1	7	7	15	36
dP_3	1	15	35	51	136
dP_4	1	31	155	187	528
dP_5	1	63	651	715	2080
dP_6	1	127	2667	2795	8256
dP_7	1	255	10795	11051	32896
dP_8	1	511	43435	43947	131328

Table 1: The discrete torsion classification of orientifolds of del Pezzo singularities. The \mathbb{F}_0 singularity and many of the dP_k , $k > 1$ singularities have discrete symmetries which relate *a priori* distinct choices of discrete torsion. The number of non-isomorphic cusps is smaller than shown here in these cases, but still very large.

There are three ways in which this paradox might be resolved. Either (i) the discrete torsion classification is incorrect, (ii) there are additional gauge theory duals which have not been found yet, or (iii) the missing cusps are not describable via perturbative gauge theories. In the remainder of this paper, we argue through a careful analysis of the dP_1 singularity that the latter possibility is the correct one. Fortunately, using a deconfinement-like trick we will nonetheless be able to construct perturbative gauge theories in the same universality class as the theories at the cusps, allowing us to describe some of their most important properties.

3 Phases of the dP_1 orientifold

We now specialize to the dP_1 orientifold described in §2. For reference, we reproduce the GLSM for the dP_1 singularity (2.1) below

$$\begin{array}{c|ccccc}
& z_1 & z_2 & z_3 & z_4 & t \\
\hline
U(1)_a & 1 & 0 & 1 & 1 & -3 \\
U(1)_b & 0 & 1 & 0 & 1 & -2
\end{array} \tag{3.1}$$

subject to the D-term conditions (2.2):

$$|z_1|^2 + |z_3|^2 + |z_4|^2 - 3|t|^2 = \xi_a \quad , \quad |z_2|^2 + |z_4|^2 - 2|t|^2 = \xi_b \quad , \tag{3.2}$$

The toric diagram and web diagram for this singularity are shown in figure 10. The Fayet-Iliopoulos (FI) parameters ξ_a and ξ_b control the resolutions of the singularity, as illustrated in figure 10(c), where the unresolved (affine) singularity corresponds to $\xi_a = \frac{3}{2}\xi_b \leq 0$.

We consider the orientifold involution $t \rightarrow -t$, as in §2.1. Blowing up in the region $\xi_a > \xi_b > 0$, the exceptional divisor $t = 0$ is dP_1 , which is wrapped by an O7 plane. Moving

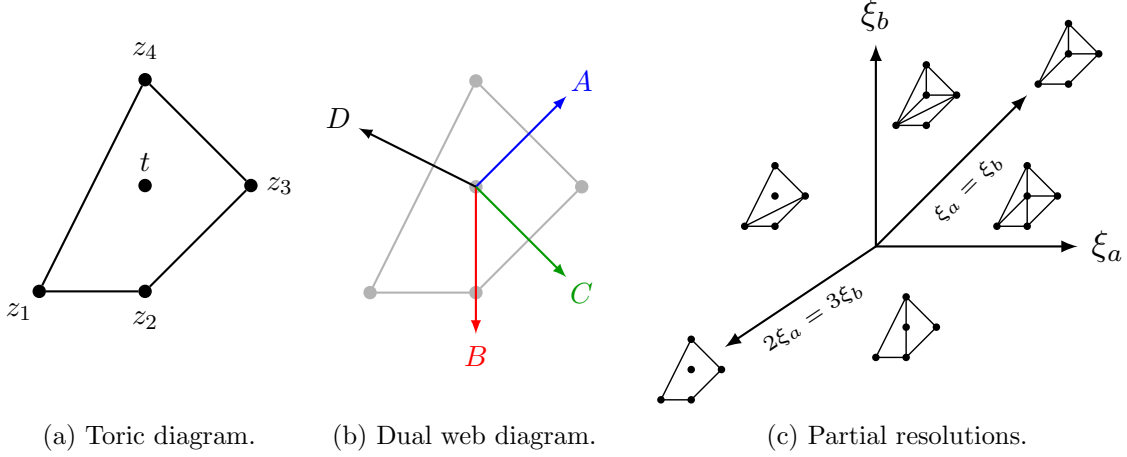


Figure 10: (a) Toric diagram associated to the complex cone over dP_1 . The labels refer to the corresponding fields in the GLSM (3.1). (b) The dual web diagram (or (p, q) diagram) for the singular geometry. The external legs are labeled and colored for future reference. (c) Partial resolutions of the dP_1 singularity are controlled by the FI parameters ξ_a and ξ_b .

to the region $\xi_b > \xi_a > 0$, the exceptional divisor develops a conifold singularity (at $\xi_a = \xi_b$) which flops, changing the topology of the divisor to dP_0 , still wrapped by an O7 plane. In the process, an O3 plane at $z_1 = z_2 = z_3 = 0$ splits off. Continuing into the region $\xi_a < \frac{3}{2}\xi_b$, $\xi_a \leq 0$, the O7 plane collapses into a $\mathbb{C}^3/\mathbb{Z}_3$ orientifold singularity, leaving behind the O3 plane. In this region, the dP_1 singularity has split into two orbifold singularities, and the \mathbb{Z}_2^2 twisted homology group of the parent singularity maps on to the \mathbb{Z}_2 twisted homology groups of the two components. Performing this partial resolution in the dual gauge theory and comparing with the known discrete torsions of orbifolds [1, 7, 9], we can read off the discrete torsion of the parent singularity.

3.1 Discrete torsion for the classical phases

We apply this approach to the orientifolds I_A and I_B discussed in §2.2. For future reference, we reproduce the charge tables for phases I_A and I_B [7] in tables 2, 3. To read off the effect of the partial resolution to a $\mathbb{C}^3/\mathbb{Z}_3$ orientifold singularity plus an O3 plane, as in the upper-left quadrant of figure 10(c), we need to identify which fields get a vev. As illustrated in figure 11, this can be done systematically by analyzing the zig-zag paths [28, 42, 43] of the dimer model, see [44]. Giving a vev to the fields where the zig-zag paths B and C cross combines the corresponding legs of the web diagram, which yields the web diagram for $\mathbb{C}^3/\mathbb{Z}_3$, hence the baryon in question corresponds to partial resolution to the $\mathbb{C}^3/\mathbb{Z}_3$ orientifold singularity, as in the upper-left quadrant of figure 10(c), where the D3 branes remain on top of the singularity.

There is another baryonic branch where the D3 branes are carried away on top of the O3 plane, corresponding to a vev for the fields where the zig-zag paths A and D cross. More

	$SU(N-4)$	$SU(N)$	$SU(2)$	$U(1)_B$	$U(1)_Y$	$U(1)_R$
A^i	\square	$\bar{\square}$	\square	$-\frac{1}{2N} - \frac{3}{2(N-4)}$	$1 + \frac{2}{N-4}$	$-\frac{2}{N-4} + \frac{2}{N}$
Y	$\bar{\square}$	$\bar{\square}$	$\mathbf{1}$	$-\frac{1}{2N} + \frac{3}{2(N-4)}$	$-1 - \frac{2}{N-4}$	$1 + \frac{2}{N-4} + \frac{2}{N}$
Z	$\overline{\square\square}$	$\mathbf{1}$	$\mathbf{1}$	$\frac{3}{N-4}$	$-1 - \frac{4}{N-4}$	$1 + \frac{4}{N-4}$
B^i	$\mathbf{1}$	\square	\square	$\frac{1}{N}$	0	$1 - \frac{4}{N}$
X	$\mathbf{1}$	\square	$\mathbf{1}$	$\frac{1}{N}$	-1	$1 - \frac{4}{N}$

Table 2: Phase I_A

	$SU(\tilde{N}+4)$	$SU(\tilde{N})$	$SU(2)$	$U(1)_B$	$U(1)_Y$	$U(1)_R$
\tilde{A}^i	\square	$\bar{\square}$	\square	$-\frac{1}{2\tilde{N}} - \frac{3}{2(\tilde{N}+4)}$	$1 - \frac{2}{\tilde{N}+4}$	$\frac{2}{\tilde{N}+4} - \frac{2}{\tilde{N}}$
\tilde{Y}	$\bar{\square}$	$\bar{\square}$	$\mathbf{1}$	$-\frac{1}{2\tilde{N}} + \frac{3}{2(\tilde{N}+4)}$	$-1 + \frac{2}{\tilde{N}+4}$	$1 - \frac{2}{\tilde{N}+4} - \frac{2}{\tilde{N}}$
\tilde{Z}	$\overline{\square\square}$	$\mathbf{1}$	$\mathbf{1}$	$\frac{3}{\tilde{N}+4}$	$-1 + \frac{4}{\tilde{N}+4}$	$1 - \frac{4}{\tilde{N}+4}$
\tilde{B}^i	$\mathbf{1}$	\square	\square	$\frac{1}{\tilde{N}}$	0	$1 + \frac{4}{\tilde{N}}$
\tilde{X}	$\mathbf{1}$	\square	$\mathbf{1}$	$\frac{1}{\tilde{N}}$	-1	$1 + \frac{4}{\tilde{N}}$

Table 3: Phase I_B

generally, some number of D3 branes can remain on the $\mathbb{C}^3/\mathbb{Z}_3$ orientifold singularity while the others are carried away on top of the O3 plane.¹⁵ The corresponding baryon – a mixture of the two described above – was identified in [7]:

$$\mathcal{O}_p = Z^{N-4-p}(XY^2)^p, \quad \tilde{\mathcal{O}}_{\tilde{p}} = \tilde{Z}^{\tilde{N}+4-\tilde{p}}(\tilde{X}\tilde{Y}^2)^{\tilde{p}}, \quad (3.3)$$

for I_A and I_B , respectively, where p and $\tilde{N} - \tilde{p}$ must be even. Turning on a vev for \mathcal{O}_p or $\tilde{\mathcal{O}}_{\tilde{p}}$ breaks

$$\begin{aligned} \mathcal{O}_p : \quad & SU(N-4) \times SU(N) \longrightarrow [SO(N-4-p) \times SU(N-p)] \times USp(p), \\ \tilde{\mathcal{O}}_{\tilde{p}} : \quad & SU(\tilde{N}+4) \times SU(\tilde{N}) \longrightarrow [USp(\tilde{N}+4-\tilde{p}) \times SU(\tilde{N}-\tilde{p})] \times SO(\tilde{p}). \end{aligned} \quad (3.4)$$

Keeping track of the chiral superfields which are Higgsed or which acquire a mass from the superpotential, we find that the $USp(p)$ and $SO(\tilde{p})$ factors decouple from the rest of the gauge group, with an $\mathcal{N} = 4$ spectrum and interactions, whereas the remaining fields and interactions reproduce those of the $\mathbb{C}^3/\mathbb{Z}_3$ orientifold studied in [7], as illustrated in figure 12(a).

¹⁵There are, of course, other directions in moduli space where the D3 branes do not lie atop either of the resulting O-planes, but these directions are not relevant to the present discussion.

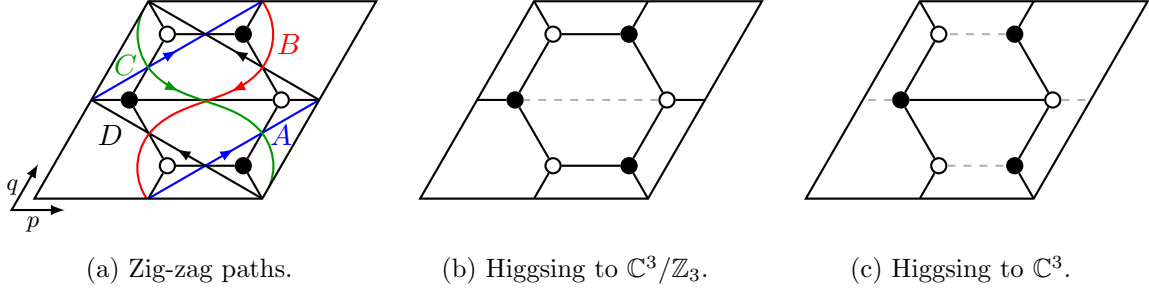


Figure 11: (a) The zig-zag paths for the dP_1 dimer model, figure 4(a). The winding numbers of the zig-zag paths reproduce the directions of the homonymous legs in the web diagram, figure 10(b). (b) Partial resolution to $\mathbb{C}^3/\mathbb{Z}_3$ corresponds to a vev for the fields where paths B and C cross. (c) Partial resolution to \mathbb{C}^3 corresponds to a vev for the fields where paths A and D cross. An $\mathcal{N} = 4$ theory is obtained upon integrating out the massive matter.

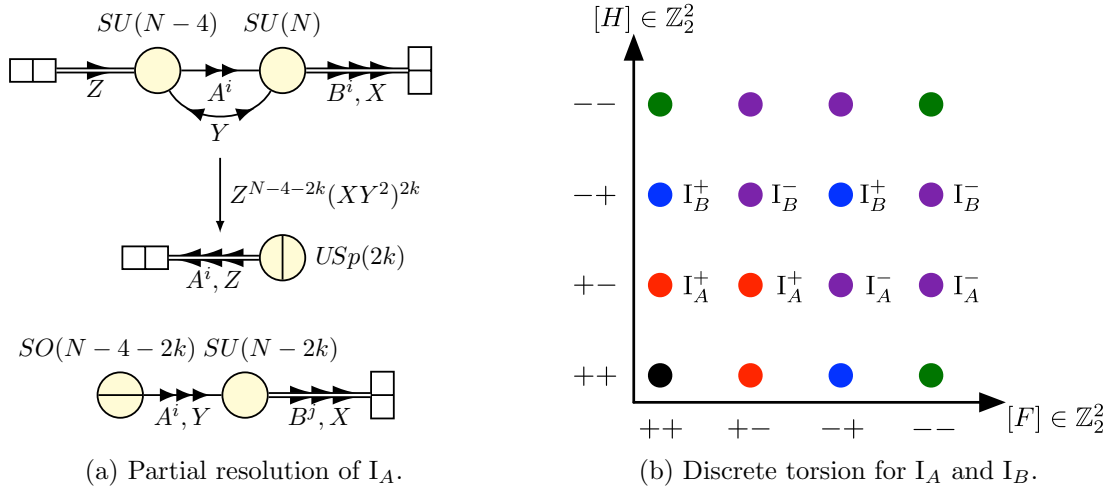


Figure 12: (a) Partial resolution of the dP_1 singularity as realized in phase I_A . Phase I_B is analogous. (b) Assignment of discrete torsions (in the basis associated to the partial resolution) to phases I_A and I_B .

We verify that this result is consistent with D3 charge conservation. The $\mathcal{N} = 4$ theories (coming from D3 branes on top of an O3 plane in a smooth background) have D3 brane charge

$$Q_{\mathbb{C}^3}^{SO(p)} = p - \frac{1}{2}, \quad Q_{\mathbb{C}^3}^{USp(p)} = p + \frac{1}{2}, \quad (3.5)$$

whereas the $\mathbb{C}^3/\mathbb{Z}_3$ orientifold theories have D3 brane charge [9]

$$Q_{\mathbb{C}^3/\mathbb{Z}_3}^{SO(p-4) \times SU(p)} = p - \frac{3}{2}, \quad Q_{\mathbb{C}^3/\mathbb{Z}_3}^{USp(p+4) \times SU(p)} = p + \frac{3}{2}, \quad (3.6)$$

where we measure the charge in the Calabi-Yau double cover, so that a mobile D3 brane has charge +2. Adding together the charges of the two components, we obtain the charge of the

dP_1 orientifold singularity in each phase:

$$Q_{I_A}^{SU(N-4) \times SU(N)} = N - 1 \quad , \quad Q_{I_B}^{SU(\tilde{N}+4) \times SU(\tilde{N})} = \tilde{N} + 1. \quad (3.7)$$

This result can be verified using the explicit construction of the fractional branes given in appendix B.

The result (3.4) encodes the discrete torsion of the parent dP_1 orientifold singularity as follows. For the $\mathcal{N} = 4$ theories as well as for the $\mathbb{C}^3/\mathbb{Z}_3$ orientifold theories, the gauge groups with an $SO(p)$ factor have torsion $[F] = (-)^p$ and $[H] = +$ and those with an $USp(p)$ factor have torsion $[F] = \pm$ and $[H] = -$, where in the latter case the two choices of $[F]$ correspond to the same cusp at different values of C_0 . Thus, the discrete torsion of the I_A theory is $[F] = ((-)^N, \pm)$ and $[H] = (+, -)$ in a basis where $(-, +)$ generates the \mathbb{Z}_2 associated to the $\mathbb{C}^3/\mathbb{Z}_3$ singularity and $(+, -)$ generates the \mathbb{Z}_2 associated to the O3 plane. Likewise, the discrete torsion for the I_B theory is $[F] = (\pm, (-)^{\tilde{N}})$ and $[H] = (-, +)$ in the same basis.

Using this information we can start filling in some of the dots in figure 9. We denote by I_A^\pm the I_A theory with $(-1)^N = \pm 1$, and similarly by I_B^\pm the I_B theory with $(-1)^{\tilde{N}} = \pm 1$. The result of the above argument is depicted in figure 12(b). Notice that I_A^- and I_B^- fall in the same $SL(2, \mathbb{Z})$ multiplet, hence they should be S-duals. Conservation of D3 charge (3.7) requires $\tilde{N} = N - 2$. This duality was already conjectured purely on the basis of field theory evidence in [7], including a non-trivial matching between the low- N dynamics. We provide further evidence for this duality in §5.1, where we match a large number of terms in the superconformal index, limited only by the running time of an optimized program. The discrete torsion assignment in figure 12 provides a much clearer picture of why this duality exists for odd N and not for even N . It also highlights the gaps in the first and last rows, including the S-duals of the even N theories, whose absence was a mystery in [7]. In fact, none of the $SL(2, \mathbb{Z})$ multiplets are complete, including the one containing the S-dual pair I_A^- and I_B^- .

3.2 Brane tilings and orientifolds

We now explain why these theories are absent, which is the first step along the way to constructing them.

While our main focus is dP_1 , we find it convenient in the present discussion to consider a generic isolated toric singularity with $k + 3$ legs in the web diagram — for which there are k two-cycles in the horizon Y_5 of the singularity, and for which the twisted homology group is \mathbb{Z}_2^{k+1} [45] — for example dP_k , $k = 0, 1, 2, 3$.

We first review the construction of dimer models from NS5-D5 systems, as discussed in e.g. [26]. Consider type IIB string theory on $T^2 \times \mathbb{R}^4$,¹⁶ with a flat background metric, where $x_4 \sim x_4 + 1$ and $x_5 \sim x_5 + 1$ parameterize the torus. We wrap N D5 branes — the double T-dual of the N D3 branes we started with — on the T^2 . To reproduce the original Calabi-Yau geometry, we introduce NS5 branes ending on one-cycles of the torus and extending outwards

¹⁶All of the branes we consider wrap the directions x_0, \dots, x_3 , and none wrap the directions x_8, x_9 .

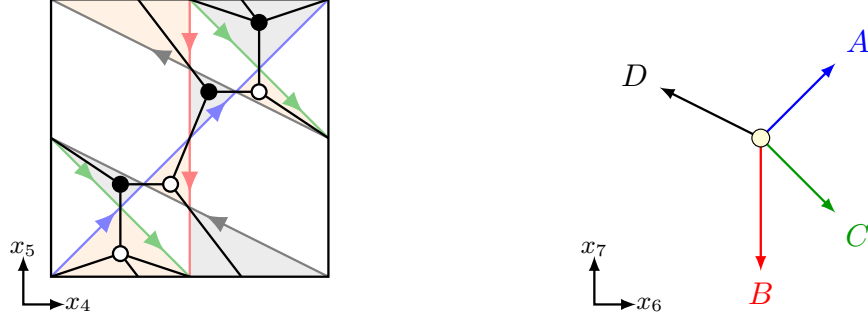


Figure 13: The brane tiling corresponding to the dP_1 singularity and the dual dimer model, c.f. figure 11(a).

along rays in the (x_6, x_7) directions. Specifically, for an NS5 brane ending on the (p, q) cycle of the torus, the corresponding ray — $(x_6, x_7) = (tp, tq)$ with $t \in [0, \infty)$ — is chosen to preserve a common $\mathcal{N} = 1$ supersymmetry with the other NS5 branes and with the D5 branes. The cycles wrapped by the NS5 branes correspond to the legs of the web diagram of the toric singularity in question, see e.g. figure 10(b).

To satisfy five-brane charge conservation, the NS5 branes cannot simply end on the torus. Instead, they divide the torus into (N, Q) D5-NS5 bound states with different Q 's, where steps in Q across the NS5 brane cycles account for the tadpole induced by the boundary of the NS5 brane. To obtain a gauge theory description, we restrict to configurations with $Q = 0, \pm 1$, where the $(N, 0)$ branes carry a $U(N)$ gauge group, whereas $(N, 1)$ and $(N, -1)$ carry only a $U(1)$ gauge group. In the low-energy limit, the $U(1)$'s become massive or decouple, and we are left with a quiver gauge theory with the $(N, 0)$ faces as nodes. Wherever two NS5 branes intersect, two of the $(N, 0)$ faces touch each other, and there is bifundamental matter, which is chiral due to the presence of the NS5 branes. For each $(N, 1)$ and $(N, -1)$ face, there is a corresponding disk diagram which generates a term in the superpotential out of the matter fields surrounding the face.

This construction is illustrated in figure 13 for dP_1 . We refer to the configuration of five branes along the torus as a “brane tiling”.¹⁷ Dualizing the brane tiling, we recover the dimer model (figure 1(a)) for dP_1 , where the $(N, 0)$ branes map to faces, the $(N, 1)$ and $(N, -1)$ branes to white and black nodes, respectively, and the NS5-brane intersections to edges. The NS5 branes correspond to zig-zag paths in the dimer model.

The above description of the NS5-D5 system is valid in the $g_s \rightarrow \infty$ limit, where the NS5 brane tension is much less than the D5 brane tension.¹⁸ In the $g_s \rightarrow 0$ limit, the NS5 branes combine into a single NS5 brane wrapping a holomorphic curve with stacks of D5 branes (whose worldvolume is topologically a disk) ending on one-cycles on the curve. The latter

¹⁷Our usage here is somewhat more specific than is common in the literature. We have reserved the phrase “brane tiling” for a physical configuration of branes, in contrast to dimer models, which represent a broader class of quiver gauge theories.

¹⁸See [26] for a precise definition of the $g_s \rightarrow \infty$ and $g_s \rightarrow 0$ limits.

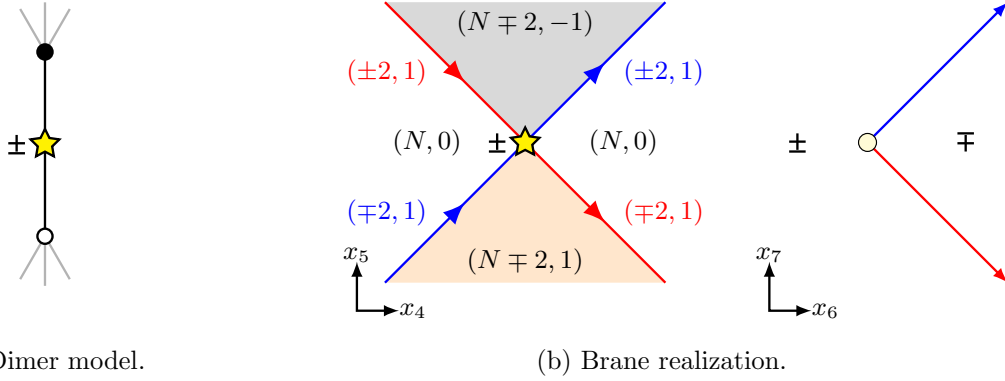


Figure 14: The T-parity of an orientifold fixed point in the dimer model (figure (a)) corresponds to the RR charge of the O5 plane in the major angle between the NS5 branes in the brane tiling (figure (b)). Here the NS5 branes carry ± 2 units of D5 charge to compensate for the mismatch in the RR charge between the major and minor angles of the O5 plane.

description is closely related to the mirror of the original toric singularity with intersecting D6 branes and a non-trivial geometry [43]. However, for the present paper we focus on the brane configuration in the $g_s \rightarrow \infty$ limit, which is easier to visualize, and will be convenient for engineering deconfinement in §4.

Orientifolding the toric singularity corresponds to introducing O5 planes in the brane tiling [31]. In particular, the “fixed-point” involutions considered in §2.2 correspond to four O5 planes located at four points along the T^2 and filling the (x_6, x_7) directions. The sign of the RR charge of the O5 plane changes each time it crosses an NS5-brane in the (x_6, x_7) plane [46]. In the standard construction, this either does not happen (when the O5 plane lies within an $(N, 0)$ face on the torus) or occurs twice (when the O5 plane sits at the intersection point of two NS5 branes on the torus). In the former case, the RR charge of the O5 plane is the same as the T-parity associated to the fixed point in the dimer model, whereas in the latter case the T-parity is the same as the RR charge of the O5 plane in the major angle (greater than 180°) between the NS5 branes in the (x_6, x_7) plane, see figure 14.

Before orientifolding, there are in general moduli corresponding to the positions of the NS5-brane cycles. Accounting for a single calibration condition and translation invariance along the torus [26], there are k such moduli for $k + 3$ legs in the web diagram. These moduli are T-dual to B_2 Wilson lines on the k two-cycles in the horizon Y_5 of the toric singularity. Likewise, their superpartners — k Wilson lines on the $k + 3$ NS5-brane worldvolumes (subject to one constraint and two gauge equivalences) — are T-dual to C_2 Wilson lines on the same two-cycles.

Upon orientifolding, these moduli are projected out. This can be seen both in the five-brane system and in the T-dual Calabi-Yau orientifold. In the former, the five-brane positions are constrained by the orientifold. We observe that no two legs of the web diagram for dP_1 (figure 10(b)) are parallel; this is due to the fact that the dP_1 singularity is isolated. Since

the O5 involution maps an NS5 brane ending on the cycle (p, q) to another NS5 brane ending on a homologous cycle, this implies that each NS5 brane is its own image under the O5 involution. Topologically, the boundary of the NS5 brane is an S^1 , and the O5 involution maps this boundary to itself with an orientation reversal. Thus, the involution has two fixed points along the boundary, i.e. each NS5 brane must pass through two of the fixed points on the torus. This completely fixes the NS5 brane moduli considered above, up to the choice of which pair of fixed points to cross (of two possible choices).

In the T-dual Calabi-Yau geometry, the B_2 Wilson lines $\oint B_2$ change sign under the involution. Accounting for the shift symmetry $\oint B_2 \cong \oint B_2 + 1$, we conclude that $\oint B_2 = 0$ or $\oint B_2 = \frac{1}{2}$, and the modulus is projected out, again up to a discrete choice. But this is exactly how $[H]$ discrete torsion arises in the dual geometry!¹⁹

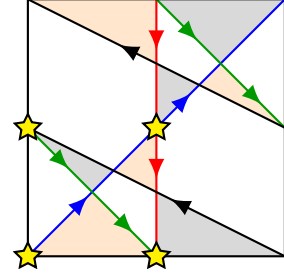
Thus, we expect that the NS5 brane positions encode $[H]$ discrete torsion. To make this more precise, we count the number of choices. Since the O5 plane charge flips each time an NS5 brane is crossed in the (x_6, x_7) directions, the number of NS5 branes crossing the corresponding fixed point on the torus must be even. After placing $k + 2$ NS5 branes, the position of the last NS5 brane is fixed by this requirement. Moreover, translation symmetry on the torus allows us to interchange the four fixed points among each other. In particular, any two NS5 branes with $(p, q) \not\equiv (p', q') \pmod{2}$ intersect at exactly one fixed point,²⁰ so picking some fiducial pair, we fix the translation symmetry on the torus by marking this fixed point. In placing the remaining k NS5 branes, we make k choices, hence there are 2^k possible distinct NS5 brane configurations.

To account for the final two choices of discrete torsion, we consider the RR charges of the four O5 planes at some fixed angle in the (x_6, x_7) plane. Supersymmetry requires that the product of the four charges is positive [31], so there are eight possible choices. However, changing the sign of one O5 plane relative to another will affect the meson sign rules of [24], hence changing the geometric involution. Thus, only an overall change of sign preserves the geometric involution, and there are two possible sign choices for the RR charges of the O5 planes at this point in the (x_6, x_7) plane, which fixes these charges everywhere, since they change sign each time an NS5 brane is crossed.

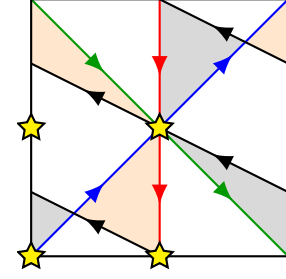
Thus, the NS5 brane positions together with the overall sign of the RR charges of the O5 planes account for 2^{k+1} possibilities, exactly the same as the number of choices of $[H]$ discrete torsion. This information can be neatly encapsulated in the *local charges* of one of the four O5 planes in each of the $k+3$ wedges in the (x_6, x_7) plane between the legs of the web diagram. In particular, these charges specify which NS5 branes cross the corresponding fixed point on the torus (the legs of the web diagram adjoining wedges of opposite local charge), which completely fixes the NS5 brane positions. The overall RR charges of the other three O5 planes can then be fixed using the supersymmetry constraint and the meson sign rules of [24].

¹⁹To be precise, this accounts for a $\mathbb{Z}_2^k \subset \mathbb{Z}_2^{k+1}$ subgroup of the twisted homology group. The remaining \mathbb{Z}_2 is generated by an $\mathbb{RP}^2 \subset X_5$ which is trivial in Y_5 , as in [1].

²⁰Here we assume that the NS5 brane winding numbers are not all congruent modulo two, as happens e.g. for \mathbb{F}_0 . In this case, the counting is different, but the end result is the same [45].

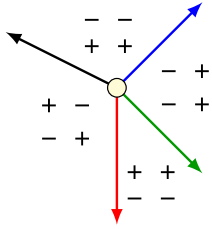


(a) Double intersections.

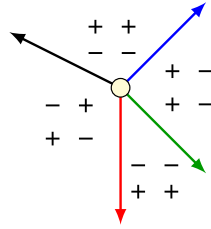


(b) Quadruple intersection.

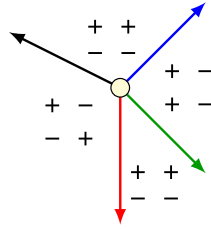
Figure 15: Possible NS5 brane positions in the brane tiling describing the dP_1 orientifold singularity. The white regions are $(N, 0)$ branes and orange and grey regions are $(N, 1)$ and $(N, -1)$ branes, respectively.



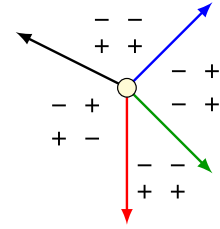
(a) I_A



(b) I_B



(c) Unknown phase (II)



(d) Unknown phase (III)

Figure 16: Local charges for the O5 planes in the four possible configurations T-dual to branes at the dP_1 orientifold singularity with the geometric involution described in the text. Configurations (a) and (b) correspond to the brane tiling in figure 15(a) and those in (c) and (d) to that in figure 15(b). The latter two are previously unknown phases.

There are 2^{k+3} choices of the local charges, but for each choice there are three equivalent ones corresponding to the local charges of the other three O5 planes, so there are 2^{k+1} inequivalent choices, as before.

Having understood the origin of $[H]$ discrete torsion in the five-brane system, we are now in a position to explain the paradoxes of §2.2–2.4. We consider dP_1 . From the general analysis given above, we expect that there are two distinct NS5 brane configurations, each of which admits two orientifolds related by an overall sign flip of the RR charges of the O5 planes, for a total of four choices corresponding to the four possible $[H]$ torsions. The two possible NS5 brane configurations are shown in figure 15 and the four corresponding choices of local charges are shown in figure 16. Using the dimer-model / brane-tiling dictionary, it is straightforward to verify (c.f. figure 13) that figure 15(a) with the local charges shown in figure 16(a) or 16(b) corresponds to the orientifolds I_A and I_B of §2.2 (see figure 4), respectively.

By contrast, the configuration in figure 15(b) is non-standard, due to the quadruple intersection of NS5 branes at one of the fixed points. We emphasize that this quadruple intersection is forced on us by the O5 involution, which projected out the NS5 brane moduli

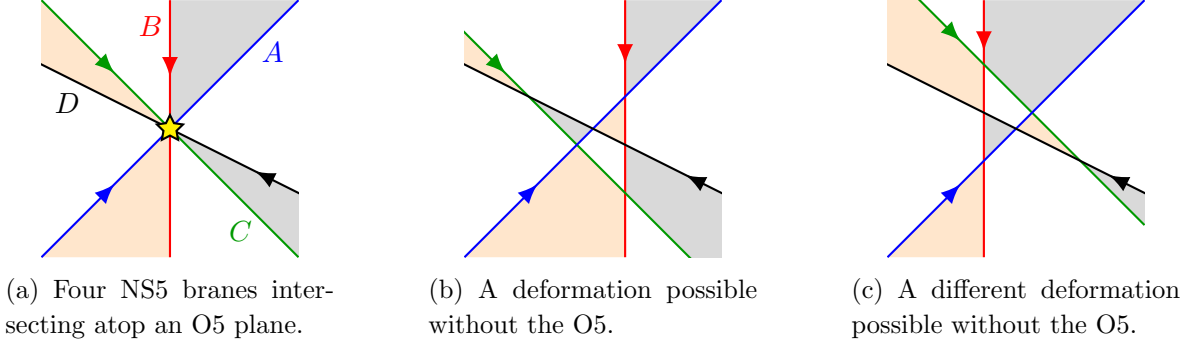


Figure 17: (a) Four NS5 branes intersecting over a O5 plane. (b)–(c) Removing the orientifold plane, there are two deformations that allow a perturbative description, related by Seiberg duality.

which would otherwise allow us to deform away from this special point in the moduli space, see figure 17. Since this deformation grows a fourth $(N, 0)$ face in the brane tiling, the special point lies at infinite coupling for one of the gauge groups, and we expect that there are intrinsically strongly coupled degrees of freedom localized at the quadruple intersection. Thus, the answer to the paradox of §2 is that the missing phases are not gauge theories at all, but something intrinsically strongly coupled!

In fact, as shown in figures 17(b) and 17(c), there are two ways in which the quadruple crossing can be resolved, related by Seiberg duality on the shrinking $(N, 0)$ face. A configuration with formally infinite coupling interpolating between two Seiberg dual phases is a familiar situation in the Hanany-Witten literature [47, 48]. However, the infinite coupling makes the gauge theory description ill-defined, and the orientifolds we consider lack a modulus to deform away from the strong-coupling point, so we need a different approach to describe the low-energy physics.

Let us take a step back and examine under what circumstances these higher multiplicity intersections are forced to occur. Since each NS5 brane crosses two fixed points, and there are four fixed points in total, it is evident that when there are more than four NS5 branes (i.e. more than four legs in the web diagram) a higher multiplicity intersection must occur at one or more of the fixed points, whereas in the case of four NS5 branes a quadruple intersection will occur for some choices of $[H]$, but not for others. This agrees exactly with what we found in §2, where there were no candidate duals for dP_2 and dP_3 and an incomplete list for dP_1 and \mathbb{F}_0 . Moreover, in the case of three NS5 branes, as for all isolated orbifold singularities, a higher multiplicity intersection is obviously impossible, in perfect agreement with the precise matching between the discrete torsion classification of orbifolds and their dual gauge theories obtained in [7, 9].

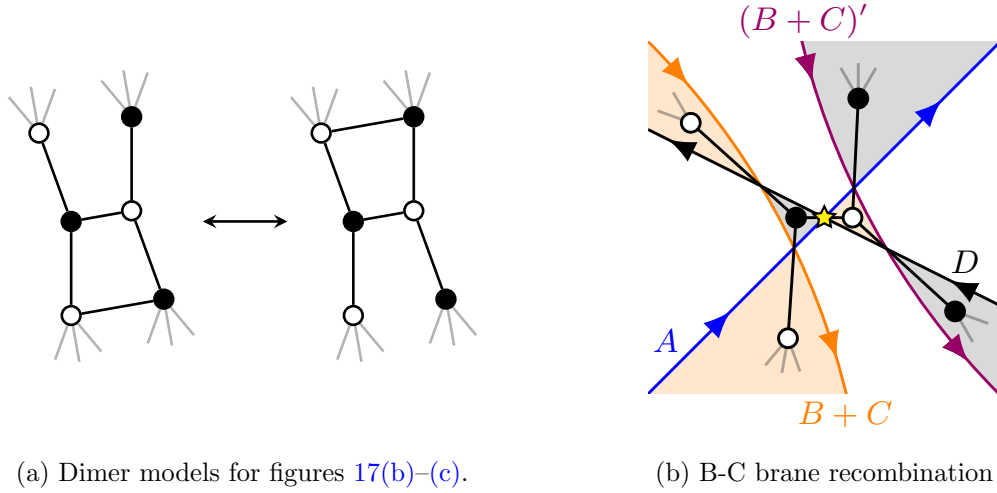


Figure 18: (a) Dimer models for the Seiberg-dual deformations of the quadruple crossing, figures 17(b)–(c). (b) A partial resolution of the quadruple crossing in 17(a), which corresponds to turning on a vev where the B and C branes intersect in 17(b)–(c).

3.3 Quad CFTs

To isolate the physics associated to the quadruple crossing and to decouple details of the rest of the brane tiling, we zoom in on the vicinity of the O5 plane, replacing T^2 with \mathbb{R}^2 , so that the four $(N, 0)$ faces in figure 17(a) become flavor branes and the superpotential terms associated to the four $(N, \pm 1)$ branes go to zero. The resulting brane configuration corresponds to a CFT in the infrared. Once these “quad” CFTs are understood, we can reintroduce gauge couplings for the non-compact branes by weakly gauging flavor symmetries of the CFT. Likewise, the missing superpotential terms can be reintroduced by deforming the CFT by a relevant operator.

Before orientifolding, the quadruple intersection can be resolved by a small deformation, as in figures 17(b)–(c), giving a pair of Seiberg dual gauge theories in the same universality class as the quad CFT, corresponding to the dimer models in figure 18(a). Heuristically, the orientifolded quad CFT corresponds to a quotient on the operator spectrum of this “parent” quad CFT. This is not quite correct, because the orientifold introduces a tadpole which must be cancelled by making ranks of the flavor branes unequal, but we expect it to be approximately true at large N , where the difference in ranks is a small effect. Thus, we can learn something about the orientifolded quad CFT by studying its parent.

We use this technique to determine the flavor symmetries associated to the quadruple crossing. In addition to the $SU(N)^4$ flavor symmetry associated to the flavor branes, there is an anomaly-free $U(1)$ flavor symmetry in the parent for each NS5 brane (zig-zag path) in the brane tiling [49], where the sum of these $U(1)$ s decouples. Thus, the manifest non-R flavor symmetry group is $SU(N)^4 \times U(1)^3$. However, the superpotential generated by the finite-area $(N, \pm 1)$ faces in figures 17(b)–(c) respects a larger $SU(2N) \times SU(N)^2 \times U(1)^2$ flavor

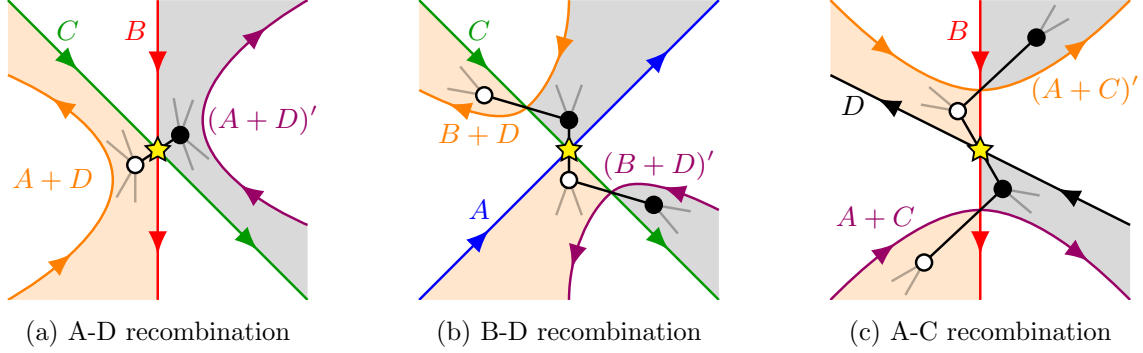


Figure 19: Possible brane recombinations which resolve the quadruple crossing, in addition to the B-C recombination shown in figure 18(b). In each case, the corresponding dimer model is superimposed on the tiling.

symmetry, where $SU(2N) \supset SU(N)^2 \times U(1)$ is broken when the flavor branes are gauged, but is conserved by the quad CFT itself.

The orientifold projection maps the NS5 branes to themselves and exchanges the $(N, 0)$ flavor branes in pairs, hence the $U(1)^3$ subgroup is invariant, whereas the $SU(N)$ factors are exchanged in pairs, leaving the manifest flavor symmetry group $SU(N) \times SU(N+p) \times U(1)^3$ after orientifolding, where p is the difference in ranks required to cancel the RR tadpole associated to the O5 plane. Thus, the orientifold projection maps the enhanced $SU(2N)$ symmetry of the parent theory to its charge conjugate, which suggests that $SU(2N)$ is broken to either $SO(2N)$ or $USp(2N)$ by the involution, where $SO(2N) \supset SU(N) \times U(1)$ or $USp(2N) \supset SU(N) \times U(1)$ is a nonabelian enhancement of the manifest flavor symmetries. This enhancement can be seen explicitly by Higgsing the baryon associated to the B-C crossing in figures 17(b)–(c), recombining the NS5 branes and giving the brane tiling shown in figure 18(b), which admits a perturbative, dimer model description. The superpotential terms associated to the finite-area $(N, \pm 1)$ faces preserve the enhanced symmetry $SO(2N)$ ($USp(2N)$) for an O5 plane of positive (negative) T-parity.

We infer that there are two classes of quad CFTs, depending on the overall sign of the RR charge of the O5 plane, with non-R flavor symmetry groups $SO(2N) \times SU(N+p) \times U(1)^2$ and $USp(2N) \times SU(N+p') \times U(1)^2$, respectively, for p and p' to be determined. We have also seen that these CFTs flow to an infrared-free theory with chiral superfields and a tree-level superpotential when we move along a baryonic branch corresponding to recombining the B and C NS5 branes. There are three other possible brane recombinations, shown in figure 19. In these cases, there are no finite-area $(N, \pm 1)$ faces, hence the infrared physics is described by free chiral superfields.

These brane recombinations — which will correspond to partial resolutions of the toric singularity when the quad CFT is embedded into T^2 — exhaust the baryonic directions in the moduli space. There are also mesonic directions coming from the gauge-singlet mesons in figure 18(a) and their orientifold images, which are composite mesons (elementary mesons

in the Seiberg dual theory). Turning on a rank k vev for the gauge-singlet mesons and their orientifold images, we obtain the rank $N - k$ quad CFT plus a residual $U(k)^2$ global symmetry and various gauge-singlet chiral superfields charged under $SU(N - k)^4 \times U(1)^3 \times U(k)^2$. These $U(k)^2$ -charged chiral fields do not appear in the superpotential, hence they decouple from the remainder of the quad CFT. When the quad CFT is embedded into T^2 , this direction in moduli space will correspond to removing an orientifold image pair of stacks of k D3 branes from the singularity without resolving it.

Thus, even without an explicit construction of the orientifolded quad CFTs, we can infer their global symmetries and the general characteristics of their moduli space. In the next section, we will construct CFTs which match these expectations, and are therefore candidate descriptions of the quadruple crossing.

4 Deconfinement and strong coupling

We now turn to the task of describing five-brane systems with quadruple intersections of NS5 branes, as in figure 15(b). We expect that these configurations are T-dual to configurations with the missing $[H]$ torsions in figure 12.

Surprisingly, even though (as we have argued) these configurations are intrinsically strongly coupled, it is still possible to construct a family of UV gauge theories in the same universality class as the strongly coupled theory. We motivate this through a brane engineering construction of the UV theories, and provide highly non-trivial evidence that our result is correct based on the quantum moduli space and superconformal index of the resulting theories, where the former matches with the five-brane description under the partial resolutions described in §3.3, and the latter passes all S-duality tests. Our construction is based on the deconfinement method of [17, 18], which we now review.

4.1 Deconfinement in the gauge theory

Consider an $USp(N - 4)$ gauge theory with N chiral superfields \hat{Z}^i in the vector representation, transforming under an $SU(N)$ flavor symmetry. It is well known [50] that this theory s-confines with the composite $Z^{ij} = \Omega^{ab} \hat{Z}_a^i \hat{Z}_b^j$ (where Ω^{ab} is the symplectic form of $USp(N - 4)$) and the superpotential

$$W = \text{Pf } Z, \quad (4.1)$$

where Z transforms in the \square representation of $SU(N)$. We consider deforming this theory by weakly gauging the $SU(N)$ flavor symmetry coupled to some set of additional chiral fields to cancel the anomalies. In the limit where the $SU(N)$ gauge coupling is small at the $USp(N - 4)$ confinement scale, the low energy dynamics of this $USp(N - 4) \times SU(N)$ gauge theory are the same as those of the $SU(N)$ gauge theory with the s-confined matter spectrum and superpotential (4.1). We can construct further duals of this theory by considering the limit where the $SU(N)$ gauge coupling becomes large before the $USp(N - 4)$ confinement scale. If there is no phase transition in between and the IR fixed point is isolated, this theory describes

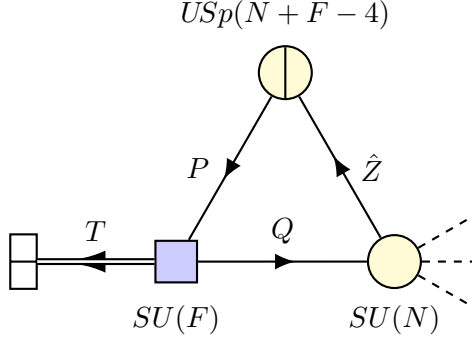


Figure 20: Deconfined description for an antisymmetric tensor.

the same infrared physics as before. In the limit where the $USp(N - 4)$ gauge coupling is small at the $SU(N)$ dynamical scale, we can replace $SU(N)$ with its Seiberg dual to obtain another theory with the same infrared fixed point. By dualizing nodes of the quiver in turn, we obtain a chain of dual descriptions [17]. This “deconfinement” technique is helpful for understanding the dynamics of the original $SU(N)$ gauge theory with antisymmetric tensor matter.

So far we have assumed that the $SU(N)$ gauge theory in question has a superpotential in the infrared of the form (4.1). To describe a theory without a superpotential, we replace $USp(N - 4)$ with $USp(N + F - 4)$ in the UV theory for some arbitrary $F > 0$, and add F additional $USp(N + F - 4)$ vectors P transforming under an $SU(F)$ flavor symmetry, as well as F antifundamentals Q of $SU(N)$ transforming under the same $SU(F)$ and a gauge-singlet T in the \square representation of $SU(F)$. This gives the quiver diagram shown in figure 20. We introduce the $SU(F)$ -invariant superpotential

$$W = PQ\hat{Z} + TP^2. \quad (4.2)$$

When the $USp(N + F - 4)$ theory s-confines, it forms the composites

$$M = \begin{pmatrix} \hat{Z}^2 & \hat{Z}P \\ -\hat{Z}P & P^2 \end{pmatrix} \quad (4.3)$$

with the confining superpotential $\text{Pf } M$. However, $\hat{Z}P$ and P^2 get a mass with Q and T respectively, via the tree-level superpotential (4.2), and can be integrated out. The F -term conditions for Q and T set $\hat{Z}P = P^2 = 0$, and the confining superpotential vanishes, leaving behind a single $SU(N)$ antisymmetric tensor $Z = \hat{Z}^2$ with no superpotential [18].

Note that the choice of $F > 0$ is arbitrary, except that $N + F$ must be even for $USp(N + F - 4)$ to exist. In the infrared, no fields are charged under the $SU(F)$. Thus, despite being unbroken, the UV symmetry $SU(F)$ is not a symmetry of the infrared fixed point, explaining how theories with different global symmetry groups in the UV and no accidental symmetries can describe the same infrared physics. We refer to such a UV global symmetry as “trivial”.

In fact, the triviality of $SU(F)$ imposes interesting *a posteriori* constraints on the moduli space and operator spectrum. Consider turning on a vev for a gauge-invariant operator in a non-trivial $SU(F)$ representation, spontaneously breaking the $SU(F)$. In the UV theory, this is a D-flat direction classically, and it is straightforward to choose an operator which also satisfies the classical F-term constraints such as T (for $F > 2$, so that T transforms under $SU(F)$). However, triviality for $SU(F)$ implies that the operator in question is lifted in the infrared, hence it is not a flat direction of the full theory. This is true for any operator in a non-trivial $SU(F)$ representation. Thus, for most practical purposes, we can treat $SU(F)$ as weakly gauged, and only consider $SU(F)$ singlet operators. Triviality of the $SU(F)$ implies the vanishing of the $SU(F)^3$ and $SU(F)^2U(1)$ anomalies, except that $SU(F)^2U(1)_R$ receives a contribution from the $SU(F)$ gauginos, and the R-symmetry is anomalous. Since the $SU(F)$ is trivial, once gauged it undergoes gaugino condensation in the infrared, resulting in F isolated vacua in the $SU(F)$ sector, and an accidental R-symmetry in the $SU(N)$ sector. While this is essentially (though not exactly) equivalent to the infrared physics of the theory before gauging the $SU(F)$, it is usually more convenient to treat $SU(F)$ as a global symmetry, keeping in mind that it is trivial, hence only $SU(F)$ singlets contribute to the IR dynamics.

To illustrate the triviality of $SU(F)$, we consider the effect of a few $SU(F)$ -breaking vevs. Turning on a vev for T gives mass to some of the P 's. If T has rank greater than one, then $USp(N + F - 4)$ develops a dynamical superpotential, and supersymmetry is broken. If T has rank one and $F > 2$, $USp(N + F - 4)$ has a quantum-deformed moduli space, $\text{Pf } M = \Lambda^{N+F-2}$, but the F-term conditions set $\text{Pf } M = 0$ as before, so supersymmetry is broken. If T has rank one and $F = 2$, then T is a $SU(F)$ singlet, and the result is different. After integrating out the P 's in the UV theory, we are left with a superpotential $W = Q^2 \hat{Z}^2$. As before, $USp(N + F - 4)$ has a quantum-deformed moduli space $\text{Pf}(\hat{Z}^2) = \Lambda^{N+F-2}$, but now the F-term conditions do not enforce $\text{Pf}(\hat{Z}^2) = 0$. Instead, $SU(N)$ is Higgsed to $USp(N)$ and Q acquires a mass, leaving $SU(F)$ trivial as before.²¹ A similar story applies to other $SU(F)$ breaking directions in the classical moduli space.

4.2 Deconfinement in the brane tiling

In this section, we engineer deconfinement of an antisymmetric tensor in the five-brane system discussed in §3.2. In the process, we will inevitably encounter non-BPS — indeed, dynamically unstable — brane configurations. This situation is not unprecedented. For instance, many of the toric phases which arise in dimer models cannot be realized by brane tilings with straight NS5 branes. These “geometrically inconsistent” phases [51, 52] do not correspond to any BPS configuration of branes, but in general they are Seiberg-dual to some geometrically consistent phase, hence they lie in the same universality class as some BPS configuration. With this example in mind, we engineer a configuration of branes which reproduces the gauge theory

²¹In fact, T plays the same role in this case as $\hat{Z}^N = \text{Pf } Z$ does for even N and $F \geq 4$ (\hat{Z}^N vanishes identically for $F = 2$).

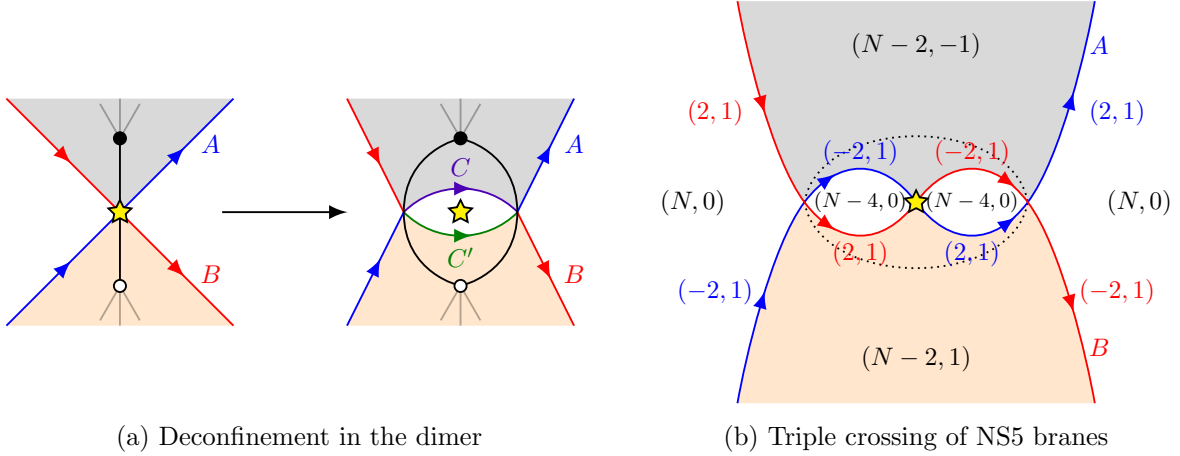


Figure 21: (a) Deconfinement corresponds to edge doubling in the dimer model. To avoid a global change in the structure of the zig-zag paths, the original paths A and B are forced to recombine into new paths C and C' on the doubled edges. (b) The configuration of branes prior to “lifting”, with a triple crossing of NS5 branes. The dashed line indicates the boundary of the region to be lifted off the D5 stack, and the shaded regions within this line will become the NS5 branes C and C' .

construction of §4.1, ignoring issues of supersymmetry and stability. We then provide some post hoc justification for why this works.

We start with the brane tiling description of a single antisymmetric tensor multiplet of $SU(N)$, see figure 14. As in §3.3, we take the worldvolume of the D5 branes to be \mathbb{R}^2 instead of T^2 , so that there is a single O5 plane, and the image pair of $(N, 0)$ faces corresponds to an $SU(N)$ flavor symmetry. The O5 plane is divided into an $O5^+$ plane and an $O5^-$ plane by the NS5 branes, with opposite D5 charges in the two parts, so the NS5 branes carry D5 charge ± 2 to cancel the tadpole [31].

Leaving aside the issue of flavors and the confining superpotential temporarily, deconfinement has an obvious description in the dimer model, see figure 21(a). The antisymmetric tensor corresponds to an edge crossing a fixed point of negative T-parity. To deconfine this tensor, we replace the edge with an image-pair of edges surrounding a two-sided face with the fixed point in the middle. The new face is an USp gauge group — $USp(N - 4)$ by anomaly cancellation — which s-confines, reproducing the antisymmetric tensor we started with. Thus, deconfinement corresponds to “doubling” in the language of [53, 54].

In order to translate this into a five-brane system, we construct the zig-zag paths of the dimer. This immediately leads to a puzzle: before doubling the edge, there are two zig-zag paths, A and B , which cross at the fixed point. After doubling, one end of A connects to the other end of B , and vice versa, so the zig-zag paths get reconnected, even though we performed a local operation in the dimer. Taking the new zig-zag paths literally leads to the conclusion that dimer models of this type are “inconsistent” [28].

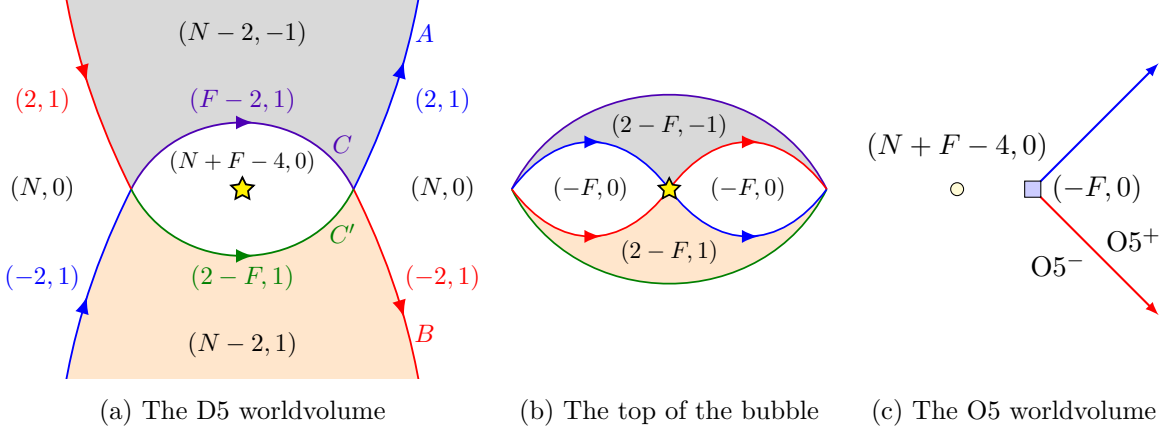


Figure 22: The configuration of branes after lifting, including the pair creation of F flavor branes. We use the same orientation conventions in (a) and (b), so that the flavor faces on the roof of the bubble appear here as $(-F, 0)$, which is the same as $(F, 0)$ oppositely oriented.

Instead, we interpret the two zig-zag paths inside the new two-sided face as new NS5 branes C and C' which appear after deconfinement, whereas the zig-zag paths outside the new face are the same NS5 branes A and B that were present before deconfinement. To understand how the two halves of A and B are joined together and how C and C' connect to A and B , we construct the entire NS5 brane configuration in two steps, as follows. First, we deform the initial brane configuration by changing the single crossing of the NS5 branes into a triple crossing, creating an image pair of “eyes” surrounding the O5 plane, as in figure 21(b). We then trace out a contour enclosing this pair of eyes, and lift the NS5 branes within the enclosing contour off of the D5 stack into the minor angle between the A and B branes in the (x_6, x_7) plane, opening up a “bubble” bounded by a new $(N-4, 0)$ face on the D5 stack and the lifted NS5 branes, which we identify as C and C' . The NS5 branes A and B now end on the upper surface of the bubble, tracing out the same double eye as before, where they fuse with the upper boundary of the branes C and C' .

We add F flavors to this configuration by pair-creating F pairs of D5 branes within the larger eye and adding half of these to the $USp(N-4)$ face to obtain $USp(N+F-4)$. Their F opposite numbers are bound to the NS5 branes C and C' on the roof of the bubble, where they fill in the pair of eyes created by the boundaries of the branes A and B , generating $(F, 0)$ faces (oriented oppositely to the $(N+F-4, 0)$ face below them) with a corresponding $SU(F)$ symmetry. The final brane configuration is illustrated in figure 22.

For completeness, we construct an explicit realization of the “deconfinement bubble” described above. This is done merely to better illustrate our argument; we emphasize that the details of the curves have no effect on our conclusions.

We take the initial configuration of branes to be $x_5 = \pm x_4$ and $x_7 = \pm x_6$, $x_6 \geq 0$, where the upper (lower) sign applies to brane A (brane B) and the D5 stack is located at

$x_6 = x_7 = 0$.²² We then deform the branes to create a triple crossing as in figure 21(b), so that their boundaries lie at $x_5 = \pm x_4 \frac{x_4^2/a^2 - 1}{x_4^2/a^2 + 1}$, where a controls the size of the deformation in the (x_4, x_5) plane. The deformation can be extended into the bulk as

$$x_5 = \pm x_4 \frac{x_4^2/a^2 + x_6^2/b^2 - 1}{x_4^2/a^2 + x_6^2/b^2 + 1}, \quad (4.4)$$

where b controls the size of the deformation in the (x_6, x_7) plane, so that the branes return to their initial shapes asymptotically as $x_4, x_6 \rightarrow \infty$.

Next, we trace out an eye surrounding the triple crossing at $x_5 = \pm \frac{a}{2}[1 - x_4^2/a^2]$ for $|x_4| \leq a$. After the lift, this describes boundary of the brane C (C') for the upper (lower) sign, and is chosen to match first derivatives with the boundaries of A and B at their mutual intersections. To implement the lift, we specify the displacement of C , C' in the positive x_6 direction by

$$x_5^2/a^2 + [1 - x_4^2/a^2] x_6^2/c^2 = \frac{1}{4}[1 - x_4^2/a^2]^2 \quad (4.5)$$

for $|x_4| \leq a$, where c controls the size of the lift and the x_4 -dependent prefactor of x_6^2 is chosen for later convenience. The branes C , C' stretch between their boundaries on the D5 branes at $x_5 = \pm \frac{a}{2}[1 - x_4^2/a^2]$ and their intersection with the branes A and B , along the pair of curves specified by

$$x_4^2/a^2 \frac{x_4^2/a^2 + x_6^2/b^2 - 1}{x_4^2/a^2 + x_6^2/b^2 + 1} + [1 - x_4^2/a^2] x_6^2/c^2 = \frac{1}{4}[1 - x_4^2/a^2]^2, \quad (4.6)$$

where we choose $c < 2b$ so that the branes intersect before the pair of eyes surrounding the O5 plane close up. The final configuration of branes in the (x_4, x_5, x_6) directions is plotted in figure 23(a).

We now describe the positions of the branes in the x_7 direction. Before lifting, we had $x_7 = \pm x_6$ for branes A and B , respectively. In order to match the slopes of the branes A and B with C and C' at their intersection point on the D5 stack, we choose $x_7 = \mp \frac{x_4}{a} x_6$ for C and C' , respectively. To ensure that A and B meet the boundary of C and C' along the curve (4.6), we deform the x_7 position of A and B by:

$$x_7^2/c^2 = x_6^2/c^2 + x_5^2/a^2 - \frac{1}{4}[1 - x_4^2/a^2]^2, \quad (4.7)$$

for $|x_4| < a$, where brane A (B) correspond to the $x_7 > 0$ ($x_7 < 0$) branch of the solution. This reproduces $x_7^2 = \frac{x_4^2}{a^2} x_6^2$ on the intersection with (4.5) and reduces to $x_7 = \pm x_6$ in the $x_6 \rightarrow \infty$ limit. Setting $x_4^2 = a^2$, we obtain $x_7^2/c^2 = x_6^2/c^2 + x_5^2/a^2$, which differs slightly from the initial configuration $x_7 = \pm x_6$ because $x_5 = \pm a \frac{x_6^2/b^2}{x_6^2/b^2 + 1} \neq 0$. In order to match onto this behavior for $|x_4| > a$, we take

$$x_7^2/c^2 = x_6^2/c^2 + \frac{[3x_4^2/a^2 - 2][2x_4^2/a^2 + x_6^2/b^2 - 2] x_6^2/b^2}{[x_4^2/a^2 + x_6^2/b^2 + 1]^2 x_4^4/a^4}, \quad (4.8)$$

²²Here we have fixed the minor angle between the branes to be 90° , but this can easily be changed.

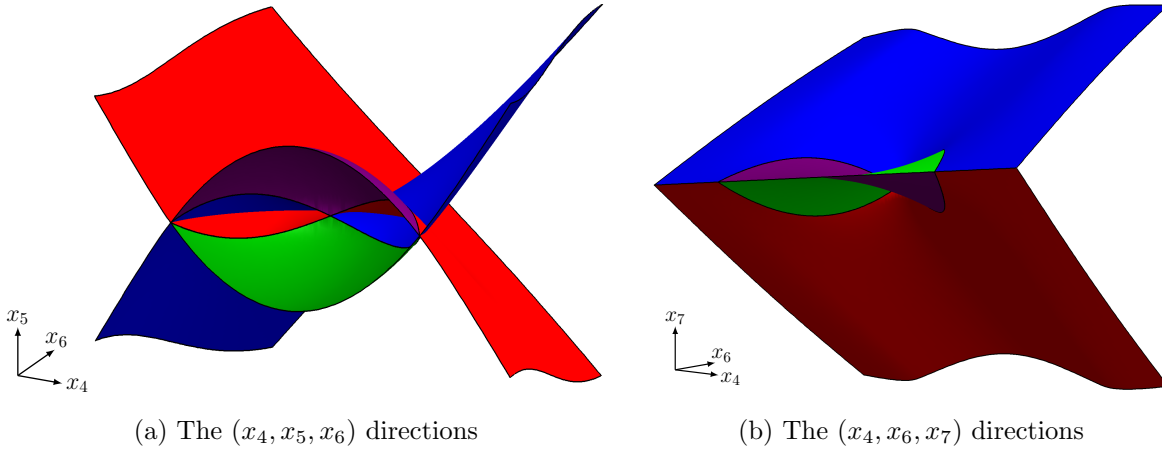


Figure 23: The deconfined NS5 branes, plotted using the equations described in the text (for $c = \sqrt{2}b$). The flavor branes are not pictured: they fill in the pair of eyes where the branes A and B intersect the branes C and C' .

for $|x_4| > a$, where the second term is chosen to match first derivatives at $|x_4| = a$ and to reproduce $x_7 \rightarrow \pm x_6$ asymptotically as $x_4, x_6 \rightarrow \infty$. The final configuration of branes in the (x_4, x_6, x_7) directions is plotted in figure 23(b).

With a complete picture of the deconfined configuration of NS5 branes, we can read off the physics of the resulting gauge theory. From the perspective of the D5 stack near the intersection of branes A and B , the F flavor branes are ordinary minor flavor branes [31, 55]. Thus, in addition to the bifundamental \hat{Z} usually generated at the intersection point, flavored fields P and Q are also present, and there is a superpotential term $\hat{Z}PQ$, as in (4.2). Similarly, from the perspective of the F flavor branes near their intersection with the O5 plane, they form part of an ordinary brane tiling, hence by analogy there is an antisymmetric tensor T of $SU(F)$ at the point of intersection with the O5 plane. By the same analogy, the image pair of NS5 branes C and C' will generate a superpotential term TP^2 formed from the fields encircling their perimeter.

Thus, the configuration of branes constructed above completely reproduces the deconfined theory of §4.1, with one exception: since the $(F, 0)$ flavor faces have finite size, the $SU(F)$ flavor symmetry is gauged. As noted in §4.1, this describes almost the same physics as an ungauged, trivial $SU(F)$. However, it is more convenient to work with a global $SU(F)$, and this is easily engineered by “puncturing” the $(F, 0)$ faces, i.e. by attaching long thin D5-brane tubes which end at infinity. When the $USp(N + F - 4)$ face confines, the $SU(F)$ flavor tubes pinch off, leaving behind a trivial $SU(F)$ flavor symmetry, as in the gauge theory description.

We conclude that the above non-BPS, unstable configuration of branes — which is a small deformation of the initial, BPS configuration — produces an $\mathcal{N} = 1$ gauge theory in the right universality class when we naively ignore the supersymmetry-breaking couplings. We can explain this heuristically as follows: we imagine deforming the full string theory by

coupling it to external currents sourcing F-term tadpoles for the transverse scalars of the branes, arranged so that the deformed theory relaxes into the configuration of curved branes we are interested in, which is now supersymmetric due to the F-term tadpoles. In general, this deformed theory will not be UV complete, but since we are interested in the infrared physics, we ignore this and consider the effect of the deformation on the infrared fixed point. Let us suppose that the deformed theory has the same flavor symmetries as the undeformed theory, without any accidental symmetries.²³ In this case, the superconformal R-symmetry in the IR is a conserved symmetry of the UV theory, and the UV deformation can only induce marginal deformations in the IR. Since these deformations are forced to be flavor singlets, they are exactly marginal [56], and the deformed theory will flow to the same conformal manifold as the undeformed theory. In particular, in the absence of exactly marginal deformations, the two theories are in the same universality class.

Leaving aside the subtleties of this heuristic reasoning, let us see how it applies to the case at hand. Introducing the above deconfinement bubble without flavor branes ($F = 0$) leads to a deformed theory with fewer flavor symmetries, due to the $USp(N-4)^2U(1)$ mixed anomalies, and we expect that the infrared physics may differ from that of the original brane configuration. Indeed, the $USp(N-4)$ s-confines and generates a confining superpotential (4.1) not present in the initial theory.²⁴ Conversely, once we add flavor branes to the deconfinement bubble in the manner described above, the symmetries of the deformed theory match those of the original theory, and indeed the infrared physics of the two descriptions match, as shown in §4.1.

Thus, by matching the flavor symmetries of the deformed and undeformed brane configurations, we gain some control over changes to the infrared physics. With this in mind, we apply the same deconfinement construction to understand the quadruple crossing of NS5 branes encountered in §3.2.

4.3 Deconfining phase II

We are interested in the local physics of four NS5 branes intersecting atop an O5 plane, as in figure 24. As above, we begin by considering the case of non-compact D5 branes with an single O5 plane in the middle, corresponding to the “quad CFTs” considered in §3.3. The deformations corresponding to deconfinement are local, so that once this configuration is understood there is no obstacle to embedding it into T^2 .

There are two phases to consider, differing by an overall sign in the local RR charges of the O5 plane. In this section, we focus on the case shown in figure 24(b). Because we will only deconfine antisymmetric (rather than symmetric) tensors, the case shown in figure 24(c) is somewhat different, and will be treated separately in §4.4.

In the same spirit as §4.2, we can imagine pairing any two adjacent legs of the web diagram and blowing up a deconfinement bubble by recombining the associated NS5 branes.

²³Non-abelian (rank-preserving) symmetry enhancements, such as occur in §4.4, do not affect this reasoning.

²⁴In the case where $SU(N)$ is not gauged, this superpotential is irrelevant in the IR, but this is not true in general when $SU(N)$ is gauged.

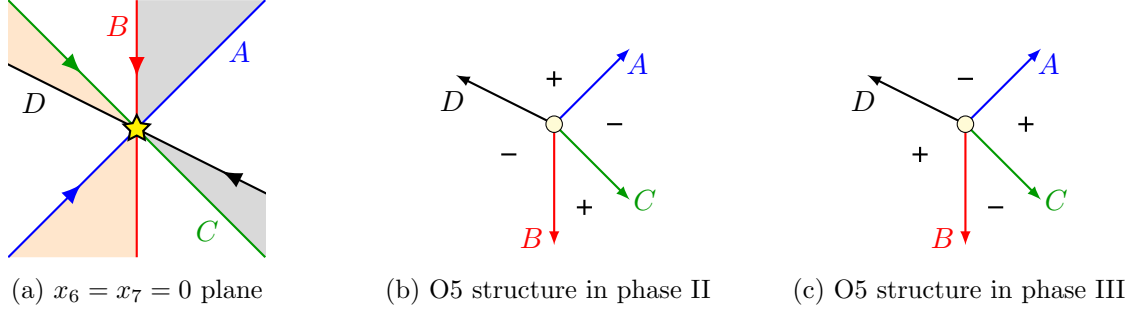


Figure 24: Neighborhood of the strongly coupled sector in phases II and III of the dP_1 orientifold.

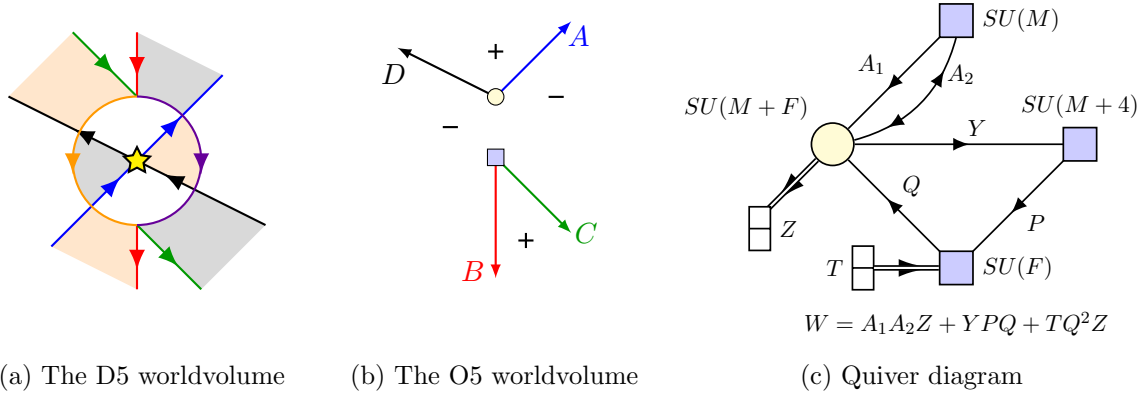


Figure 25: Local picture for the deconfinement in phase II obtained by deforming B and C together. In (b) the intersection of the O5 with the $x_6 = x_7 = 0$ plane where the tiling lives is indicated by the yellow circle. After deconfinement the B and C branes no longer intersect over this point (they rather intersect over the flavor stack, indicated by the blue square), but A and D still do.

Analogous to deconfinement of an antisymmetric tensor, we choose to pair only legs that enclose an O5 plane with positive charge in their minor angle. Thus, for phase II we can either recombine B and C or recombine A and D . We consider the former combination for now, returning to the latter shortly. After recombination, the brane configuration is the same as in §4.2, but with the branes A and D superimposed on top, see figure 25. Since the deconfinement bubble is contained within the minor angle between branes B and C , A and D do not intersect it off the D5 brane stack. Moreover, the quadruple intersection has been resolved, and we can read off the resulting gauge theory exactly as in §3.2, accounting for the flavor branes as in the same way as in §4.2.

The resulting quiver gauge theory is shown in figure 25(c), and the corresponding charge table is shown in table 4, where the tree-level superpotential is

$$W = A_1 A_2 Z + Y P Q + T Q^2 Z. \quad (4.9)$$

	$SU(M+F)$	$SU(M)$	$SU(M+4)$	$SU(F)$	$U(1)_B$	$U(1)_X$	$U(1)_Y$	$U(1)_R$
A_1	\square	\square	$\mathbf{1}$	$\mathbf{1}$	$-\frac{1}{M+F}$	1	$-\frac{M+4}{M+F}$	$1 - \frac{2}{M+F}$
A_2	\square	\square	$\mathbf{1}$	$\mathbf{1}$	$-\frac{1}{M+F}$	-1	$-\frac{M+4}{M+F}$	$1 - \frac{2}{M+F}$
Y	\square	$\mathbf{1}$	\square	$\mathbf{1}$	$\frac{1}{M+F}$	0	$-1 + \frac{M+4}{M+F}$	$\frac{2}{M+F}$
Z	\square	$\mathbf{1}$	$\mathbf{1}$	$\mathbf{1}$	$\frac{2}{M+F}$	0	$\frac{2(M+4)}{M+F}$	$\frac{4}{M+F}$
P	$\mathbf{1}$	$\mathbf{1}$	\square	\square	$\frac{1}{F}$	0	1	2
Q	\square	$\mathbf{1}$	$\mathbf{1}$	\square	$-\frac{1}{M+F} - \frac{1}{F}$	0	$-\frac{M+4}{M+F}$	$-\frac{2}{M+F}$
T	$\mathbf{1}$	$\mathbf{1}$	$\mathbf{1}$	\square	$\frac{2}{F}$	0	0	2

Table 4: A deconfined description of the quad CFT associated to phase II

The a -maximized R-charge [57] is

$$U(1)_R^{(\text{sc})} = U(1)_R + \left(-\frac{4}{3} + \frac{M}{4}(\alpha_M - 1)^2 + \alpha_M(\alpha_M - 2) \right) U(1)_B + \alpha_M U(1)_Y, \quad (4.10)$$

where α_M is the smallest non-negative root of

$$9(M+4)\alpha_M^3 - 9M\alpha_M^2 - 3(3M+4)\alpha_M + M = 0. \quad (4.11)$$

Our task is now to argue that the infrared fixed point of this gauge theory describes the CFT associated to the quadruple crossing of NS5 branes we started with. However, we notice immediately that this gauge theory depends on the number of flavors, F , introduced during deconfinement. As a first consistency check, we show that the infrared fixed point depends only on the parity of F , and that the $SU(F)$ global symmetry is otherwise trivial.

Our proof works by relating this resolved configuration of branes to the configuration where branes A and D are recombined into a bubble and branes B and C cross the O5 plane, illustrated in figure 26(c). To do so, we first deconfine the antisymmetric tensor Z with G flavors, generating a new $USp(M+F+G-4)$ face, where we require $F+G \equiv M \pmod{2}$. We then take the Seiberg dual of the $SU(M+F)$ node, which turns into an $SU(M+G)$ node. Keeping track of the interactions and integrating out massive matter, we find that the $USp(M+F+G-4)$ node is again s-confining, where now the roles of $SU(F)$ and $SU(G)$ have flipped. Moving to the s-confined description, all $SU(F)$ -charged states become massive, and we conclude that the $SU(F)$ is trivial. The resulting gauge theory corresponds to the deconfined brane tiling 26(c), now with G flavors. This chain of dualities, which we refer to as “deconfinement duality”, is closely related to Seiberg duality, and does not affect the infrared physics. Notice that G still encodes the parity of F , due to the constraint $F+G \equiv M \pmod{2}$, but otherwise different values of F correspond to the same infrared physics. Likewise, by construction $SU(G)$ is trivial, and the physics only depends on $(-1)^G = (-1)^{M+F}$.

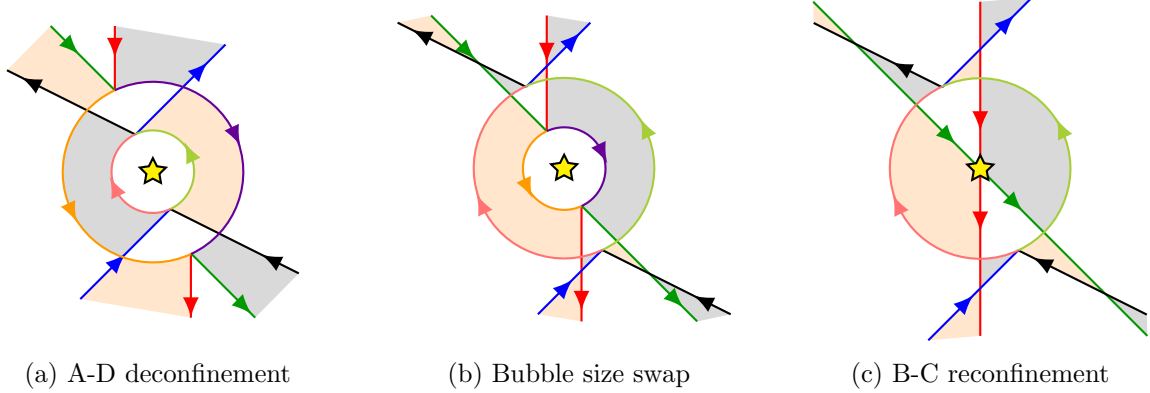
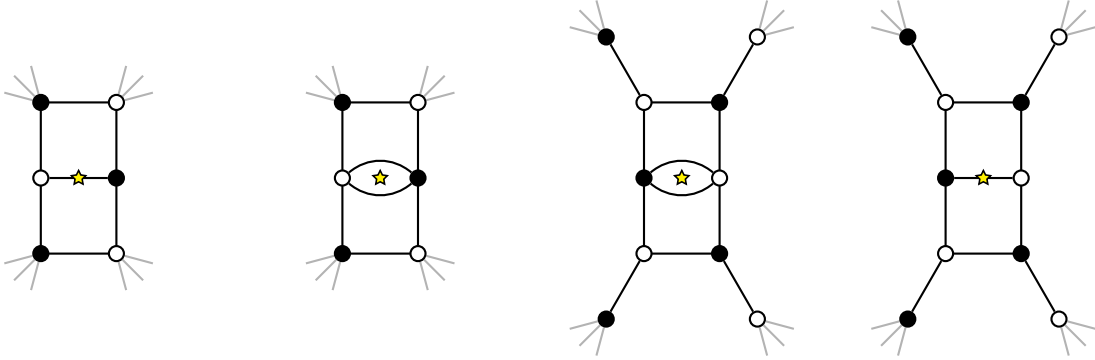


Figure 26: Deconfinement duality in the brane tiling for the local configuration in phase II. (a) We deconfine the antisymmetric tensor Z where NS5 branes A and D cross. (b) Seiberg duality on the mirror-image pair of wedge-shaped faces corresponds to passing the boundaries of the two deconfinement bubbles through each other. (c) Reconfining the central face, we obtain a dual description.



(a) Dimer for fig. 25(a) (b) Dimer for fig. 26(a) (c) Dimer for fig. 26(b) (d) Dimer for fig. 26(c)

Figure 27: Deconfinement duality from the point of view of the dimer model. (a) We start with dimer model corresponding to the the B-C deconfined brane tiling shown in 25(a). (b) We deconfine the antisymmetric tensor. (c) We apply Seiberg duality to the SU gauge group (recall figure 1(c)), and integrate out massive matter. (d) Reconfining the central USp node, we obtain the dimer model corresponding to the A-D deconfined brane tiling shown in figure 26(c).

This chain of dualities can be described in the brane tiling using deconfinement bubbles, as in figure 26, and likewise admits a simple description in the dimer model, see figure 27. However, we emphasize that the above argument is based on field theory reasoning, and does not rely on the string theory realization.

The residual dependence on the parity of F is important: there are additional data associated to the original BPS configuration that we have so far ignored. In particular, the

dual Calabi-Yau singularity has moduli associated to Wilson lines of both B_2 and C_2 before orientifolding. We argued in §3.2 that the B_2 Wilson lines are projected to discrete values after orientifolding and contribute to the $[H]$ discrete torsion, where in the dual brane tiling these discrete Wilson lines correspond to NS5 brane positions. So far we have ignored the analogous C_2 discrete Wilson lines, which contribute to $[F]$ discrete torsion by the same argument. These correspond to Wilson lines on the NS5 branes in the dual brane tiling [58], and we expect that they are likewise projected to discrete values by the O5 involution. A natural guess is that $(-1)^F$ is fixed by a combination of Wilson lines localized at the quadruple intersection, hence it contributes to RR discrete torsion. This view will be confirmed when we study the S-duality properties of these theories.

Besides the trivial $SU(F)$ symmetry, the remaining $SU(M) \times SU(M+4) \times U(1)^3 \times U(1)_R$ flavor symmetry group displayed in table 4 matches the brane picture laid out in §3.3. Moreover, the gauge theory enjoys an accidental non-abelian enhancement to $USp(2M) \supset SU(M) \times U(1)_X$ not manifest in the brane picture, in perfect agreement with the expectations outlined in §3.3.

We now describe the moduli space of these theories. The gauge-invariant chiral operators consist of mesons and baryons of $SU(M+F)$.²⁵ However, due to the triviality of $SU(F)$, only the $SU(F)$ -invariant subsector of these operators can correspond to flat directions in the moduli space. The other directions break $SU(F)$, hence they are lifted by quantum effects. The $SU(F)$ -invariant mesons and baryons are

$$\Phi_i = A_i Y \quad , \quad \mathcal{O}_k = A_1^k A_2^{M-k} Q^F \quad , \quad \tilde{\mathcal{O}}_k = Z^{\frac{F+k-4}{2}} Y^{M+4-k} . \quad (4.12)$$

In the former case, $0 \leq k \leq M$ is arbitrary, whereas in the latter case $0 \leq k \leq M+4$ must satisfy $(-1)^k = (-1)^F$.²⁶

Note that due to the F-term constraint for Z , the baryons \mathcal{O}_k combine into a single irrep of $USp(2M)$, the M -index antisymmetric tensor of dimension $\frac{(2M+2)!}{(M+1)!(M+2)!}$. This curious fact will have an interesting analog in phase III in §4.4.

We can identify the baryons with partial resolutions as in §3.3. The procedure is similar to that of §3.1. A partial resolution which combines two adjacent legs of the web diagram corresponds to vevs for the baryons where the corresponding NS5 branes cross.²⁷ Thus, \mathcal{O}_0 describes the B-D partial resolution (figure 19(b)), whereas \mathcal{O}_M describes the A-C partial resolution (figure 19(c)), and \mathcal{O}_k for $0 < k < M$ interpolates between the two, much as in §3.1. Turning on a vev for \mathcal{O}_k , the $SU(M+F)$ gauge group is completely Higgsed, and all $SU(F)$ -charged matter becomes massive. The remaining massless fields, shown on the left side of figure 28, do not interact, and fall in the expected representations of the flavor brane symmetries inherited from the quad CFT, c.f. figures 18(b), 19, with the necessary addition

²⁵Here we ignore chiral operators containing glueballs ($W_\alpha W^\alpha$) for simplicity.

²⁶We assume $F \geq 3$ for simplicity. For $F = 1$ ($F = 2$), $\tilde{\mathcal{O}}_1$ ($\tilde{\mathcal{O}}_0$) is not defined, and we should replace $\tilde{\mathcal{O}}_1 \rightarrow P$ ($\tilde{\mathcal{O}}_0 \rightarrow T$), which is an $SU(F)$ -invariant only for this value of F .

²⁷For this purpose, we consider the edge of the deconfinement bubble as equivalent to either of its constituent NS5 branes.

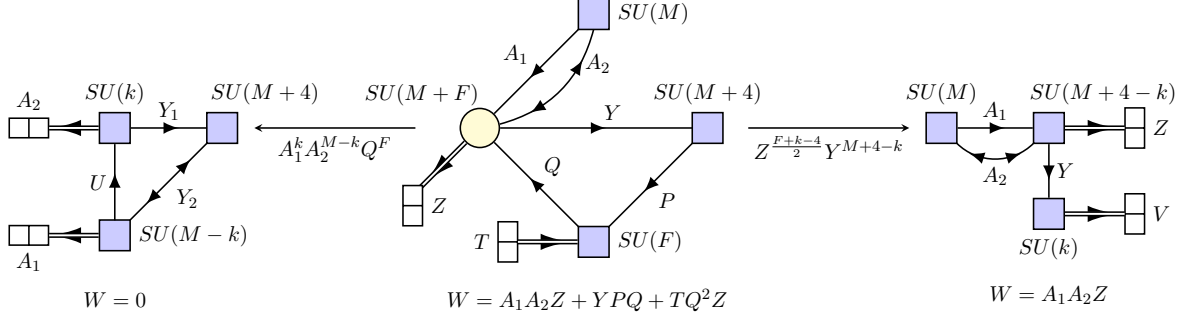


Figure 28: Partial resolutions of the quad CFT for phase II. The left hand resolutions correspond to recombining B-D / A-C (cf. figures 19(b), 19(c)), whereas the right-hand resolutions correspond to recombining B-C / A-D (cf. figures 18(b), 19(a)). The fields U and Y are Goldstone bosons for $SU(M) \rightarrow SU(M-k) \times SU(k)$ and $SU(M+4) \rightarrow SU(M+4-k) \times SU(k)$ breaking, respectively.

of Goldstone bosons due to the breaking of global symmetries (these will be eaten when the flavor branes are gauged).

Likewise $\tilde{\mathcal{O}}_0$ describes the B-C partial resolution (figure 18(b)), whereas $\tilde{\mathcal{O}}_{M+4}$ describes the A-D partial resolution (figure 19(a)), and $\tilde{\mathcal{O}}_k$ interpolates between the two. Turning on a vev for $\tilde{\mathcal{O}}_k$, the gauge group is Higgsed to $USp(F+k-4)$. Integrating out the massive matter, $USp(F+k-4)$ reconfines much as in §4.1, generating a composite antisymmetric tensor V without a superpotential. The entire spectrum — including a tree-level superpotential — is shown on the right-hand side of figure 28. As before, the results agree with figures 19(c), 19(b)), except for the inevitable appearance of Goldstone bosons.

Finally, turning on a rank k vev for Φ_1 (equivalently Φ_2), we obtain the rank- $(M-k)$ theory together with a residual $U(k)$ flavor symmetry and non-interacting chiral superfields charged under it and under the global symmetries of the CFT, in agreement with the behavior of the parent theory discussed in §3.3.

Thus, the candidate CFT constructed above has the same global symmetries and moduli space as anticipated for the quad CFT in §3.3. Moreover, one can show using the a -maximized R-charge (4.10) that this CFT has no exactly marginal deformations. Therefore, the deconfinement trick of §4.2 appears to generate a gauge theory *in the same universality class* as the theory on four intersecting NS5 branes. Since the UV gauge theory (in contrast to the IR fixed point) depends on F , this is the strongest claim that can be made, and is consistent with the intuition that the higher multiplicity intersection of NS5 branes is intrinsically strongly coupled. We obtain further non-trivial evidence for this claim in §5, where we consider S-duality of the dP_1 orientifold phases constructed from this CFT.

4.4 Deconfining phase III

We now construct a deconfined description of the quad CFT for phase III. Much of the discussion is analogous to phase II, described above, so we will be brief. The worldvolume of

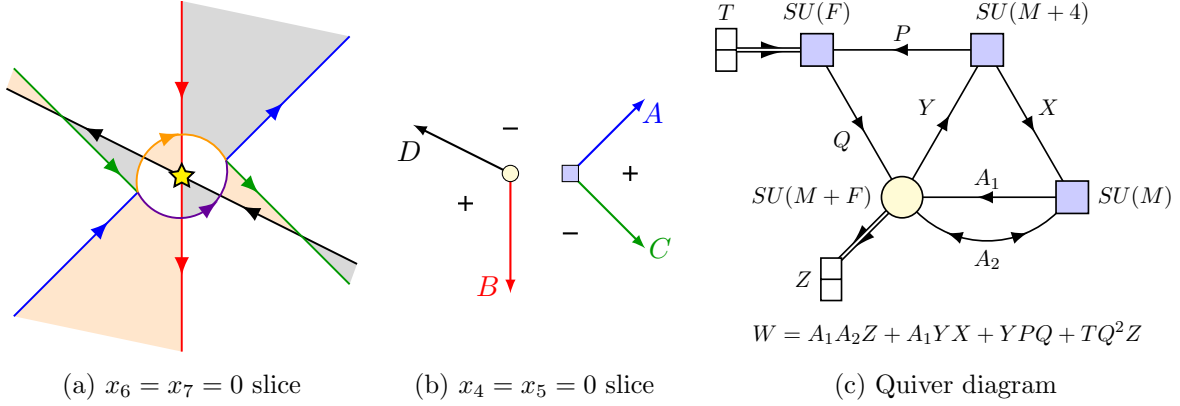


Figure 29: Local picture for the deconfinement in phase III obtained by deforming A and C together. After deconfinement the A and C branes no longer intersect the intersection of the tiling with the orientifold plane (depicted as the yellow circle in (b)) but B and D still do.

the O5 plane coincident with the quadruple intersection of NS5 branes is shown in figure 24(c). As before, we blow up a deconfinement bubble by pairing two adjacent NS5 branes enclosing an $O5^+$ in their minor angle. In this case, we can form the bubble using either B and D or A and C . The two choices will be related via deconfinement duality, hence their infrared physics is the same. The configuration with A and C combined into a bubble is shown in figure 29(a)–(b), and the resulting quiver gauge theory is shown in figure 29(c), with the charge table shown in table 5 and the tree-level superpotential

$$W = A_1 A_2 Z + A_1 Y X + Y P Q + T Q^2 Z. \quad (4.13)$$

Note that this is a superpotential deformation of table 4 plus the gauge singlet meson X , where we have chosen to redefine

$$U(1)_Y^{(\text{III})} = U(1)_Y^{(\text{II})} - \frac{M+4}{2} U(1)_B \quad (4.14)$$

for later convenience. The a -maximized R-charge is now

$$U(1)_R^{(\text{sc})} = U(1)_R + \left(-\frac{4}{3} + \frac{M}{4} (1 - \tilde{\alpha}_M^2) \right) U(1)_B + \tilde{\alpha}_M U(1)_X, \quad (4.15)$$

where $\tilde{\alpha}_M$ is the smallest non-negative root of

$$9M\tilde{\alpha}_M^3 - 9(M+4)\tilde{\alpha}_M^2 - 3(3M+8)\tilde{\alpha}_M + (M+4) = 0. \quad (4.16)$$

Because of the close relationship between tables 5 and 4, many of the consistency checks performed in the previous section go through analogously for this theory. Consequently, we only discuss the novel aspects of this theory, leaving the basic checks as an exercise.

Applying deconfinement duality, we obtain a dual theory with $G \equiv M+F \pmod{2}$ flavors which is isomorphic to the original theory. Thus, for even M the theory is self-dual (with a

	$SU(M+F)$	$SU(M)$	$SU(M+4)$	$SU(F)$	$U(1)_B$	$U(1)_X$	$U(1)_Y$	$U(1)_R$
A_1	$\bar{\square}$	\square	$\mathbf{1}$	$\mathbf{1}$	$-\frac{1}{M+F}$	1	$-\frac{M+4}{2(M+F)}$	$1 - \frac{2}{M+F}$
A_2	$\bar{\square}$	$\bar{\square}$	$\mathbf{1}$	$\mathbf{1}$	$-\frac{1}{M+F}$	-1	$-\frac{M+4}{2(M+F)}$	$1 - \frac{2}{M+F}$
X	$\mathbf{1}$	$\bar{\square}$	\square	$\mathbf{1}$	0	-1	1	1
Y	\square	$\mathbf{1}$	$\bar{\square}$	$\mathbf{1}$	$\frac{1}{M+F}$	0	$-1 + \frac{M+4}{2(M+F)}$	$\frac{2}{M+F}$
Z	\square	$\mathbf{1}$	$\mathbf{1}$	$\mathbf{1}$	$\frac{2}{M+F}$	0	$\frac{M+4}{M+F}$	$\frac{4}{M+F}$
P	$\mathbf{1}$	$\mathbf{1}$	\square	$\bar{\square}$	$\frac{1}{F}$	0	$1 - \frac{M+4}{2F}$	2
Q	$\bar{\square}$	$\mathbf{1}$	$\mathbf{1}$	\square	$-\frac{1}{M+F} - \frac{1}{F}$	0	$\frac{M+4}{2F} - \frac{M+4}{2(M+F)}$	$-\frac{2}{M+F}$
T	$\mathbf{1}$	$\mathbf{1}$	$\mathbf{1}$	$\bar{\square}$	$\frac{2}{F}$	0	$-\frac{M+4}{F}$	2

Table 5: A deconfined description of the quad CFT associated to phase III

non-trivial mapping of the operator spectrum to itself), whereas for odd M the two choices of flavor parity are dual to each other.

As in phase II, the manifest non-R symmetries are $SU(M+4) \times SU(M) \times U(1)^3$. However, contrary to our expectations from §3.3, there is no accidental non-abelian enhancement visible in the gauge theory. Naively, we expect an enhancement $SU(M+4) \times U(1) \rightarrow SO(2(M+4))$ for some $U(1) \subset U(1)^3$, but the gauge theory has no such symmetry.

The resolution is that the enhanced symmetry emerges accidentally in the infrared. In fact, the deconfinement duality discussed above already provides some hint of this. The even- M self-duality maps $SU(M+4) \times U(1)_Y$ to its charge conjugate, leaving the other global symmetries invariant, hence the infrared CFT can have only self-conjugate (real or pseudo-real) representations of $SU(M+4) \times U(1)_Y$. This is consistent with an accidental enhancement to $SO(2(M+4))$ because the latter has only self-conjugate representations for even M . Conversely, for odd M there is no self-duality, in agreement with the fact that $SO(2(M+4))$ has complex spinor representations for odd M .

We obtain further evidence for such an enhancement by examining the gauge-invariant operators parameterizing the moduli space. Similar to phase II, we find the following $SU(F)$ -invariant mesons and baryons:

$$\Phi_1 = X \quad , \quad \Phi_2 = A_2 Y \quad , \quad \mathcal{O}_k = A_1^k A_2^{M-k} Q^F \quad , \quad \tilde{\mathcal{O}}_k = Z^{\frac{F+k-4}{2}} Y^{M+4-k} . \quad (4.17)$$

Here Φ_1 and Φ_2 transform as \square_1 and $\bar{\square}_{-1}$ under $SU(M+4) \times U(1)_Y$, respectively, hence they fill out a vector of $SO(2(M+4))$. Likewise, \mathcal{O}_k is not charged under $SU(M+4) \times U(1)_Y$, hence it is an $SO(2(M+4))$ singlet. Finally, $\tilde{\mathcal{O}}_k$ transforms as

$$[k]_{k-\frac{M+4}{2}} \quad , \quad (-1)^k = (-1)^F \quad (4.18)$$

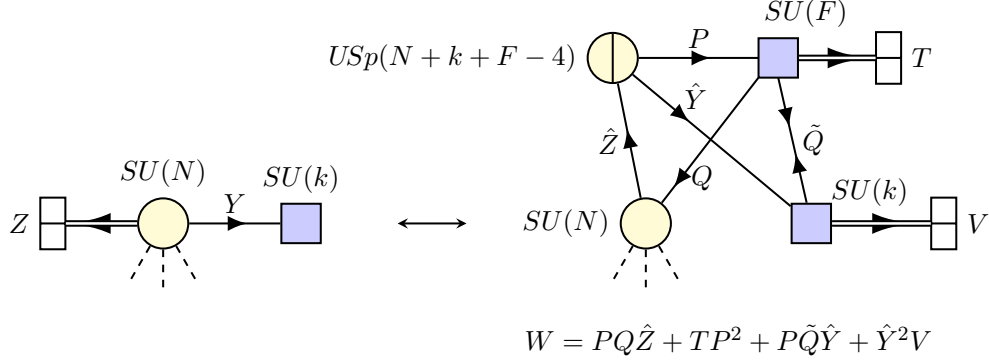


Figure 30: A variant of deconfinement where an antisymmetric tensor is deconfined together with k flavors. Figure 20 is the special case $k = 0$.

under $SU(M+4) \times U(1)_Y$, where $[k]$ denotes the k -index antisymmetric tensor representation. Collecting all permissible values of k , we recognize the spinor representation S (\bar{S}) of $SO(2(M+4))$ for even F (odd F). Thus, the family of operators $\tilde{\mathcal{O}}_k$ combine to form a single irrep of $SO(2(M+4))$, a spinor of dimension $2^{M+3}!$

Note that the spinor representations S and \bar{S} are related by the \mathbb{Z}_2 outer automorphism of $SO(2(M+4))$. This suggests that the two F -parities describe equivalent quad CFTs related by a non-trivial mapping on the operator spectrum (the \mathbb{Z}_2 outer automorphism). We have already seen that this is the case for odd M . To prove it for even M we employ the deconfinement variant shown in figure 30, where an antisymmetric tensor is deconfined at the same time as k flavors. We apply this variant to deconfine Z together with $M+4-k$ out of the $M+4$ Y 's, which explicitly breaks $SU(M+4) \rightarrow SU(M+4-k)_1 \times SU(k)_2 \times U(1)_A$, so that $SU(M+4)$ is an accidental non-abelian enhancement in the confined theory. It is convenient to take linear combinations $U(1)_{1,2}$ of $U(1)_Y$ and $U(1)_A$ such that Φ_1 decomposes as $(\square_1, \mathbf{1}_0) \oplus (\mathbf{1}_0, \square_1)$ under $U(M+4-k)_1 \times U(k)_2 \subset U(M+4)$ and likewise Φ_2 decomposes as $(\bar{\square}_{-1}, \mathbf{1}_0) \oplus (\mathbf{1}_0, \bar{\square}_{-1})$.

The gauge group of the deconfined theory is $SU(M+F) \times USp(2M+F+G-k)$, where G is the number of flavors introduced during deconfinement, constrained by $(-1)^G = (-1)^{F+k}$. The Seiberg-dual of the $SU(M+F)$ gauge group factor is $SU(M+G)$, where the $USp(2M+F+G-k)$ factor retains a confining spectrum in the dual. Reconfining, we obtain a description with G flavors and an accidental enhancement $U(M+4-k)_1 \times \overline{U(k)}_2 \rightarrow U(M+4)$. This dual theory is isomorphic to the original theory up to charge conjugation of the $U(k)$ factor. Choosing any odd value of k , we obtain a duality between even and odd flavor parities, hence the two are equivalent.

In fact, this variant of deconfinement duality (the usual case being $k = M+4$) is powerful enough to prove — under mild assumptions — that the infrared theory has the full $SO(2(M+4))$ symmetry, since the dual descriptions have different $U(M+4)$ subgroups as manifest

symmetries, and the smallest group which contains all of these subgroups is $SO(2(M+4))$.²⁸ Moreover, we can verify that the mapping induced by the deconfinement duality lies within $SO(2(M+4))$ for even k — when the flavor parity is unchanged — whereas it is a non-trivial $SO(2(M+4))$ outer automorphism for odd k — when the flavor parity flips. To show this, we consider the standard embedding of $U(n)$ inside $SO(2n)$ via the complexification

$$z_i = x_{2i-1} + ix_{2i}. \quad (4.19)$$

Charge conjugating k of the z_i coordinates corresponds to flipping the sign of k of the x_{2j} 's, hence for even k the transformation lies within $SO(2n)$, whereas for odd k it lies in the disconnected component of $O(2k)$, i.e. it is a parity flip which exchanges the two Weyl-spinor irreps of $SO(2n)$, S and \bar{S} .

It is interesting to compare the physics we have just described with the quad CFT for phase II, where we previously argued that the two choices of flavor parity give distinct CFTs. The difference arises because the quad CFT for phase II is not self-dual under deconfinement duality. Applying the above variant of the duality leads to a distinct dual description with no $U(M+4-k)_1 \times U(k)_2 \rightarrow U(M+4)$ enhancement of the manifest flavor symmetries, hence we cannot conclude that the two choices of flavor parity are equivalent. In fact, the two flavor parities give distinct spectra of the $\tilde{\mathcal{O}}_k$ baryons under the manifest global symmetries, whereas a further non-abelian enhancement is not consistent with the operator spectrum, therefore — in the absence of rank-enhancing accidental symmetries — we conclude that the two flavor parities of phase II give rise to inequivalent CFTs.

Finally, we note that deformations and gaugings of this CFT may break $SO(2(M+4))$, leading to distinct results for the different flavor parities. For instance, phase II can be reached by giving X a mass with an additional gauge singlet \bar{X} . Since this breaks $SO(2(M+4)) \rightarrow U(M+4)$, the result will depend on the parity of F . In particular, a deconfinement duality that flips the F -parity will also change the deformation to a different deformation in which parts of \bar{X} are coupled to components of the composite meson Φ_2 . Gauging the flavor faces in the brane tiling also breaks $SO(2(M+4))$, and will have a similar effect.

4.5 On symmetric tensor deconfinement

We note in passing that there is a symmetric tensor analog of deconfinement [60, 61], which is based on the observation that $SO(N+4)$ with N vectors \hat{Z} in the fundamental representation of $SU(N)$ confines with the composite $Z = \hat{Z}^2$ in the $\square\square$ representation of $SU(N)$. There are four branches of moduli space, two equivalent branches with a runaway superpotential and two equivalent branches with no superpotential [5, 62]. Thus, treating the $SO(N+4)$ theory with N vectors on one of the latter branches analogously to the s-confining $USp(N-4)$ theory

²⁸Since deconfinement and Seiberg duality are integral identities at the level of the superconformal index [59], this is sufficient to prove that the index respects the full $SO(2(M+4))$ symmetry, assuming that it can be reliably computed in the UV theory. We have computed low lying states in the index for small values of M , verifying that they fill out complete $SO(2(M+4))$ representations.

with N vectors, the procedure of §4.1 can be repeated to obtain a deconfined description of the symmetric tensor.

However, there are conceptual differences between the two cases. Since there is no dynamically generated superpotential, $F > 0$ is no longer strictly necessary. Instead, the case $F = 0$ is distinguished by reduced flavor symmetries in the UV theory, which only conserves $U(1)$ symmetries under which the symmetric tensor is uncharged, with the remainder emerging as accidental symmetries in the infrared. Moreover, since the vector representation is not a faithful representation of $SO(N)$, it cannot screen all Wilson loops, hence there are gauge-invariant order-parameters which distinguish between confining and Higgs phases and the moduli space (in particular the Kähler potential) will not smoothly interpolate between the two [63].

Nonetheless, the success of the approach in §4.2–4.4 in describing the quad CFTs suggests that a similar construction could be done using symmetric tensor deconfinement. In particular, none of the details of §4.2 depended strongly on the distinction between symmetric and antisymmetric tensors, and one can check that theories with the correct flavor symmetries and moduli space can be built along the lines of §4.3–4.4.

The primary issue with these theories is their lack of an apparent analog of flavor parity, since an $SU(N)$ symmetric tensor can be deconfined with any number of flavors of either parity. As noted above, flavor parity will play an important role in determining the RR torsion when the quadruple crossing is incorporated into the brane tiling. Consistency demands that there is an analogous quantity in the symmetric tensor deconfined description.

A natural resolution to this puzzle is that — like the deconfined description of a single symmetric tensor — the theory has two supersymmetric branches of moduli space, which are no longer equivalent, but are distinguished by different spectra of light operators. For instance, consider the symmetric tensor description of phase III, whose quiver is similar to figure 25(c) with symmetric tensors replacing the antisymmetric tensors and slightly different ranks for the nodes. The $SO(2(M+4))$ flavor symmetry is now manifest but the baryons do not form a spinor of $SO(2(M+4))$. Instead, they occupy the $(M+4)$ -index antisymmetric tensor representation, which splits into self-dual (imaginary self-dual) and anti-self-dual (imaginary anti-self-dual) irreps for even M (odd M).

One can show that — just as $\tilde{\mathcal{O}}_k$ in (4.17) fills out a spinor of $SO(2(M+4))$ — products $\tilde{\mathcal{O}}_{k_1}\tilde{\mathcal{O}}_{k_2}$ fill out an $(M+4)$ -index antisymmetric tensor, which is either (imaginary) self-dual or (imaginary) anti-self-dual, depending on the flavor parity. Thus, the symmetric-tensor deconfined theory exhibits aspects of both flavor parities in its spectrum, consistent with our hypothesis that the flavor parities correspond to distinct branches of the quantum moduli space. While it would be interesting to probe this idea further, antisymmetric tensor deconfinement presents a clearer picture which is sufficient for our purposes. We leave further development of the symmetric tensor deconfinement viewpoint on quad CFTs as an interesting open problem.

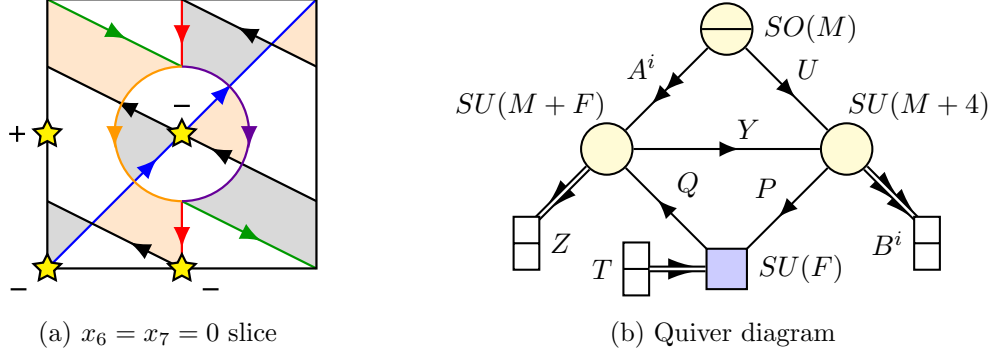


Figure 31: Deconfinement of the configuration in figure 15(b) for phase II. (a) The deconfined brane tiling, where we hide the flavor branes for simplicity. (b) The corresponding quiver gauge theory.

5 S-duality for all phases of dP_1

With a description of the quad CFTs in hand, it is now straightforward to construct the missing phases of the dP_1 orientifold by embedding these CFTs into the brane tiling for phases II and III, figure 15(b).

Notionally, this will take the form of a deformation / gauging of the quad CFT. In general, we might want to distinguish between deforming the deconfined gauge theory in the UV versus deforming the quad CFT itself. In the present discussion, however, we will not distinguish between these two viewpoints, leaving a more careful treatment to future work. Our main result is an index, which is insensitive to such distinctions.

Embedding the deconfined description of the phase II quad-CFT into the brane tiling leads to the deconfined tiling shown in figure 31(a), corresponding to the quiver gauge theory in figure 31(b) with the superpotential

$$W = \frac{1}{2} \varepsilon_{ij} A^i A^j Z + Y P Q + T Q^2 Z + \varepsilon_{ij} A^i Y B^j U. \quad (5.1)$$

The corresponding charge table is shown in table 6, where we have chosen yet another basis for the $U(1)$ symmetries for future convenience. Here the gauging has broken $USp(2M) \rightarrow SO(M) \times SU(2)$. For even M , there is an additional \mathbb{Z}_2 discrete symmetry of the form $\mathcal{P}(-1)^{B_1+B_2}$, where \mathcal{P} denotes the \mathbb{Z}_2 outer automorphism of $SO(M)$, under which $SO(M)$ baryons are charged, and $B_{1,2}$ denote the baryon numbers associated to $SU(M+F)$ and $SU(M+4)$, respectively.

These theories fall into four classes according to $(-1)^F$ and $(-1)^M$, where the latter “color parity” is preserved along the mesonic moduli space due to the necessity of removing D3 branes in orientifold-image pairs in the dual Calabi-Yau geometry. We use the shorthand Π_f^m with $f = (-1)^F$ and $m = (-1)^M$ to distinguish the four classes.

To relate these theories to the brane tilings discussed in §3, we use partial resolution to read off the discrete torsion, as in §3.1. First, we need to identify the relevant baryons.

	$SU(M+F)$	$SO(M)$	$SU(M+4)$	$SU(F)$	$SU(2)$	$U(1)_B$	$U(1)_Y$	$U(1)_R$
A^i	$\bar{\square}$	\square	$\mathbf{1}$	$\mathbf{1}$	\square	$-\frac{1}{2(M+F)}$	$\frac{M+3}{2(M+F)}$	$1 - \frac{M-1}{2(M+F)}$
B^i	$\mathbf{1}$	$\mathbf{1}$	\square	$\mathbf{1}$	\square	$-\frac{2}{M+4}$	$1 - \frac{2}{M+4}$	$-\frac{2}{M+4}$
U	$\mathbf{1}$	\square	$\bar{\square}$	$\mathbf{1}$	$\mathbf{1}$	$\frac{1}{M+4}$	$-1 + \frac{1}{M+4}$	$1 + \frac{1}{M+4}$
Y	\square	$\mathbf{1}$	$\bar{\square}$	$\mathbf{1}$	$\mathbf{1}$	$\frac{1}{2(M+F)} + \frac{1}{M+4}$	$-\frac{M+3}{2(M+F)} + \frac{1}{M+4}$	$\frac{M-1}{2(M+F)} + \frac{1}{M+4}$
Z	\square	$\mathbf{1}$	$\mathbf{1}$	$\mathbf{1}$	$\mathbf{1}$	$\frac{1}{M+F}$	$-\frac{M+3}{M+F}$	$\frac{M-1}{M+F}$
P	$\mathbf{1}$	$\mathbf{1}$	\square	$\bar{\square}$	$\mathbf{1}$	$-\frac{1}{M+4} + \frac{3}{2F}$	$-\frac{1}{M+4} - \frac{M+1}{2F}$	$2 - \frac{1}{M+4} + \frac{M-3}{2F}$
Q	$\bar{\square}$	$\mathbf{1}$	$\mathbf{1}$	\square	$\mathbf{1}$	$-\frac{1}{2(M+F)} - \frac{3}{2F}$	$\frac{M+3}{2(M+F)} + \frac{M+1}{2F}$	$-\frac{M-1}{2(M+F)} - \frac{M-3}{2F}$
T	$\mathbf{1}$	$\mathbf{1}$	$\mathbf{1}$	$\bar{\square}$	$\mathbf{1}$	$\frac{3}{F}$	$-\frac{M+1}{F}$	$2 + \frac{M-3}{F}$

Table 6: A deconfined description of phase II

Fortunately, we can rely on the similar calculation shown in figure 28 to find the correct baryon in the quad CFT, dressing it with baryons from the remainder of the brane tiling according to the standard procedure [44], as reviewed in §3.1. We find (c.f. (4.12))

$$\mathcal{O}_k = Y^{2(M+4-k)} Z^{F+k-4} U^{2k} \quad (5.2)$$

where k is constrained by $(-1)^k = (-1)^F$, and controls the distribution of D3 branes between the residual $\mathbb{C}^3/\mathbb{Z}_3$ orientifold singularity and the O3 plane.

Turning on a vev for this baryon will Higgs

$$SU(M+F) \times SO(M) \times SU(M+4) \longrightarrow USp(F+k-4) \times SO(M-k) \times SU(M+4-k) \times SO(k). \quad (5.3)$$

Just as in figure 28, the $USp(F+k-4)$ is confining, and we obtain the $SO(M-k) \times SU(M+4-k)$ $\mathbb{C}^3/\mathbb{Z}_3$ orientifold theory together with the $SO(k)$ $\mathcal{N}=4$ theory.

Recall that for these orbifold components, the $SO(p) \times (\dots)$ gauge groups have torsion $[F] = (-)^p$ and $[H] = +$ and the $USp(2p) \times (\dots)$ gauge groups have torsion $[F] = \pm$ and $[H] = -$, where in the latter case $[F]$ combines with C_0 to determine the theta angle. Thus, II_+^\pm has $[F]$ torsion $(\pm, +)$ whereas II_-^\pm has $[F]$ torsion $(\mp, -)$, and all four cases have trivial $[H]$ torsion. We can also read off the D3 charge by combining the charge of the components. We obtain

$$Q_{\text{II}} = (M+4-k-3/2) + (k-1/2) = M+2. \quad (5.4)$$

We now turn to phase III. Embedding the deconfined description of the quad CFT from §4.4 into the brane tiling shown in figure 15(b) leads to the deconfined brane tiling shown in figure 32(a). The corresponding quiver diagram, figure 32(b), has the tree-level superpotential

$$W = ZA_1A_2 + A_1YX + YPQ + TQ^2Z + B_1XU + B_2A_2YU, \quad (5.5)$$

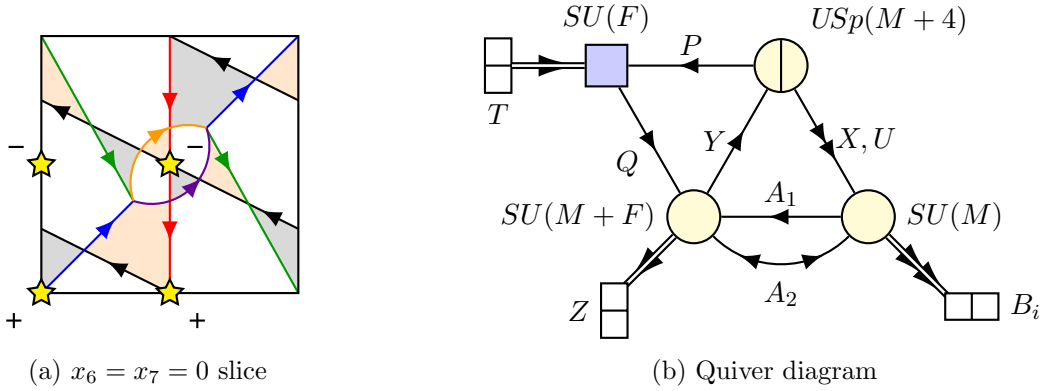


Figure 32: Deconfined phase III. (a) The deconfined brane tiling, where the flavor branes are hidden as before. (b) The associated quiver gauge theory.

	$SU(M+F)$	$SU(M)$	$USp(M+4)$	$SU(F)$	$U(1)_B$	$U(1)_X$	$U(1)_Y$	$U(1)_R$
A_1	$\bar{\square}$	\square	$\mathbf{1}$	$\mathbf{1}$	$\frac{1}{M+F} - \frac{1}{M}$	$-\frac{M+4}{2(M+F)}$	$\frac{1}{M} - \frac{M+2}{2(M+F)}$	$\frac{M+1}{M} + \frac{1}{M+F}$
A_2	$\bar{\square}$	$\bar{\square}$	$\mathbf{1}$	$\mathbf{1}$	$\frac{1}{M} + \frac{1}{M+F}$	$-\frac{M+4}{2(M+F)}$	$-\frac{1}{M} - \frac{M+2}{2(M+F)}$	$\frac{M-1}{M} + \frac{1}{M+F}$
B_1	$\mathbf{1}$	$\square\square$	$\mathbf{1}$	$\mathbf{1}$	$-\frac{2}{M}$	-1	$1 + \frac{2}{M}$	$\frac{2}{M}$
B_2	$\mathbf{1}$	$\square\square$	$\mathbf{1}$	$\mathbf{1}$	$-\frac{2}{M}$	1	$1 + \frac{2}{M}$	$\frac{2}{M}$
U	$\mathbf{1}$	$\bar{\square}$	\square	$\mathbf{1}$	$\frac{1}{M}$	0	$-1 - \frac{1}{M}$	$\frac{M-1}{M}$
X	$\mathbf{1}$	$\bar{\square}$	\square	$\mathbf{1}$	$\frac{1}{M}$	1	$-\frac{1}{M}$	$\frac{M-1}{M}$
Y	\square	$\mathbf{1}$	\square	$\mathbf{1}$	$-\frac{1}{M+F}$	$-1 + \frac{M+4}{2(M+F)}$	$\frac{M+2}{2(M+F)}$	$-\frac{1}{M+F}$
Z	$\square\square$	$\mathbf{1}$	$\mathbf{1}$	$\mathbf{1}$	$-\frac{2}{M+F}$	$\frac{M+4}{M+F}$	$\frac{M+2}{M+F}$	$-\frac{2}{M+F}$
P	$\mathbf{1}$	$\mathbf{1}$	\square	$\bar{\square}$	$-\frac{1}{F}$	$1 - \frac{M+4}{2F}$	$\frac{M+2}{2F}$	$2 - \frac{3}{F}$
Q	$\bar{\square}$	$\mathbf{1}$	$\mathbf{1}$	\square	$\frac{1}{F} + \frac{1}{M+F}$	$\frac{M+4}{2F} - \frac{M+4}{2(M+F)}$	$-\frac{M+2}{2F} - \frac{M+2}{2(M+F)}$	$\frac{3}{F} + \frac{1}{M+F}$
T	$\mathbf{1}$	$\mathbf{1}$	$\mathbf{1}$	$\bar{\square}$	$-\frac{2}{F}$	$-\frac{M+4}{F}$	$\frac{M+2}{F}$	$2 - \frac{6}{F}$

Table 7: A deconfined description of phase III

and the charge table shown in table 7.

For even F , there is an additional \mathbb{Z}_2 discrete symmetry of the form $(-1)^{B_1+B_3}$, where $B_{1,3}$ denotes the baryon number associated to $SU(M+F)$ and $SU(F)$, respectively.²⁹

Here the gauging has broken $SO(2(M+4)) \rightarrow USp(M+4) \times SU(2)$, but the $SU(2)$ is not manifest because the original deconfined description only conserved $U(M+4) \subset SO(2(M+4))$. Instead, only $U(1)_X \in SU(2)$ is visible. Deconfinement duality corresponds to charge conjugation on $U(1)_X$, which is half-integrally quantized for gauge invariant operators, hence

²⁹Since $SU(F)$ is trivial, we only consider $SU(F)$ invariants, for which B_3 is integrally quantized.

only (pseudo) real representations of $U(1)_X$ with integer or half-integer charges can appear in the operator spectrum, consistent with an $SU(2)$ enhancement.³⁰

Since $USp(M+4)$ is only defined for even M , these theories fall into two classes, which we denote III_f with $f = (-1)^F$. A similar procedure can be used to identify the baryons corresponding to the partial resolution to $\mathbb{C}^3/\mathbb{Z}_3$. We find (c.f. 4.17):

$$\mathcal{O}_k = A_1^k A_2^{M-k} Q^F U^{2k}, \quad (5.6)$$

where k is even. Turning on a vev for this baryon will Higgs

$$SU(M+F) \times SU(M) \times USp(M+4) \longrightarrow [USp(M+4-k) \times SU(M-k)] \times USp(k) \quad (5.7)$$

where all $SU(F)$ -charged matter becomes massive, and the remaining light fields are those of the $USp(M+4-k) \times SU(M-k)$ $\mathbb{C}^3/\mathbb{Z}_3$ orientifold theory together with the $USp(k)$ $\mathcal{N}=4$ theory. Thus, the phase III theories have $[H]$ torsion $(-, -)$. We can read off the D3 charge by adding up the charge of the components, giving

$$Q_{\text{III}} = (M - k + 3/2) + (k + 1/2) = M + 2, \quad (5.8)$$

as in phase II.

To determine the $[F]$ torsion from the above computation, we would need to compare theta angle of the $\mathcal{N}=4$ theory with the phase of the exactly marginal coupling in the $\mathbb{C}^3/\mathbb{Z}_3$ theory, determined in [7]. Such a calculation is beyond the scope of this work. Instead, we note that there are two inequivalent choices, (\pm, \pm) and (\pm, \mp) , where in either case the two sign choices combine with C_0 to determine the phase of an exactly marginal coupling in the gauge theory. The S-dual of the theory with trivial $[F]$ torsion is II_-^+ , which has a \mathbb{Z}_2 discrete symmetry, therefore III_+ must correspond to $[F]$ torsion (\pm, \pm) and III_- to $[F]$ torsion (\pm, \mp) . This is a natural guess, since then even F and M corresponds to trivial $[F]$ torsion, as in phase II.

Thus, as illustrated in figure 33, the phase II and phase III theories obtained via deconfinement neatly fill in the gaps in figure 12(b). Besides the $\text{I}_A^- \longleftrightarrow \text{I}_B^-$ duality already discovered in [7], this figure predicts several new S-dualities:

$$\text{I}_A^+ \longleftrightarrow \text{II}_-^- \quad , \quad \text{I}_B^+ \longleftrightarrow \text{II}_+^- \quad , \quad \text{II}_-^+ \longleftrightarrow \text{III}_+ \quad , \quad \text{I}_A^- \longleftrightarrow \text{I}_B^- \longleftrightarrow \text{III}_- \quad , \quad (5.9)$$

where the previously known duality is now a triality and II_+^+ is expected to be self-dual. In particular, both I_A^+ and I_B^+ have distinct S-duals, answering a puzzle from [7]. The relative ranks of the duals are predicted by matching the D3 charges,

$$Q_{\text{D3}} = N - 1 = \tilde{N} + 1 = M + 2. \quad (5.10)$$

The same result is obtained by anomaly matching, where the $U(1)$ bases in tables 6, 7 were chosen to match those in tables 2, 3.

³⁰In particular, this ensures that the superconformal index fills out complete $SU(2)$ multiplets.

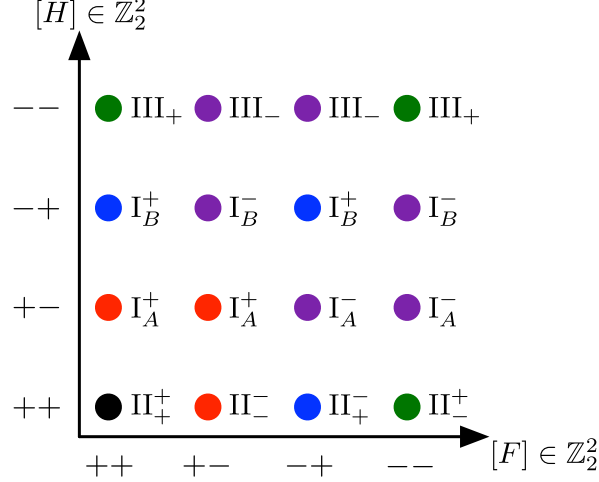


Figure 33: Discrete torsion for all phases of the dP_1 orientifold. Except for the relative position of III_+ and III_- , all torsions are fixed by the partial resolution to the $\mathbb{C}^3/\mathbb{Z}_3$ orientifold singularity plus an O3 plane. The $[F]$ torsion assignment for phase III is obtained by matching discrete symmetries between prospective S-duals.

5.1 Matching the superconformal index

With an extensive set of predicted S-dualities in hand, we need a way to test these dualities. Anomaly matching is not sensitive enough, because all the theories with the same D3 charge (5.10) have matching anomalies regardless of $[F]$ and $[H]$ torsion, apart from the mismatch of the $SU(2)^3$ Witten anomalies between I_A^+ and I_B^+ noted in [7], which persists in their duals.³¹ Based on the \mathbb{Z}_2 discrete symmetry discussed above and on the quantization condition for $U(1)_B$ (which is integral for $\text{I}_{A/B}^-$, III_\pm , and II_+^+ , and otherwise half-integral), we can rule out any further dualities between the dP_1 theories besides those in (5.9).

To do better, we could match the operator spectra of the dual theories. This can be subtle due to the large number of gauge invariant operators in a quiver gauge theory, quantum constraints on the moduli space, etc., and we leave a more extensive treatment to future work. Instead, we rely on a conceptually simple but very sensitive test: we match the superconformal indices between the dual theories.

The superconformal index [64, 65] counts shortened superconformal multiplets of the theory quantized on $S^3 \times \mathbb{R}$ up to recombination:

$$\mathcal{I} = \text{Tr}_{\mathcal{H}=0} \left[(-1)^F t^{R+2J_L} x^{2J_R} f \right], \quad (5.11)$$

where $J_{L,R}$ generate the Cartan of $SU(2)_{L,R}$, R denotes the R-charge, and f is an arbitrary fugacity of the flavor symmetry group. The trace is taken over states annihilated by

$$\mathcal{H} \equiv H - 2J_L - \frac{3}{2}R, \quad (5.12)$$

³¹We have not computed the Witten anomaly or the $SU(2)^2\mathbb{Z}_2$ anomaly in phase III, where only $U(1)_X \subset SU(2)$ is manifest.

with H the Hamiltonian, which is the anticommutator of a supercharge Q in the superconformal algebra with its conjugate (hence the index counts Q cohomology classes.)

The superconformal index can be shown to agree between Seiberg dual theories [66], where it reduces to an integral identity for elliptic hypergeometric functions [59]. In the case of other dualities, such as S-dualities, the index should likewise agree, but the appropriate integral identities are not always known, see e.g. [67, 68].

The index is invariant under continuous deformations [66], so in particular when a weakly-coupled UV description is available — and in the absence of rank-enhancing accidental symmetries along the flow — the index can be computed in the UV. We have

$$\mathcal{I} = \int dg \, PE \left[\sum_a i_a(t, x, g, f) \right], \quad (5.13)$$

where $PE[f(x)] \equiv \exp \left(\sum_{k=1}^{\infty} \frac{1}{k} f(x^k) \right)$ is the plethystic exponential, the integral is taken over the gauge group with the Haar measure, and i_a is the “letter” for the a th field, of the form

$$i_V = \frac{2t^2 - t(x + x^{-1})}{(1 - tx)(1 - tx^{-1})} \chi_V, \quad i_{\Phi} = \frac{t^R \chi_{\Phi} - t^{2-R} \chi_{\Phi^\dagger}}{(1 - tx)(1 - tx^{-1})}, \quad (5.14)$$

for vector and chiral superfields, respectively. Here R is the a -maximized R-charge of the chiral field and χ_V and χ_{Φ} denote the group characters of the representation under the gauge and global symmetries. In effect, (5.13) counts gauge-invariants in the symmetric product of the states in the letter, where negative contributions to the letter anticommute.

In general, the integral over the gauge group is very difficult to perform, except at large N , where it simplifies [65]. Instead, we perform a series expansion in t to count low-lying states in the index. Using

$$\int dg \, \chi_r(g) = \delta_{r,1}, \quad \chi_r(g) \chi_{r'}(g) = \chi_{r \times r'}(g), \quad (5.15)$$

for representations r, r' , where $\delta_{r,1}$ denotes the number of singlet irreps in r , it becomes straightforward in principle to compute the index to any fixed order in t , provided that all the chiral fields satisfy $0 < R < 2$.

Unfortunately, the a -maximized R-charges of the fundamental fields in the UV theory need not satisfy this inequality, even in the absence of accidental symmetries which mix with the R-symmetry in the infrared. For instance, the deconfined description of an $SU(N)$ antisymmetric tensor, figure 20, has the a -maximized R-charges:

$$R(\hat{Z}) = \frac{1}{3}, \quad R(P) = -\frac{N-6}{3F}, \quad R(Q) = \frac{5}{3} + \frac{N-6}{3F}, \quad R(T) = 2 + 2\frac{N-6}{3F}, \quad (5.16)$$

where F is the number of flavors in the deconfined description, with $(-1)^F = (-1)^N$. These charges satisfy the bound $0 < R < 2$ for $N < 6$ and violate it otherwise, whereas in either case the infrared fixed point consists of free chiral multiplets with R-charge $2/3$, by construction.

The resolution is that the states with negative powers of t completely cancel out of the index. To see how this work, consider the marginal case $N = 6$ in the above deconfined theory, so that $R(P) = R(\bar{T}) = 0$, where \bar{T} denotes the negative contribution to the letter for T . Naively, there are an infinite number of contributions to the index at $\mathcal{O}(t^0)$. However, it is straightforward to check that integrating over the symplectic group gives:

$$\int dg PE[y\chi_{\square}(g)\chi_{\square}(f)] = PE\left[y^2\chi_{\square}(f)\right], \quad (5.17)$$

i.e. the gauge invariant operator P^{2k} transforms in k th symmetric power of the conjugate antisymmetric representation of $SU(F)$, so that the contributions of P^{2k} and \bar{T}^k to the $\mathcal{O}(t^0)$ term in the index cancel.

In fact, this cancellation is guaranteed by the integral identities of [59], since the re-confinement of the deconfined description is a special case of Seiberg duality for symplectic groups, but it serves to illustrate the difficulties which arise in computing the index in more general theories whose fundamental fields do not satisfy $0 < R < 2$.

The a -maximized R-charge for tables 2, 3, 6, 7 is

$$U(1)_R^{(\text{sc})} = U(1)_R + (4 - \beta) U(1)_Y + Q_{D3} \left(\frac{3}{\beta} - \frac{\beta}{4} \right) U(1)_B \quad (5.18)$$

where Q_{D3} is given by (5.10), and β is the unique root of the quartic equation

$$(\beta - 2)(\beta - 6)(3\beta^2 - 8\beta - 12)Q_{D3}^2 + 16\beta^2(9 - 2\beta) = 0 \quad (5.19)$$

satisfying $\frac{2}{3}(2 + \sqrt{13}) < \beta \leq 4$ for $Q_{D3} \geq 4$, with $\frac{2}{3}(2 + \sqrt{13}) \approx 3.737$. From this, one can check that the a -maximized R-charges in tables 2, 3 satisfy $0 < R < 2$ for $Q_{D3} > 4$,³² whereas those in table 6 satisfy the constraint for $4 < Q_{D3} \leq 13$ with $F = 1$ and for $4 < Q_{D3} \leq 12$ with $F = 2$, and those in table 7 satisfy it for $4 < Q_{D3} \leq 10$ with $F = 1, 2$.

For the present paper, we confine our attention to $4 < Q_{D3} \leq 10$, for which the index can be computed as an expansion in t in all the phases of dP_1 .³³ This already allows for very non-trivial tests of the duality.

Consider for example $Q_{D3} = 9$. The superconformal index in phase I_A^+ is:

$$1 + b^{\frac{1}{2}}y^{-5}t_{(1.294)}^{-17+\frac{27}{2\beta}+\frac{31\beta}{8}} + b^{\frac{1}{2}}y^{-4}X_1t_{(1.488)}^{-13+\frac{27}{2\beta}+\frac{23\beta}{8}} + b^{\frac{1}{2}}y^{-3}X_2t_{(1.683)}^{-9+\frac{27}{2\beta}+\frac{15\beta}{8}} + b^{\frac{1}{2}}y^{-2}X_3t_{(1.877)}^{-5+\frac{27}{2\beta}+\frac{7\beta}{8}} \\ - (1 + X_2)t^2 + \dots + [J_1(3 + 7X_2 + 4X_4) - 2J_3(1 + X_2)]t^5 + \dots \quad (5.20)$$

up to order t^5 , where y and b are the flavor fugacities for $U(1)_Y$ and $U(1)_B$, respectively, and X_i and J_i denote the characters for the spin $i/2$ representation of the $SU(2)$ flavor symmetry

³² $Q_{D3} = 4$ is a special case where there is confinement with chiral symmetry breaking in the infrared [7].

³³Besides finding a systematic way to deal with the large degree of cancellation in the index, another way to proceed for $Q_{D3} > 10$ would be to expand in a different fugacity. One can show that there is always a *conserved* R-symmetry (not necessarily the a -maximized one) satisfying $0 < R < 2$ for any $Q_{D3} > 4$ and $F > 0$, hence there is a corresponding fugacity with only positive powers in the letter, allowing a systematic expansion which avoids the above issues.

and of $SU(2)_R$, respectively. In cases where t is raised to an irrational exponent, we indicate a decimal approximant in the subscript. Note that we have shown only the first and last few terms in the expansion (5.20). The full expression, shown in §C.3, has 180 terms, of which only 12 have been given above!

The index for I_B^+ and $Q_{D3} = 9$ is

$$1 + b^{\frac{3}{2}} y^{-4} t_{(1.021)}^{-12 + \frac{81}{2\beta} + \frac{5\beta}{8}} - (1 + X_2) t^2 + b^{\frac{3}{2}} y^{-4} J_1 t_{(2.021)}^{-11 + \frac{81}{2\beta} + \frac{5\beta}{8}} + b^3 y^{-8} t_{(2.041)}^{-24 + \frac{81}{\beta} + \frac{5\beta}{4}} - y X_1 t_{(2.194)}^{6-\beta} \\ + b^{-\frac{1}{2}} X_4 t_{(2.734)}^{2 - \frac{27}{2\beta} + \frac{9\beta}{8}} + \dots + [J_1 (3 + 7X_2 + 4X_4) - 2J_3 (1 + X_2)] t^5 + \dots \quad (5.21)$$

up to order t^5 , where the full expression, shown in §C.4, has 154 terms. We see immediately that (5.20) and (5.21) do not match, hence I_A^+ and I_B^+ are not dual, as anticipated in [7] and borne out by figure 33. By contrast, computing the index for II_- to the same order gives back all 180 terms of (5.20), and computing the index for II_+ gives back all 154 terms of (5.21)! This is highly non-trivial evidence in favor of the dualities $I_A^+ \longleftrightarrow II_-$ and $I_B^+ \longleftrightarrow II_+$.

Likewise, the index for I_A^- and $Q_{D3} = 8$ is

$$1 - (1 + X_2) t^2 - y X_1 t_{(2.178)}^{6-\beta} + b y^{-7} t_{(2.39)}^{-23 + \frac{24}{\beta} + 5\beta} + b y^{-6} X_1 t_{(2.568)}^{-19 + \frac{24}{\beta} + 4\beta} + 2b y^{-5} X_2 t_{(2.746)}^{-15 + \frac{24}{\beta} + 3\beta} \\ + \dots + [9 + 10X_2 + 3X_4 - 2X_6 + 2J_2 (3 + 8X_2 + 3X_4) - 2J_4 (1 + X_2)] t^6 + \dots \quad (5.22)$$

up to order t^6 . The full result in §C.2 has 215 terms, all of which are reproduced in both I_B^- and III_- ! This is highly non-trivial evidence for the duality $I_A^- \longleftrightarrow I_B^-$ proposed in [7], now expanded into a triality $I_A^- \longleftrightarrow I_B^- \longleftrightarrow III_-$.

Finally, the index for II_-^+ and $Q_{D3} = 8$ is³⁴

$$1 + b^{-1} y^4 X_5 t_{(1.077)}^{15 - \frac{24}{\beta} - 2\beta} - (1 + X_2) t^2 + b^{-1} y^4 J_1 X_5 t_{(2.077)}^{16 - \frac{24}{\beta} - 2\beta} + b^{-2} y^8 (X_2 + X_6 + X_{10}) t_{(2.153)}^{30 - \frac{48}{\beta} - 4\beta} \\ - y t_{(2.178)}^{6-\beta} X_1 + \dots + [J_1 (5 + 14X_2 + 12X_4 + 7X_6 + 4X_8) - 2J_3 (1 + X_2)] t^5 + \dots \quad (5.23)$$

up to order t^5 , where the full result in §C.1 has 216 terms, all of which are reproduced in III_+ ! This confirms the last remaining duality $II_-^+ \longleftrightarrow III_+$ from figure 33.

For completeness, we also give the first few terms of the index for II_+^+ and $Q_{D3} = 8$:

$$1 + \frac{b^{3/2} t_{(0.830)}^{-\frac{21}{2} + \frac{36}{\beta} + \frac{\beta}{2}}}{y^{7/2}} + \frac{\sqrt{b} t_{(1.017)}^{-\frac{31}{2} + \frac{12}{\beta} + \frac{7\beta}{2}}}{y^{9/2}} + \frac{y^4 X_5 t_{(1.077)}^{15 - \frac{24}{\beta} - 2\beta}}{b} + \frac{\sqrt{b} X_1 t_{(1.195)}^{-\frac{23}{2} + \frac{12}{\beta} + \frac{5\beta}{2}}}{y^{7/2}} \\ + \frac{\sqrt{b} X_2 t_{(1.373)}^{-\frac{15}{2} + \frac{12}{\beta} + \frac{3\beta}{2}}}{y^{5/2}} + \frac{\sqrt{b} X_3 t_{(1.551)}^{-\frac{7}{2} + \frac{12}{\beta} + \frac{\beta}{2}}}{y^{3/2}} + \frac{b^3 t_{(1.660)}^{-21 + \frac{72}{\beta} + \beta}}{y^7} + \frac{\sqrt{b} X_4 t_{(1.729)}^{\frac{1}{2} + \frac{12}{\beta} - \frac{\beta}{2}}}{\sqrt{y}} + \dots \quad (5.24)$$

Notice that (5.24) does not match (5.22) or (5.23), just as (5.20) and (5.21) do not match, even for the first few terms. Thus, the superconformal index is a highly sensitive test of

³⁴We omit the fugacity for the \mathbb{Z}_2 discrete symmetry for simplicity.

Q_{D3}	$I_A^+ = II_-^-$		$I_B^+ = II_+^-$		Q_{D3}	$I_A^- = I_B^- = III_-$		$II_-^+ = III_+$	
	Terms	Order	Terms	Order		Terms	Order	Terms	Order
5	*275	$\mathcal{O}(t^2)$	*222	$\mathcal{O}(t^2)$	6	145	$\mathcal{O}(t^4)$	*135	$\mathcal{O}(t^3)$
7	221	$\mathcal{O}(t^4)$	*187	$\mathcal{O}(t^4)$	8	215	$\mathcal{O}(t^6)$	216	$\mathcal{O}(t^5)$
9	180	$\mathcal{O}(t^5)$	154	$\mathcal{O}(t^5)$	10	110	$\mathcal{O}(t^6)$	1	$\mathcal{O}(t^{5/4})$

Table 8: Summary of S-duality checks using the superconformal index. For III_+ and $Q_{D3} = 10$, we are unable to compute any non-vanishing terms in the index beyond the leading 1, but can show that several contributions cancel as required to match the S-dual theory. The starred theories have accidental symmetries, but the index still matches for the manifest flavor symmetries.

S-dualities. The S-dual theories in figure 33 have indices which match hundreds of terms (and conjecturally exactly), whereas the dP_1 theories which are not S-dual have indices which disagree even in the first few terms!³⁵

We have also matched the superconformal indices between the dual theories for other values of $Q_{D3} \leq 10$. Our results are summarized in table 8.

6 Conclusions

In this paper we have argued that in studying $\mathcal{N} = 1$ S-duality in Calabi-Yau orientifolds, as initiated in [7–9], one is forced to include strongly-coupled sectors. In toric examples, these sectors arise from more than two NS5 branes intersecting atop an O5 plane on a D5 brane stack, such as the quad CFTs described in §3.3 and constructed in §4.

In the cases we have studied, these sectors have simple yet non-trivial properties. They are characterized by a large flavor symmetry group and a moduli space with mesonic and baryonic directions, where the mesonic directions relate CFTs with different ranks, and the baryonic directions relate the CFT to weakly-coupled chiral superfields describing brane recombinations which avoid the higher-multiplicity intersection. A remarkable property of these CFTs is the appearance of spinor representations of the $SO(2(M+4))$ flavor symmetry in the baryonic spectrum for arbitrary M . This property is hidden in the deconfined gauge theory description, and indeed it is difficult to imagine how it could have been manifest, since the dimension of the spinor representation grows exponentially with M , in conflict with asymptotic freedom. This confirms the intrinsically strongly-coupled (non-Lagrangian) nature of the quad CFTs.

By coupling these quad CFTs to quiver gauge theories, as dictated by the brane tiling construction, we have obtained a complete picture of S-dualities in the dP_1 orientifold considered in this paper. Our description has been subjected to stringent consistency checks using

³⁵To be precise, the leading baryons generally disagree. For larger values of Q_{D3} , these baryons will appear with higher powers of t and the leading $\mathcal{O}(b^0)$ terms will match, even between non-S-dual theories, as the index approaches a large N limit.

one of the best instruments available in minimally supersymmetric theories, the superconformal index. We expect that similar ingredients can be used to understand S-duality in a broad class of toric orientifolds [45], if not beyond.

The quad CFTs — and similar strongly-coupled sectors arising from $2k$ NS5 branes intersecting atop an O5 plane with $k > 2$ — are interesting in their own right, and deserve further study. It would be instructive to determine the string-theory origin of the non-abelian enhancement to $USp(2M)$ or $SO(2(M+4))$, and in particular the appearance of spinor representations in the latter case. Other descriptions of these CFTs, such as by symmetric tensor deconfinement, could be developed further. The superconformal index of these CFTs may admit a description which is independent of the deconfinement procedure, making their properties and symmetries manifest. It would also be interesting to determine whether these same CFTs play a role in orientifolds of non-toric Calabi-Yau singularities.

Recently, there has been some progress in describing certain S-dualities of chiral $\mathcal{N} = 1$ theories in terms of a 6d $(1,0)$ theory compactified on a punctured Riemann surface [13–15]. It remains to be seen if our S-dualities fall into this class, in which case they might form part of a yet-unknown unified picture of $\mathcal{N} = 1$ dualities.

Finally, while our discussion has focused on the brane tiling in the $g_s \rightarrow \infty$ limit, it should be possible to describe the new phases in the $g_s \rightarrow 0$ limit as well as in the mirror description with intersecting D6 branes. At present, this is an open problem.

Acknowledgments

We thank A. Hanany for discussions, and T. Wrase for collaboration in related previous work [7, 9]. BH is supported by the Fundamental Laws Initiative of the Harvard Center for the Fundamental Laws of Nature. I. G.-E. thanks N. Hasegawa for kind encouragement and constant support.

A Del Pezzo orientifold singularities

In this appendix, we construct the ten del Pezzo singularities and their orientifolds with the del Pezzo as an isolated fixed plane.³⁶

The del Pezzo singularities for dP_k , $k \geq 5$, are complete intersection singularities. Let $P_r^{(a_1, \dots, a_p)}$ denote a generic quasi-homogeneous polynomial of weight r in p variables with weights (a_1, \dots, a_p) . The dP_6 , dP_7 , and dP_8 singularities are the hypersurfaces $P_3^{(1,1,1,1)} = 0$, $P_4^{(1,1,1,2)} = 0$ and $P_6^{(1,1,2,3)} = 0$ in \mathbb{C}^4 , respectively, whereas the dP_5 singularity is the complete intersection of two quadrics $P_2^{(1,1)} = R_2^{(1,1)} = 0$ in \mathbb{C}^5 . In each case, the involution σ reflects the odd-weight coordinates and leaves the even-weight coordinates invariant.

The del Pezzo surfaces dP_k for $k \leq 3$ and \mathbb{F}_0 are toric, as are the corresponding singularities. These singularities are most easily described as the classical moduli space of a gauged

³⁶Embeddings for the non-toric del Pezzo singularities are taken from [21] and references therein.

linear sigma model (GLSM) with vanishing Fayet-Iliopoulos (FI) parameters:

$$dP_0 : \frac{}{\mathbb{Z}_3} \left| \begin{array}{ccc} x & y & z \\ \omega_3 & \omega_3 & \omega_3 \end{array} \right., \quad dP_1 : \frac{}{U(1)} \left| \begin{array}{cccc} x & y & z & w \\ 2 & 2 & -1 & -3 \end{array} \right., \quad \mathbb{F}_0 : \frac{}{\mathbb{Z}_2} \left| \begin{array}{cccc} y & z & w & u \\ 1 & -1 & -1 & 1 \\ + & - & - & + \end{array} \right., \quad (\text{A.1})$$

$$dP_2 : \frac{}{U(1)_1} \left| \begin{array}{ccccc} x & y & z & w & u \\ 2 & 2 & -1 & -3 & 0 \\ 0 & 1 & -1 & -1 & 1 \end{array} \right|, \quad dP_3 : \frac{}{U(1)_2} \left| \begin{array}{ccccc} x & y & z & w & u & v \\ 2 & 2 & -1 & -3 & 0 & 0 \\ 0 & 1 & -1 & -1 & 1 & 0 \\ 1 & 0 & -1 & -1 & 0 & 1 \end{array} \right|, \quad (\text{A.2})$$

where σ reflects x, y, z for dP_k and takes $z \rightarrow iz$, $w \rightarrow iw$ for \mathbb{F}_0 . Note that the dP_0 and \mathbb{F}_0 singularities are orbifolds of \mathbb{C}^3 and the conifold, respectively.

By contrast, the dP_4 singularity is neither toric nor a complete intersection singularity. A hybrid approach is most convenient. Consider the affine variety defined by the GLSM

$$\frac{}{U(1)} \left| \begin{array}{ccccc} z_1 & z_2 & z_3 & u_1 & u_2 \\ 1 & 1 & 1 & -1 & -1 \end{array} \right|, \quad (\text{A.3})$$

with vanishing FI parameter. The dP_4 singularity is the hypersurface $P_2(z)u_1 + R_2(z)u_2 = 0$ in this variety for generic quadrics P_2 and R_2 . The involution σ takes $z_i \rightarrow -z_i$.

B Exceptional collections and brane charges

In this appendix we study the dynamics of D3 branes probing the dP_1 singularity from the point of view of exceptional collections. This allows us to prove, without needing to resolve the singularity, that the rank relations necessary for the duality to work are equivalent to D3 charge conservation. In [9] it was proposed that the microscopic process behind the duality is a somewhat mysterious orientifold transition for (collapsed) O7 planes, and this was verified for the dP_0 singularity. The exceptional collection language will allow us to see that the same process is compatible with the duality $\Gamma_A^- \longleftrightarrow \Gamma_B^-$ proposed in [7]. Somewhat unsatisfactorily, the discussion below is limited to the “classical” phases of dP_1 , since we lack a description in terms of exceptional collections of the strongly-coupled phases which are the main focus of our paper. It would be very interesting to understand if a generalization of the orientifold transition could generate the strongly coupled phases as well.

A standard basis for projective objects on dP_1 is given by:

$$\mathcal{P} = \{\mathcal{O}, \mathcal{O}(e), \mathcal{O}(\ell), \mathcal{O}(2\ell)\}, \quad (\text{B.1})$$

where ℓ is the hyperplane class of dP_1 , and e the class of the exceptional \mathbb{P}^1 . The basis of fractional branes obtained by mutation of (B.1) has the following Chern characters:

$$\text{ch}(\mathcal{E}_1) = 1, \quad \text{ch}(\mathcal{E}_2) = e - \frac{1}{2}\ell^2, \quad \text{ch}(\mathcal{E}_3) = -2 - 2e + \ell + \frac{3}{2}\ell^2, \quad \text{ch}(\mathcal{E}_4) = 1 + e - \ell, \quad (\text{B.2})$$

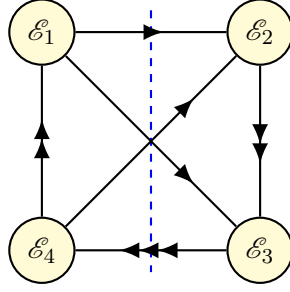


Figure 34: The map between sheaves and nodes in the quiver for the dP_1 singularity. The dashed line indicates the orientifold involution studied in the text.

and the resulting quiver is shown in figure 34, which reproduces the dP_1 quiver studied in the text.

Now consider an O7 plane on the contracting dP_1 . Clearly the basis (B.2) cannot be invariant under the large volume orientifold action [9]

$$i_*\mathcal{E}[k] \longrightarrow i_*(\mathcal{E}^\vee \otimes K_{\mathcal{S}} \otimes \mathcal{L}_{2B_2})[2-k]. \quad (\text{B.3})$$

For instance, \mathcal{E}_2 is the only sheaf with rank 0, and (B.3) preserves rank. Instead, we will find that the orientifold action on this basis is one of the \mathfrak{a} orientifolds introduced in [9].

Let us motivate the particular \mathfrak{a} orientifold we will study by comparing with the description of the orientifolded $\mathbb{C}^3/\mathbb{Z}_3$ [9]. As we found in §3.1, one can go from the dP_1 quiver in figure 34 to the quiver for phase 1 of $\mathbb{C}^3/\mathbb{Z}_3$ by giving a vev to the field Z between \mathcal{E}_1 and \mathcal{E}_2 . Under the blow down map $\pi: dP_1 \rightarrow \mathbb{P}^2$, the exceptional divisor e contracts to a point, and the hyperplane ℓ in dP_1 becomes the hyperplane in \mathbb{P}^2 . By looking to the Chern characters in (B.2), and the fractional basis for \mathbb{P}^2 given in [9], a very plausible description of the Higgsing in terms of sheaves is given by

$$\pi_*(\mathcal{E}_1 + \mathcal{E}_2) = \mathcal{O} \quad ; \quad \pi_*\mathcal{E}_3 = \Omega(1)[1] \quad ; \quad \pi_*\mathcal{E}_4 = \mathcal{O}(-1)[2]. \quad (\text{B.4})$$

From this point of view, it is no surprise that the collection (B.2) is not invariant under the ordinary orientifold action (B.3), since in the \mathbb{P}^2 case we would need to compose (B.3) with an auto-equivalence of the category to be able to exchange $\pi_*\mathcal{E}_3$ and $\pi_*\mathcal{E}_4$, leaving $\pi_*(\mathcal{E}_1 + \mathcal{E}_2)$ invariant. Given this correspondence, and the form of the quantum monodromy in the $\mathbb{C}^3/\mathbb{Z}_3$ case, we can make a natural suggestion for the auto-equivalence in dP_1 :

$$\mathcal{M}_q = \mathfrak{L}^{-1} \cdot \mathfrak{M}_{\mathcal{O}(-\ell)} \cdot \mathfrak{L}, \quad (\text{B.5})$$

where \mathfrak{L} is the operation of tensoring a sheaf with $\mathcal{O}(-\ell)$, and $\mathfrak{M}_{\mathcal{O}(-\ell)}$ is the monodromy around the locus where $\mathcal{O}(-\ell)$ becomes massless, which we assume to exist, in analogy with the $\mathbb{C}^3/\mathbb{Z}_3$ case. Acting on the Chern characters, we have:

$$\text{ch}(\mathfrak{M}_{\mathcal{O}(-\ell)}\mathcal{F}) = \text{ch}(\mathcal{F}) - \langle \mathcal{F}, \mathcal{O}(-\ell) \rangle \text{ch}(\mathcal{O}(-\ell)). \quad (\text{B.6})$$

After acting with \mathcal{M}_q , we have a new basis of branes given by:

$$\mathcal{E}_1 = \mathcal{O}[2] \ , \ \mathcal{E}_2 = \mathcal{O}(e)[0] \ , \ \mathcal{E}_3 = \mathcal{O}(2e - \ell)[1] \ , \ \mathcal{E}_4 = \mathcal{O}(\ell - e)[1] . \quad (\text{B.7})$$

It is now straightforward to verify that this basis is invariant under the orientifold action (B.3) with $\mathcal{L}_{2B} = \mathcal{O}(3\ell)$, giving the involution on the quiver shown in figure 34. The corresponding charge vectors are given by:

$$\begin{aligned} e^{-B}\Gamma(\mathcal{E}_1) &= 1 - \frac{1}{2}e + \frac{1}{24}\ell^2 , & e^{-B}\Gamma(\mathcal{E}_3) &= -1 - \frac{3}{2}e + \ell + \frac{11}{24}\ell^2 , \\ e^{-B}\Gamma(\mathcal{E}_2) &= 1 + \frac{1}{2}e + \frac{1}{24}\ell^2 , & e^{-B}\Gamma(\mathcal{E}_4) &= -1 + \frac{3}{2}e - \ell + \frac{11}{24}\ell^2 . \end{aligned} \quad (\text{B.8})$$

After applying the orientifold action (B.3) we could apply \mathcal{M}_q in order to obtain the action on the original basis of branes, but for simplicity we will stay with the basis (B.7) for the remainder of this section.

The spectrum for the quiver can now be computed using the same techniques as in [9]. We first consider an $\text{O}7^+$ plane wrapping the contracting dP_1 surface, which requires a configuration of the form $\text{O}7^+ + 4(\mathcal{E}_3 + \mathcal{E}_4) + (N - 4)\text{D}3$ s in order to cancel tadpoles, where $N - 4$ counts D3 branes in covering space conventions. The resulting gauge group is $SU(N - 4) \times SU(N)$, and the matter content of the theory is given in the following table:

$SU(N - 4)$	$SU(N)$	$SU(2)$
\square	$\bar{\square}$	\square
\square	$\bar{\square}$	1
$\overline{\square\square}$	1	1
1	\square	\square
1	\square	1

(B.9)

We identify this configuration as phase I_A . To understand the origin of the $SU(2)$ flavor symmetry, we note that dP_1 is the moduli space of the gauged linear sigma model

	x_0	x_1	x_2	x_3
\mathbb{C}^*	-1	1	0	1
\mathbb{C}^*	1	0	1	0

(B.10)

Notice that $x_1 = 0$ and $x_3 = 0$ are linearly equivalent divisors, and thus there is a $SU(2)$ symmetry rotating the corresponding sections. As an example, the doublet between \mathcal{E}_1 and \mathcal{E}_4 comes from:

$$\text{Ext}_X^1(i_*\mathcal{E}_1, \mathcal{E}_4) = \text{Ext}_X^0(i_*\mathcal{O}, i_*\mathcal{O}(\ell - e)) = \text{Ext}_{\mathcal{S}}^0(\mathcal{O}, \mathcal{O}(\ell - e)) = \{x_1, x_3\} = \mathbb{C}^2 , \quad (\text{B.11})$$

where $\mathcal{S} = dP_1$, and $\{x_1, x_3\}$ denotes the space spanned by the x_1, x_3 sections. The $\mathbf{3} = \mathbf{2} + \mathbf{1}$ split in the bifundamentals between \mathcal{E}_3 and \mathcal{E}_4 can be understood in a similar way:

$$\begin{aligned} \text{Ext}_X^1(i_*\mathcal{E}_4, i_*\mathcal{E}_3) &= \text{Ext}_{\mathcal{S}}^1(\mathcal{O}(\ell - e), \mathcal{O}(2e - \ell)) \\ &= \left\{ \frac{1}{x_1 x_3} x_0, \frac{1}{x_1 x_3} x_2 \frac{1}{x_1}, \frac{1}{x_1 x_3} x_2 \frac{1}{x_3} \right\} = \mathbb{C} \otimes \mathbb{C}^2 , \end{aligned} \quad (\text{B.12})$$

where we have used the “rationom” counting procedure of [69–71] for representing the generators of $H^1(dP_1, \mathcal{O}(3e - 2\ell))$.

Applying S-duality to I_A^- , we expected a transition in the orientifold type of the form

$$O7^+ + 8(\mathcal{E}_3 + \mathcal{E}_4) \longleftrightarrow O7^- + n D3s. \quad (\text{B.13})$$

Charge conservation implies $n = 6$, and we obtain a dual theory given by:

$SU(N+2)$	$SU(N-2)$	$SU(2)$	
\square	$\bar{\square}$	\square	
$\bar{\square}$	$\bar{\square}$	1	
$\bar{\bar{\square}}$	1	1	(B.14)
1	$\square\square$	\square	
1	$\square\square$	1	

which we identify as phase I_B with $\tilde{N} = N - 2$, agreeing with our discussion in [7] and §3.

C Results for the superconformal index of dP_1

In this appendix, we present a number of lengthy formulas for the superconformal index of the dP_1 theories expanded in powers of t . Our conventions are explained in §5.1. The code that we used for our computations, based around the computer algebra package `LiE` [72], is attached to the `arXiv` submission.

C.1 $\Pi_-^+ = \text{III}_+, Q_{D3} = 8$

$$\begin{aligned}
& 1 + b^{-1}y^4t_{(1.077)}^{15-\frac{24}{\beta}-2\beta}X_5 + t^2(-1 - X_2) + b^{-1}y^4J_1t_{(2.077)}^{16-\frac{24}{\beta}-2\beta}X_5 + b^{-2}y^8t_{(2.153)}^{30-\frac{48}{\beta}-4\beta}(X_2 + X_6 + X_{10}) \\
& - yt_{(2.178)}^{6-\beta}X_1 + by^{-7}t_{(2.39)}^{-23+\frac{24}{\beta}+5\beta} + by^{-6}t_{(2.568)}^{-19+\frac{24}{\beta}+4\beta}X_1 + 2by^{-5}t_{(2.746)}^{-15+\frac{24}{\beta}+3\beta}X_2 \\
& - y^{-1}J_1t_{(2.822)}^{-1+\beta}X_1 - b^{-1}y^3t_{(2.899)}^{13-\frac{24}{\beta}-\beta}X_4 + by^{-4}t_{(2.923)}^{-11+\frac{24}{\beta}+2\beta}(X_1 + 2X_3) - 2t^3J_1(1 + X_2) \\
& + b^{-1}y^4t_{(3.077)}^{17-\frac{24}{\beta}-2\beta}(-X_3 + (-2 + J_2)X_5 - X_7) + by^{-3}t_{(3.101)}^{-7+\frac{24}{\beta}+\beta}(2 + X_2 + 2X_4) \\
& + b^{-2}y^8J_1t_{(3.153)}^{31-\frac{48}{\beta}-4\beta}(1 + X_2 + X_4 + X_6 + X_8 + X_{10}) - yJ_1t_{(3.178)}^{7-\beta}(X_1 + X_3) \\
& + b^{-3}y^{12}t_{(3.23)}^{45-\frac{72}{\beta}-6\beta}(X_3 + X_5 + X_7 + X_9 + X_{11} + X_{15}) - b^{-1}y^5t_{(3.254)}^{21-\frac{24}{\beta}-3\beta}(X_2 + X_4 + X_6) \\
& + by^{-2}t_{(3.279)}^{-3+\frac{24}{\beta}}(X_1 + X_3 + X_5) + b^3y^{-9}t_{(3.304)}^{-27+\frac{72}{\beta}+3\beta} + by^{-7}J_1t_{(3.39)}^{-22+\frac{24}{\beta}+5\beta} + by^{-1}t_{(3.457)}^{1+\frac{24}{\beta}-\beta}(X_2 + X_6) \\
& + y^{-3}t_{(3.466)}^{-8+3\beta}(X_1 + X_3 + X_5) + by^{-6}J_1t_{(3.568)}^{-18+\frac{24}{\beta}+4\beta}X_1 + y^{-2}t_{(3.644)}^{-4+2\beta}(1 + 4X_2 + 2X_4 + X_6) \\
& + 2by^{-5}J_1t_{(3.746)}^{-14+\frac{24}{\beta}+3\beta}X_2 - y^{-1}t_{(3.822)}^{\beta}((-5 + J_2)X_1 - 7X_3 - 2(2X_5 + X_7)) \\
& - b^{-1}y^3J_1t_{(3.899)}^{14-\frac{24}{\beta}-\beta}(X_2 + 2X_4 + X_6) + by^{-4}J_1t_{(3.923)}^{-10+\frac{24}{\beta}+2\beta}(X_1 + 2X_3) \\
& - b^{-2}y^7t_{(3.975)}^{28-\frac{48}{\beta}-3\beta}(X_1 + X_3 + X_5 + X_7 + X_9) + t^4(1 + 8X_2 - 2J_2(1 + X_2) + 8X_4 + 4X_6 + 2X_8) \\
& - b^{-1}y^4t_{(4.077)}^{18-\frac{24}{\beta}-2\beta}(-J_3X_5 + J_1(X_1 + 3(X_3 + 2X_5 + X_7))) + by^{-3}J_1t_{(4.101)}^{-6+\frac{24}{\beta}+\beta}(2 + X_2 + 2X_4) \\
& + b^{-2}y^8t_{(4.153)}^{32-\frac{48}{\beta}-4\beta}(-2X_2 - X_4 - 2X_6 - X_8 - 2X_{10} + J_2(1 + 2X_2 + X_4 + 2X_6 + X_8 + 2X_{10}) - X_{12}) \\
& - yt_{(4.178)}^{8-\beta}((-6 + J_2)X_1 + (-9 + J_2)X_3 - 2(4X_5 + 2X_7 + X_9)) \\
& + b^{-3}y^{12}J_1t_{(4.23)}^{46-\frac{72}{\beta}-6\beta}(X_1 + 2X_3 + 3X_5 + 3X_7 + 2X_9 + 2X_{11} + X_{13} + X_{15}) \\
& - b^{-1}y^5J_1t_{(4.254)}^{22-\frac{24}{\beta}-3\beta}(1 + 2X_2 + 3X_4 + 3X_6 + X_8) + by^{-2}J_1t_{(4.279)}^{-2+\frac{24}{\beta}}(X_1 + X_3 + X_5) \\
& + b^3y^{-9}J_1t_{(4.304)}^{-26+\frac{72}{\beta}+3\beta} + b^{-4}y^{16}t_{(4.306)}^{60-\frac{96}{\beta}-8\beta}(1 + 2X_4 + X_6 + 2X_8 + X_{10} + 2X_{12} + X_{14} + X_{16} + X_{20}) \\
& - b^{-2}y^9t_{(4.331)}^{36-\frac{48}{\beta}-5\beta}(X_1 + 2X_3 + 2X_5 + 2X_7 + X_9 + X_{11}) + y^2t_{(4.356)}^{12-2\beta}(2 + 4X_2 + 4X_4 + 5X_6 + 2X_8 + X_{10}) \\
& + by^{-7}t_{(4.39)}^{-21+\frac{24}{\beta}+5\beta}(-1 + J_2 - 2X_2) + by^{-1}J_1t_{(4.457)}^{2+\frac{24}{\beta}-\beta}(X_2 + X_6) + y^{-3}J_1t_{(4.466)}^{-7+3\beta}(X_1 + X_3 + 2X_5) \\
& + y^3t_{(4.534)}^{16-3\beta}(X_1 + 2X_3 + 2X_5 + 2X_7 + X_9 + X_{11}) + b^{-1}yt_{(4.543)}^{7-\frac{24}{\beta}+\beta}(3X_2 + 2X_4 + 3X_6 + X_8 + X_{10}) \\
& + by^{-6}t_{(4.568)}^{-17+\frac{24}{\beta}+4\beta}((-3 + J_2)X_1 - 3X_3) + y^{-2}J_1t_{(4.644)}^{-3+2\beta}(2 + 3X_2 + 3X_4 + 2X_6) \\
& + b^{-1}y^2t_{(4.721)}^{11-\frac{24}{\beta}}(5X_1 + 8X_3 + 7X_5 + 6X_7 + 2X_9 + X_{11}) + by^{-5}t_{(4.746)}^{-13+\frac{24}{\beta}+3\beta}(-4 + 2(-3 + J_2)X_2 - 5X_4) \\
& + b^2y^{-14}t_{(4.779)}^{-46+\frac{48}{\beta}+10\beta} + y^{-1}t_{(4.822)}^{1+\beta}(-J_3X_1 + J_1(7X_1 + 10X_3 + 6X_5 + 4X_7)) \\
& - b^{-1}y^3t_{(4.899)}^{15-\frac{24}{\beta}-\beta}(-8 + (-13 + J_2)X_2 + (-19 + 3J_2)X_4 - 14X_6 + 2J_2X_6 - 11X_8 - 4X_{10} - 2X_{12}) \\
& + by^{-4}t_{(4.923)}^{-9+\frac{24}{\beta}+2\beta}((-8 + J_2)X_1 + (-9 + 2J_2)X_3 - 5X_5) + b^2y^{-13}t_{(4.957)}^{-42+\frac{48}{\beta}+9\beta}X_1 \\
& - b^{-2}y^7J_1t_{(4.975)}^{29-\frac{48}{\beta}-3\beta}(3X_1 + 4X_3 + 4X_5 + 4X_7 + 3X_9 + X_{11}) \\
& + t^5(-2J_3(1 + X_2) + J_1(5 + 14X_2 + 12X_4 + 7X_6 + 4X_8)) + \dots
\end{aligned}$$

C.2 $\Gamma_A^- = \Gamma_B^- = \text{III}_-, Q_{D3} = 8$

$$\begin{aligned}
& 1 + t^2(-1 - X_2) - yt_{(2.178)}^{6-\beta} X_1 + by^{-7}t_{(2.39)}^{-23+\frac{24}{\beta}+5\beta} + by^{-6}t_{(2.568)}^{-19+\frac{24}{\beta}+4\beta} X_1 + 2by^{-5}t_{(2.746)}^{-15+\frac{24}{\beta}+3\beta} X_2 \\
& - y^{-1}J_1t_{(2.822)}^{-1+\beta} X_1 + by^{-4}t_{(2.923)}^{-11+\frac{24}{\beta}+2\beta} (X_1 + 2X_3) - 2t^3J_1(1 + X_2) + by^{-3}t_{(3.101)}^{-7+\frac{24}{\beta}+\beta} (2 + X_2 + 2X_4) \\
& - yJ_1t_{(3.178)}^{7-\beta} (X_1 + X_3) + by^{-2}t_{(3.279)}^{-3+\frac{24}{\beta}} (X_1 + X_3 + X_5) + b^3y^{-9}t_{(3.304)}^{-27+\frac{72}{\beta}+3\beta} + by^{-7}J_1t_{(3.39)}^{-22+\frac{24}{\beta}+5\beta} \\
& + by^{-1}t_{(3.457)}^{1+\frac{24}{\beta}-\beta} (X_2 + X_6) + by^{-6}J_1t_{(3.568)}^{-18+\frac{24}{\beta}+4\beta} X_1 + y^{-2}t_{(3.644)}^{-4+2\beta} X_2 + 2by^{-5}J_1t_{(3.746)}^{-14+\frac{24}{\beta}+3\beta} X_2 \\
& - y^{-1}t_{(3.822)}^{\beta} (J_2X_1 - X_3) + by^{-4}J_1t_{(3.923)}^{-10+\frac{24}{\beta}+2\beta} (X_1 + 2X_3) + t^4(-2 + X_2 - 2J_2(1 + X_2) + X_4) \\
& + by^{-3}J_1t_{(4.101)}^{-6+\frac{24}{\beta}+\beta} (2 + X_2 + 2X_4) - yt_{(4.178)}^{8-\beta} ((-1 + J_2)X_1 + (-1 + J_2)X_3 - X_5) \\
& + by^{-2}J_1t_{(4.279)}^{-2+\frac{24}{\beta}} (X_1 + X_3 + X_5) + b^3y^{-9}J_1t_{(4.304)}^{-26+\frac{72}{\beta}+3\beta} + y^2t_{(4.356)}^{12-2\beta} (1 + X_6) \\
& + by^{-7}t_{(4.39)}^{-21+\frac{24}{\beta}+5\beta} (-1 + J_2 - 2X_2) + by^{-1}J_1t_{(4.457)}^{2+\frac{24}{\beta}-\beta} (X_2 + X_6) \\
& + b^{-1}yt_{(4.543)}^{7-\frac{24}{\beta}+\beta} (2X_2 + X_4 + X_6) + by^{-6}t_{(4.568)}^{-17+\frac{24}{\beta}+4\beta} ((-3 + J_2)X_1 - 3X_3) \\
& + y^{-2}J_1t_{(4.644)}^{-3+2\beta} (1 + X_2) + 2b^{-1}y^2t_{(4.721)}^{11-\frac{24}{\beta}} (2X_1 + 3X_3 + 2X_5 + X_7) \\
& + by^{-5}t_{(4.746)}^{-13+\frac{24}{\beta}+3\beta} (-4 + 2(-3 + J_2)X_2 - 5X_4) + b^2y^{-14}t_{(4.779)}^{-46+\frac{48}{\beta}+10\beta} \\
& + y^{-1}t_{(4.822)}^{1+\beta} (-J_3X_1 + 3J_1(X_1 + X_3)) + 3b^{-1}y^3t_{(4.899)}^{15-\frac{24}{\beta}-\beta} (2 + 3X_2 + 4X_4 + 2X_6 + X_8) \\
& + by^{-4}t_{(4.923)}^{-9+\frac{24}{\beta}+2\beta} ((-8 + J_2)X_1 + (-9 + 2J_2)X_3 - 5X_5) + b^2y^{-13}t_{(4.957)}^{-42+\frac{48}{\beta}+9\beta} X_1 \\
& + t^5(-2J_3(1 + X_2) + J_1(3 + 7X_2 + 4X_4)) + b^{-1}y^4t_{(5.077)}^{19-\frac{24}{\beta}-2\beta} (10X_1 + 14X_3 + 13X_5 + 7X_7 + 3X_9) \\
& + by^{-3}t_{(5.101)}^{-5+\frac{24}{\beta}+\beta} (-4 - 12X_2 - 9X_4 + J_2(2 + X_2 + 2X_4) - 5X_6) - b^3y^{-10}t_{(5.126)}^{-29+\frac{72}{\beta}+4\beta} X_1 \\
& + 3b^2y^{-12}t_{(5.135)}^{-38+\frac{48}{\beta}+8\beta} X_2 + yt_{(5.178)}^{9-\beta} (-J_3(X_1 + X_3) + 3J_1(2X_1 + 2X_3 + X_5)) \\
& - by^{-8}J_1t_{(5.212)}^{-24+\frac{24}{\beta}+6\beta} X_1 + b^{-1}y^5t_{(5.254)}^{23-\frac{24}{\beta}-3\beta} (11X_2 + 2(1 + 5X_4 + 5X_6 + 2X_8 + X_{10})) \\
& + by^{-2}t_{(5.279)}^{-1+\frac{24}{\beta}} ((-7 + J_2)X_1 + (-10 + J_2)X_3 - 7X_5 + J_2X_5 - 3X_7) + b^3y^{-9}t_{(5.304)}^{-25+\frac{72}{\beta}+3\beta} (-1 + J_2 - X_2) \\
& + b^2y^{-11}t_{(5.313)}^{-34+\frac{48}{\beta}+7\beta} (3X_1 + 4X_3) + y^2J_1t_{(5.356)}^{13-2\beta} (1 + 2X_2 + 2X_4 + X_6) \\
& - by^{-7}t_{(5.39)}^{-20+\frac{24}{\beta}+5\beta} (-J_3 + J_1(4 + 5X_2)) + b^{-1}y^6t_{(5.432)}^{27-\frac{24}{\beta}-4\beta} (3X_1 + 5X_3 + 5X_5 + 4X_7 + 2X_9 + X_{11}) \\
& + by^{-1}t_{(5.457)}^{3+\frac{24}{\beta}-\beta} (-3 + (-5 + J_2)X_2 - 6X_4 - 4X_6 + J_2X_6 - 2X_8) \\
& - y^{-3}t_{(5.466)}^{-6+3\beta} X_1 - b^3y^{-8}t_{(5.482)}^{-21+\frac{72}{\beta}+2\beta} X_1 + b^2y^{-10}t_{(5.491)}^{-30+\frac{48}{\beta}+6\beta} (7 + 5X_2 + 7X_4) \\
& + b^{-1}yJ_1t_{(5.543)}^{8-\frac{24}{\beta}+\beta} (2X_2 + X_4 + X_6) - by^{-6}t_{(5.568)}^{-16+\frac{24}{\beta}+4\beta} (-J_3X_1 + 2J_1(5X_1 + 4X_3)) \\
& + b^{-1}y^7t_{(5.61)}^{31-\frac{24}{\beta}-5\beta} (1 + X_4 + X_8) - bt_{(5.635)}^{7+\frac{24}{\beta}-2\beta} (X_1 + 2X_3 + 2X_5 + X_7) \\
& + y^{-2}t_{(5.644)}^{-2+2\beta} (-X_2 + J_2(2 + X_2) - 2X_4) + b^2y^{-9}t_{(5.669)}^{-26+\frac{48}{\beta}+5\beta} (11X_1 + 11X_3 + 7X_5) \\
& + b^4y^{-16}t_{(5.694)}^{-50+\frac{96}{\beta}+8\beta} + 2b^{-1}y^2J_1t_{(5.721)}^{12-\frac{24}{\beta}} (2X_1 + 3X_3 + 2X_5 + X_7) \\
& - 2by^{-5}t_{(5.746)}^{-12+\frac{24}{\beta}+3\beta} (-J_3X_2 + J_1(5 + 9X_2 + 6X_4)) + b^2y^{-14}J_1t_{(5.779)}^{-45+\frac{48}{\beta}+10\beta} \\
& + y^{-1}t_{(5.822)}^{2+\beta} ((4 + 7J_2 - J_4)X_1 + 5J_2X_3 - 2X_5) + b^2y^{-8}t_{(5.847)}^{-22+\frac{48}{\beta}+4\beta} (4 + 23X_2 + 12X_4 + 9X_6) \\
& + b^4y^{-15}t_{(5.872)}^{-46+\frac{96}{\beta}+7\beta} X_1 + b^{-1}y^3J_1t_{(5.899)}^{16-\frac{24}{\beta}-\beta} (6 + 8X_2 + 11X_4 + 6X_6 + 3X_8) \\
& - by^{-4}t_{(5.923)}^{-8+\frac{24}{\beta}+2\beta} (-J_3(X_1 + 2X_3) + J_1(20X_1 + 24X_3 + 13X_5)) - b^3y^{-11}J_1t_{(5.948)}^{-32+\frac{72}{\beta}+5\beta} \\
& + 2b^2y^{-13}J_1t_{(5.957)}^{-41+\frac{48}{\beta}+9\beta} X_1 + t^6(9 + 10X_2 - 2J_4(1 + X_2) + 3X_4 + 2J_2(3 + 8X_2 + 3X_4) - 2X_6) + \dots
\end{aligned}$$

C.3 $I_A^+ = \Pi_-$, $Q_{D3} = 9$

$$\begin{aligned}
& 1 + b^{\frac{1}{2}} y^{-5} t_{(1.294)}^{-17 + \frac{27}{2\beta} + \frac{31\beta}{8}} + b^{\frac{1}{2}} y^{-4} t_{(1.488)}^{-13 + \frac{27}{2\beta} + \frac{23\beta}{8}} X_1 + b^{\frac{1}{2}} y^{-3} t_{(1.683)}^{-9 + \frac{27}{2\beta} + \frac{15\beta}{8}} X_2 \\
& + b^{\frac{1}{2}} y^{-2} t_{(1.877)}^{-5 + \frac{27}{2\beta} + \frac{7\beta}{8}} X_3 + t^2 (-1 - X_2) + b^{\frac{1}{2}} y^{-1} t_{(2.072)}^{-1 + \frac{27}{2\beta} - \frac{\beta}{8}} X_4 - y t_{(2.194)}^{6-\beta} X_1 \\
& + b^{\frac{1}{2}} t_{(2.266)}^{3 + \frac{27}{2\beta} - \frac{9\beta}{8}} X_5 + b^{\frac{1}{2}} y^{-5} J_1 t_{(2.294)}^{-16 + \frac{27}{2\beta} + \frac{31\beta}{8}} + b^{\frac{1}{2}} y^{-4} J_1 t_{(2.488)}^{-12 + \frac{27}{2\beta} + \frac{23\beta}{8}} X_1 + b y^{-10} t_{(2.588)}^{-34 + \frac{27}{\beta} + \frac{31\beta}{4}} \\
& + b^{\frac{1}{2}} y^{-3} J_1 t_{(2.683)}^{-8 + \frac{27}{2\beta} + \frac{15\beta}{8}} X_2 + b y^{-9} t_{(2.783)}^{-30 + \frac{27}{\beta} + \frac{27\beta}{4}} X_1 - y^{-1} J_1 t_{(2.806)}^{-1+\beta} X_1 + b^{\frac{1}{2}} y^{-2} J_1 t_{(2.877)}^{-4 + \frac{27}{2\beta} + \frac{7\beta}{8}} X_3 \\
& + 2b y^{-8} t_{(2.977)}^{-26 + \frac{27}{\beta} + \frac{23\beta}{4}} X_2 - 2t^3 J_1 (1 + X_2) + b^{\frac{1}{2}} y^{-1} J_1 t_{(3.072)}^{\frac{27}{2\beta} - \frac{\beta}{8}} X_4 + b y^{-7} t_{(3.171)}^{-22 + \frac{27}{\beta} + \frac{19\beta}{4}} (X_1 + 2X_3) \\
& - y J_1 t_{(3.194)}^{7-\beta} (X_1 + X_3) + b^{\frac{1}{2}} J_1 t_{(3.266)}^{4 + \frac{27}{2\beta} - \frac{9\beta}{8}} X_5 + b^{\frac{1}{2}} y^{-5} t_{(3.294)}^{-15 + \frac{27}{2\beta} + \frac{31\beta}{8}} (-1 + J_2 - X_2) \\
& + b y^{-6} t_{(3.366)}^{-18 + \frac{27}{\beta} + \frac{15\beta}{4}} (2 + X_2 + 3X_4) + b^{\frac{1}{2}} y^{-4} t_{(3.488)}^{-11 + \frac{27}{2\beta} + \frac{23\beta}{8}} ((-2 + J_2) X_1 - 2X_3) \\
& + b y^{-5} t_{(3.56)}^{-14 + \frac{27}{\beta} + \frac{11\beta}{4}} (2X_1 + 2X_3 + 3X_5) + b y^{-10} J_1 t_{(3.588)}^{-33 + \frac{27}{\beta} + \frac{31\beta}{4}} + y^{-2} t_{(3.611)}^{-4+2\beta} X_2 + b^3 y^{-10} t_{(3.653)}^{-30 + \frac{81}{\beta} + \frac{13\beta}{4}} \\
& + b^{\frac{1}{2}} y^{-3} t_{(3.683)}^{-7 + \frac{27}{2\beta} + \frac{15\beta}{8}} (-1 + (-3 + J_2) X_2 - 2X_4) + b y^{-4} t_{(3.755)}^{-10 + \frac{27}{\beta} + \frac{7\beta}{4}} (4X_2 + 2X_4 + 3X_6) \\
& + 2b y^{-9} J_1 t_{(3.783)}^{-29 + \frac{27}{\beta} + \frac{27\beta}{4}} X_1 - y^{-1} t_{(3.806)}^{\beta} (J_2 X_1 - X_3) + b^{\frac{1}{2}} y^{-2} t_{(3.877)}^{-3 + \frac{27}{2\beta} + \frac{7\beta}{8}} (-2X_1 + (-3 + J_2) X_3 - 2X_5) \\
& + b^{\frac{3}{2}} y^{-15} t_{(3.882)}^{-51 + \frac{81}{2\beta} + \frac{93\beta}{8}} + b y^{-3} t_{(3.949)}^{-6 + \frac{27}{\beta} + \frac{3\beta}{4}} (2X_1 + 3X_3 + 2(X_5 + X_7)) + b y^{-8} J_1 t_{(3.977)}^{-25 + \frac{27}{\beta} + \frac{23\beta}{4}} (1 + 3X_2) \\
& + t^4 (-2 + X_2 - 2J_2 (1 + X_2) + X_4) + b^{\frac{1}{2}} y^{-1} t_{(4.072)}^{1 + \frac{27}{2\beta} - \frac{\beta}{8}} (-1 - 2X_2 + (-3 + J_2) X_4 - 2X_6) \\
& + b^{\frac{3}{2}} y^{-14} t_{(4.077)}^{-47 + \frac{81}{2\beta} + \frac{85\beta}{8}} X_1 - b^{\frac{1}{2}} y^{-6} J_1 t_{(4.1)}^{-18 + \frac{27}{2\beta} + \frac{39\beta}{8}} X_1 + b y^{-2} t_{(4.143)}^{-2 + \frac{27}{\beta} - \frac{\beta}{4}} (2 + X_2 + 3X_4 + X_6 + 2X_8) \\
& + 2b y^{-7} J_1 t_{(4.171)}^{-21 + \frac{27}{\beta} + \frac{19\beta}{4}} (X_1 + 2X_3) + b^{-\frac{3}{2}} y^5 t_{(4.174)}^{21 - \frac{81}{2\beta} - \frac{13\beta}{8}} (X_2 + X_6) \\
& - y t_{(4.194)}^{8-\beta} ((-1 + J_2) X_1 + (-1 + J_2) X_3 - X_5) - b^{\frac{1}{2}} t_{(4.266)}^{5 + \frac{27}{2\beta} - \frac{9\beta}{8}} (X_1 + 2X_3 + 3X_5 - J_2 X_5 + X_7) \\
& + 2b^{\frac{3}{2}} y^{-13} t_{(4.271)}^{-43 + \frac{81}{2\beta} + \frac{77\beta}{8}} X_2 - b^{\frac{1}{2}} y^{-5} t_{(4.294)}^{-14 + \frac{27}{2\beta} + \frac{31\beta}{8}} (-J_3 + 4J_1 (1 + X_2)) \\
& + b y^{-1} t_{(4.338)}^{2 + \frac{27}{\beta} - \frac{5\beta}{4}} (X_1 + X_3 + X_5 + X_7 + X_9) + b y^{-6} J_1 t_{(4.366)}^{-17 + \frac{27}{\beta} + \frac{15\beta}{4}} (2 + 3X_2 + 5X_4) \\
& + b^{-\frac{3}{2}} y^6 t_{(4.368)}^{25 - \frac{81}{2\beta} - \frac{21\beta}{8}} (X_1 + 2X_3 + X_5 + X_7) + y^2 t_{(4.389)}^{12-2\beta} (1 + X_6) - b^{\frac{1}{2}} y t_{(4.461)}^{9 + \frac{27}{2\beta} - \frac{17\beta}{8}} (X_2 + X_4 + X_6) \\
& + b^{\frac{3}{2}} y^{-12} t_{(4.465)}^{-39 + \frac{81}{2\beta} + \frac{69\beta}{8}} (X_1 + 3X_3) - b^{\frac{1}{2}} y^{-4} t_{(4.488)}^{-10 + \frac{27}{2\beta} + \frac{23\beta}{8}} (-J_3 X_1 + J_1 (8X_1 + 6X_3)) \\
& + b t_{(4.532)}^{6 + \frac{27}{\beta} - \frac{9\beta}{4}} (X_2 + X_6 + X_{10}) + b y^{-5} J_1 t_{(4.56)}^{-13 + \frac{27}{\beta} + \frac{11\beta}{4}} (3X_1 + 4X_3 + 6X_5) \\
& + b^{-\frac{3}{2}} y^7 t_{(4.563)}^{29 - \frac{81}{2\beta} - \frac{29\beta}{8}} (1 + X_2 + 2X_4 + X_6 + X_8) + b y^{-10} t_{(4.588)}^{-32 + \frac{27}{\beta} + \frac{31\beta}{4}} (-1 + 2J_2 - X_2) \\
& + y^{-2} J_1 t_{(4.611)}^{-3+2\beta} (1 + X_2) + b^3 y^{-10} J_1 t_{(4.653)}^{-29 + \frac{81}{\beta} + \frac{13\beta}{4}} + b^{\frac{3}{2}} y^{-11} t_{(4.66)}^{-35 + \frac{81}{2\beta} + \frac{61\beta}{8}} (3 + 2X_2 + 4X_4) \\
& - b^{\frac{1}{2}} y^{-3} t_{(4.683)}^{-6 + \frac{27}{2\beta} + \frac{15\beta}{8}} (-J_3 X_2 + J_1 (4 + 10X_2 + 7X_4)) + b y^{-4} J_1 t_{(4.755)}^{-9 + \frac{27}{\beta} + \frac{7\beta}{4}} (1 + 5X_2 + 5X_4 + 5X_6) \\
& + b^{-\frac{3}{2}} y^8 t_{(4.757)}^{33 - \frac{81}{2\beta} - \frac{37\beta}{8}} (X_3 + X_5 + X_9) + b y^{-9} t_{(4.783)}^{-28 + \frac{27}{\beta} + \frac{27\beta}{4}} ((-1 + 3J_2) X_1 - 2X_3) \\
& + y^{-1} t_{(4.806)}^{1+\beta} (-J_3 X_1 + 3J_1 (X_1 + X_3)) + b^{\frac{3}{2}} y^{-10} t_{(4.854)}^{-31 + \frac{81}{2\beta} + \frac{53\beta}{8}} (5X_1 + 4X_3 + 5X_5) \\
& - b^{\frac{1}{2}} y^{-2} t_{(4.877)}^{-2 + \frac{27}{2\beta} + \frac{7\beta}{8}} (-J_3 X_3 + J_1 (6X_1 + 11X_3 + 7X_5)) + b^{\frac{3}{2}} y^{-15} J_1 t_{(4.882)}^{-50 + \frac{81}{2\beta} + \frac{93\beta}{8}} \\
& + b^{\frac{1}{2}} y^{-7} t_{(4.905)}^{-21 + \frac{27}{2\beta} + \frac{47\beta}{8}} X_2 + b^{\frac{7}{2}} y^{-15} t_{(4.947)}^{-47 + \frac{189}{2\beta} + \frac{57\beta}{8}} + b y^{-3} J_1 t_{(4.949)}^{-5 + \frac{27}{\beta} + \frac{3\beta}{4}} (3X_1 + 5X_3 + 4(X_5 + X_7)) \\
& + b y^{-8} t_{(4.977)}^{-24 + \frac{27}{\beta} + \frac{23\beta}{4}} (-1 - 4X_2 + J_2 (1 + 5X_2) - 4X_4) + t^5 (-2J_3 (1 + X_2) + J_1 (3 + 7X_2 + 4X_4)) + \dots
\end{aligned}$$

$$\text{C.4} \quad \mathbf{I}_B^+ = \mathbf{II}_+^-, Q_{D3} = 9$$

$$\begin{aligned}
& 1 + b^{\frac{3}{2}} y^{-4} t_{(1.021)}^{-12 + \frac{81}{2\beta} + \frac{5\beta}{8}} + t^2 (-1 - X_2) + b^{\frac{3}{2}} y^{-4} J_1 t_{(2.021)}^{-11 + \frac{81}{2\beta} + \frac{5\beta}{8}} + b^3 y^{-8} t_{(2.041)}^{-24 + \frac{81}{\beta} + \frac{5\beta}{4}} - y t_{(2.194)}^{6-\beta} X_1 \\
& + b^{-\frac{1}{2}} t_{(2.734)}^{2 - \frac{27}{\beta} + \frac{9\beta}{8}} X_4 - y^{-1} J_1 t_{(2.806)}^{-1+\beta} X_1 - b^{\frac{3}{2}} y^{-5} t_{(2.826)}^{-14 + \frac{81}{2\beta} + \frac{13\beta}{8}} X_1 + b^{-\frac{1}{2}} y t_{(2.928)}^{6 - \frac{27}{2\beta} + \frac{\beta}{8}} (X_1 + X_3 + X_5) \\
& + b y^{-8} t_{(2.977)}^{-26 + \frac{27}{\beta} + \frac{23\beta}{4}} - 2t^3 J_1 (1 + X_2) + b^{\frac{3}{2}} y^{-4} t_{(3.021)}^{-10 + \frac{81}{2\beta} + \frac{5\beta}{8}} (-1 + J_2 - X_2) + b^3 y^{-8} J_1 t_{(3.041)}^{-23 + \frac{81}{\beta} + \frac{5\beta}{4}} \\
& + b^{\frac{9}{2}} y^{-12} t_{(3.062)}^{-36 + \frac{243}{2\beta} + \frac{15\beta}{8}} + b^{-\frac{1}{2}} y^2 t_{(3.123)}^{10 - \frac{27}{2\beta} - \frac{7\beta}{8}} (2X_2 + X_4 + X_6) + b y^{-7} t_{(3.171)}^{-22 + \frac{27}{\beta} + \frac{19\beta}{4}} X_1 \\
& - y J_1 t_{(3.194)}^{7-\beta} (X_1 + X_3) - b^{\frac{3}{2}} y^{-3} t_{(3.215)}^{-6 + \frac{81}{2\beta} - \frac{3\beta}{8}} X_1 + b^{-\frac{1}{2}} y^3 t_{(3.317)}^{14 - \frac{27}{2\beta} - \frac{15\beta}{8}} (X_1 + X_3 + X_5 + X_7) \\
& + 2b y^{-6} t_{(3.366)}^{-18 + \frac{27}{\beta} + \frac{15\beta}{4}} X_2 + b^{-\frac{1}{2}} y^4 t_{(3.512)}^{18 - \frac{27}{2\beta} - \frac{23\beta}{8}} (1 + X_4 + X_8) + b y^{-5} t_{(3.56)}^{-14 + \frac{27}{\beta} + \frac{11\beta}{4}} (X_1 + 2X_3) \\
& + y^{-2} t_{(3.611)}^{-4 + 2\beta} X_2 - b^{\frac{3}{2}} y^{-6} J_1 t_{(3.632)}^{-17 + \frac{81}{2\beta} + \frac{21\beta}{8}} + b^{-\frac{1}{2}} J_1 t_{(3.734)}^{3 - \frac{27}{2\beta} + \frac{9\beta}{8}} X_4 + b y^{-4} t_{(3.755)}^{-10 + \frac{27}{\beta} + \frac{7\beta}{4}} (2 + X_2 + 3X_4) \\
& - y^{-1} t_{(3.806)}^{\beta} (J_2 X_1 - X_3) - 2b^{\frac{3}{2}} y^{-5} J_1 t_{(3.826)}^{-13 + \frac{81}{2\beta} + \frac{13\beta}{8}} X_1 - b^3 y^{-9} t_{(3.847)}^{-26 + \frac{81}{\beta} + \frac{9\beta}{4}} X_1 \\
& + b^{-\frac{1}{2}} y J_1 t_{(3.928)}^{7 - \frac{27}{2\beta} + \frac{\beta}{8}} (X_1 + X_3 + X_5) + 2b y^{-3} t_{(3.949)}^{-6 + \frac{27}{\beta} + \frac{3\beta}{4}} (X_1 + X_3 + X_5) + b y^{-8} J_1 t_{(3.977)}^{-25 + \frac{27}{\beta} + \frac{23\beta}{4}} \\
& + b^{\frac{5}{2}} y^{-12} t_{(3.998)}^{-38 + \frac{135}{2\beta} + \frac{51\beta}{8}} + t^4 (-2 + X_2 - 2J_2 (1 + X_2) + X_4) - b^{\frac{3}{2}} y^{-4} t_{(4.021)}^{-9 + \frac{81}{2\beta} + \frac{5\beta}{8}} (-J_3 + 3J_1 (1 + X_2)) \\
& + b^3 y^{-8} t_{(4.041)}^{-22 + \frac{81}{\beta} + \frac{5\beta}{4}} (-1 + 2J_2 - X_2) + b^{\frac{9}{2}} y^{-12} J_1 t_{(4.062)}^{-35 + \frac{243}{2\beta} + \frac{15\beta}{8}} + b^6 y^{-16} t_{(4.083)}^{-48 + \frac{162}{\beta} + \frac{5\beta}{2}} \\
& + b^{-\frac{1}{2}} y^2 J_1 t_{(4.123)}^{11 - \frac{27}{2\beta} - \frac{7\beta}{8}} (2X_2 + X_4 + X_6) + b y^{-2} t_{(4.143)}^{-2 + \frac{27}{\beta} - \frac{\beta}{4}} (3X_2 + X_4 + 2X_6) \\
& + b y^{-7} J_1 t_{(4.171)}^{-21 + \frac{27}{\beta} + \frac{19\beta}{4}} X_1 + b^{\frac{5}{2}} y^{-11} t_{(4.192)}^{-34 + \frac{135}{2\beta} + \frac{43\beta}{8}} X_1 - y t_{(4.194)}^{8-\beta} ((-1 + J_2) X_1 + (-1 + J_2) X_3 - X_5) \\
& - b^{\frac{3}{2}} y^{-3} J_1 t_{(4.215)}^{-5 + \frac{81}{2\beta} - \frac{3\beta}{8}} (2X_1 + X_3) - b^3 y^{-7} t_{(4.236)}^{-18 + \frac{81}{\beta} + \frac{\beta}{4}} X_1 + b^{-\frac{1}{2}} y^3 J_1 t_{(4.317)}^{15 - \frac{27}{2\beta} - \frac{15\beta}{8}} (X_1 + X_3 + X_5 + X_7) \\
& + b y^{-1} t_{(4.338)}^{2 + \frac{27}{\beta} - \frac{5\beta}{4}} (X_1 + X_3 + X_5 + X_7) + 2b y^{-6} J_1 t_{(4.366)}^{-17 + \frac{27}{\beta} + \frac{15\beta}{4}} X_2 + 2b^{\frac{5}{2}} y^{-10} t_{(4.387)}^{-30 + \frac{135}{2\beta} + \frac{35\beta}{8}} X_2 \\
& + y^2 t_{(4.389)}^{12-2\beta} (1 + X_6) + b^{\frac{3}{2}} y^{-7} t_{(4.437)}^{-20 + \frac{81}{2\beta} + \frac{29\beta}{8}} X_1 + b^{-\frac{1}{2}} y^4 J_1 t_{(4.512)}^{19 - \frac{27}{2\beta} - \frac{23\beta}{8}} (1 + X_4 + X_8) \\
& + b t_{(4.532)}^{6 + \frac{27}{\beta} - \frac{9\beta}{4}} (1 + X_4 + X_8) - b^{-\frac{1}{2}} y^{-1} t_{(4.539)}^{-27 + \frac{17\beta}{8}} X_3 + b y^{-5} J_1 t_{(4.56)}^{-13 + \frac{27}{\beta} + \frac{11\beta}{4}} (X_1 + 2X_3) \\
& + b^{\frac{5}{2}} y^{-9} t_{(4.581)}^{-26 + \frac{135}{2\beta} + \frac{27\beta}{8}} (X_1 + 2X_3) + y^{-2} J_1 t_{(4.611)}^{-3+2\beta} (1 + X_2) - b^{\frac{3}{2}} y^{-6} t_{(4.632)}^{-16 + \frac{81}{2\beta} + \frac{21\beta}{8}} (J_2 - X_2) \\
& - b^3 y^{-10} J_1 t_{(4.653)}^{-29 + \frac{81}{\beta} + \frac{13\beta}{4}} - b^{-\frac{1}{2}} t_{(4.734)}^{4 - \frac{27}{2\beta} + \frac{9\beta}{8}} (1 + 2X_2 - (-3 + J_2) X_4 + X_6) \\
& + b y^{-4} J_1 t_{(4.755)}^{-9 + \frac{27}{\beta} + \frac{7\beta}{4}} (2 + X_2 + 4X_4) + b^{\frac{5}{2}} y^{-8} t_{(4.775)}^{-22 + \frac{135}{2\beta} + \frac{19\beta}{8}} (2 + X_2 + 3X_4) \\
& + y^{-1} t_{(4.806)}^{1+\beta} (-J_3 X_1 + 3J_1 (X_1 + X_3)) - b^{\frac{3}{2}} y^{-5} t_{(4.826)}^{-12 + \frac{81}{2\beta} + \frac{13\beta}{8}} (3J_2 X_1 - 2X_3) - 3b^3 y^{-9} J_1 t_{(4.847)}^{-25 + \frac{81}{\beta} + \frac{9\beta}{4}} X_1 \\
& - b^{\frac{9}{2}} y^{-13} t_{(4.868)}^{-38 + \frac{243}{2\beta} + \frac{23\beta}{8}} X_1 + b^{-\frac{1}{2}} y t_{(4.928)}^{8 - \frac{27}{2\beta} + \frac{\beta}{8}} ((-4 + J_2) X_1 + (-6 + J_2) X_3 - 5X_5 + J_2 X_5 - 2X_7) \\
& + 3b y^{-3} J_1 t_{(4.949)}^{-5 + \frac{27}{\beta} + \frac{3\beta}{4}} (X_1 + X_3 + X_5) + 2b^{\frac{5}{2}} y^{-7} t_{(4.97)}^{-18 + \frac{135}{2\beta} + \frac{11\beta}{8}} (X_1 + X_3 + X_5) \\
& + b y^{-8} t_{(4.977)}^{-24 + \frac{27}{\beta} + \frac{23\beta}{4}} (-1 + J_2 - 2X_2) + 2b^{\frac{5}{2}} y^{-12} J_1 t_{(4.998)}^{-37 + \frac{135}{2\beta} + \frac{51\beta}{8}} \\
& + t^5 (-2J_3 (1 + X_2) + J_1 (3 + 7X_2 + 4X_4)) + \dots
\end{aligned}$$

References

- [1] E. Witten, *Baryons and branes in anti-de Sitter space*, *JHEP* **9807** (1998) 006, [[hep-th/9805112](#)].
- [2] R. G. Leigh and M. J. Strassler, *Exactly marginal operators and duality in four-dimensional $N=1$ supersymmetric gauge theory*, *Nucl.Phys.* **B447** (1995) 95–136, [[hep-th/9503121](#)].
- [3] P. C. Argyres, K. A. Intriligator, R. G. Leigh, and M. J. Strassler, *On inherited duality in $\mathcal{N} = 1$ $d = 4$ supersymmetric gauge theories*, *JHEP* **0004** (2000) 029, [[hep-th/9910250](#)].
- [4] F. Benini, Y. Tachikawa, and B. Wecht, *Sicilian gauge theories and $N=1$ dualities*, *JHEP* **1001** (2010) 088, [[arXiv:0909.1327](#)].
- [5] N. Seiberg, *Electric-magnetic duality in supersymmetric non-Abelian gauge theories*, *Nucl.Phys.* **B435** (1995) 129–146, [[hep-th/9411149](#)].
- [6] N. Seiberg, *The Power of duality: Exact results in 4D SUSY field theory*, *Int.J.Mod.Phys.* **A16** (2001) 4365–4376, [[hep-th/9506077](#)].
- [7] I. García-Etxebarria, B. Heidenreich, and T. Wrase, *New $\mathcal{N} = 1$ dualities from orientifold transitions – Part I: Field Theory*, *JHEP* **1310** (2013) 007, [[arXiv:1210.7799](#)].
- [8] M. Bianchi, G. Inverso, J. F. Morales, and D. R. Pacifici, *Unoriented Quivers with Flavour*, *JHEP* **1401** (2014) 128, [[arXiv:1307.0466](#)].
- [9] I. García-Etxebarria, B. Heidenreich, and T. Wrase, *New $\mathcal{N} = 1$ dualities from orientifold transitions – Part II: String Theory*, *JHEP* **1310** (2013) 006, [[arXiv:1307.1701](#)].
- [10] A. M. Uranga, *Comments on nonsupersymmetric orientifolds at strong coupling*, *JHEP* **0002** (2000) 041, [[hep-th/9912145](#)].
- [11] S. Sugimoto, *Confinement and Dynamical Symmetry Breaking in non-SUSY Gauge Theory from S-duality in String Theory*, *Prog.Theor.Phys.* **128** (2012) 1175–1209, [[arXiv:1207.2203](#)].
- [12] A. Hook and G. Torroba, *S-duality of nonsupersymmetric gauge theories*, *Phys.Rev.* **D89** (2014), no. 2 025006, [[arXiv:1309.5948](#)].
- [13] D. Gaiotto and S. S. Razamat, *$N = 1$ theories of class S_k* , [arXiv:1503.05159](#).
- [14] S. Franco, H. Hayashi, and A. Uranga, *Charting Class S_k Territory*, [arXiv:1504.05988](#).
- [15] A. Hanany and K. Maruyoshi, *Chiral theories of class S* , [arXiv:1505.05053](#).
- [16] S. Franco and G. Torroba, *Gauge theories from D7-branes over vanishing 4-cycles*, *JHEP* **1101** (2011) 017, [[arXiv:1010.4029](#)].
- [17] M. Berkooz, *The Dual of supersymmetric $SU(2k)$ with an antisymmetric tensor and composite dualities*, *Nucl.Phys.* **B452** (1995) 513–525, [[hep-th/9505067](#)].
- [18] P. Pouliot, *Duality in SUSY $SU(N)$ with an antisymmetric tensor*, *Phys.Lett.* **B367** (1996) 151–156, [[hep-th/9510148](#)].
- [19] E. Witten, *Phases of $N=2$ theories in two-dimensions*, *Nucl.Phys.* **B403** (1993) 159–222, [[hep-th/9301042](#)].
- [20] P. A. Griffiths and J. Harris, *Principles of algebraic geometry*. Wiley New York, 1978.

- [21] D. Malyshev, *Del Pezzo singularities and SUSY breaking*, *Adv.High Energy Phys.* **2011** (2011) 630892, [[arXiv:0705.3281](#)].
- [22] A. Hanany and K. D. Kennaway, *Dimer models and toric diagrams*, [hep-th/0503149](#).
- [23] S. Franco, A. Hanany, K. D. Kennaway, D. Vegh, and B. Wecht, *Brane dimers and quiver gauge theories*, *JHEP* **0601** (2006) 096, [[hep-th/0504110](#)].
- [24] S. Franco, A. Hanany, D. Krefl, J. Park, A. M. Uranga, et al., *Dimers and orientifolds*, *JHEP* **0709** (2007) 075, [[arXiv:0707.0298](#)].
- [25] K. D. Kennaway, *Brane Tilings*, *Int.J.Mod.Phys.* **A22** (2007) 2977–3038, [[arXiv:0706.1660](#)].
- [26] M. Yamazaki, *Brane Tilings and Their Applications*, *Fortsch.Phys.* **56** (2008) 555–686, [[arXiv:0803.4474](#)].
- [27] A. Ishii and K. Ueda, *On moduli spaces of quiver representations associated with dimer models*, *RIMS Kôkyûroku Bessatsu* **B9** (2008) 127–141, [[arXiv:0710.1898](#)].
- [28] A. Hanany and D. Vegh, *Quivers, tilings, branes and rhombi*, *JHEP* **0710** (2007) 029, [[hep-th/0511063](#)].
- [29] B. Feng, A. Hanany, and Y.-H. He, *D-brane gauge theories from toric singularities and toric duality*, *Nucl.Phys.* **B595** (2001) 165–200, [[hep-th/0003085](#)].
- [30] C. E. Beasley and M. R. Plesser, *Toric duality is Seiberg duality*, *JHEP* **0112** (2001) 001, [[hep-th/0109053](#)].
- [31] Y. Imamura, K. Kimura, and M. Yamazaki, *Anomalies and O-plane charges in orientifolded brane tilings*, *JHEP* **0803** (2008) 058, [[arXiv:0801.3528](#)].
- [32] C. Angelantonj, M. Bianchi, G. Pradisi, A. Sagnotti, and Y. Stanev, *Chiral asymmetry in four-dimensional open string vacua*, *Phys.Lett.* **B385** (1996) 96–102, [[hep-th/9606169](#)].
- [33] J. D. Lykken, E. Poppitz, and S. P. Trivedi, *M(ore) on chiral gauge theories from D-branes*, *Nucl.Phys.* **B520** (1998) 51–74, [[hep-th/9712193](#)].
- [34] Z. Kakushadze, *Gauge theories from orientifolds and large N limit*, *Nucl.Phys.* **B529** (1998) 157–179, [[hep-th/9803214](#)].
- [35] M. Wijnholt, *Large volume perspective on branes at singularities*, *Adv.Theor.Math.Phys.* **7** (2004) 1117–1153, [[hep-th/0212021](#)].
- [36] M. Wijnholt, *Geometry of Particle Physics*, *Adv.Theor.Math.Phys.* **13** (2009) [[hep-th/0703047](#)].
- [37] B. Heidenreich. Unpublished notes.
- [38] J. Evslin, *What does(n't) K-theory classify?*, [hep-th/0610328](#).
- [39] A. Hanany and B. Kol, *On orientifolds, discrete torsion, branes and M theory*, *JHEP* **0006** (2000) 013, [[hep-th/0003025](#)].
- [40] A. Hatcher, *Algebraic Topology*. Cambridge University Press, 2002.
<http://www.math.cornell.edu/~hatcher/AT/ATpage.html>.
- [41] C.-H. Liu, *On the isolated singularity of a seven space obtained by rolling Calabi-Yau threefolds through extremal transitions*, [hep-th/9801175](#).

- [42] R. Kenyon, *An introduction to the dimer model*, *ArXiv Mathematics e-prints* (Oct., 2003) [[math/0310326](#)].
- [43] B. Feng, Y.-H. He, K. D. Kennaway, and C. Vafa, *Dimer models from mirror symmetry and quivering amoebae*, *Adv.Theor.Math.Phys.* **12** (2008) 489–545, [[hep-th/0511287](#)].
- [44] I. Garcia-Etxebarria, F. Saad, and A. M. Uranga, *Quiver gauge theories at resolved and deformed singularities using dimers*, *JHEP* **0606** (2006) 055, [[hep-th/0603108](#)].
- [45] I. García-Etxebarria and B. Heidenreich. To appear.
- [46] N. J. Evans, C. V. Johnson, and A. D. Shapere, *Orientifolds, branes, and duality of 4-D gauge theories*, *Nucl.Phys.* **B505** (1997) 251–271, [[hep-th/9703210](#)].
- [47] A. Hanany and E. Witten, *Type IIB superstrings, BPS monopoles, and three-dimensional gauge dynamics*, *Nucl.Phys.* **B492** (1997) 152–190, [[hep-th/9611230](#)].
- [48] A. Giveon and D. Kutasov, *Brane dynamics and gauge theory*, *Rev.Mod.Phys.* **71** (1999) 983–1084, [[hep-th/9802067](#)].
- [49] Y. Imamura, *Global symmetries and 't Hooft anomalies in brane tilings*, *JHEP* **0612** (2006) 041, [[hep-th/0609163](#)].
- [50] K. A. Intriligator and P. Pouliot, *Exact superpotentials, quantum vacua and duality in supersymmetric $SP(N(c))$ gauge theories*, *Phys.Lett.* **B353** (1995) 471–476, [[hep-th/9505006](#)].
- [51] N. Broomhead, *Dimer models and Calabi-Yau algebras*, [arXiv:0901.4662](#).
- [52] A. Hanany, C. P. Herzog, and D. Vegh, *Brane tilings and exceptional collections*, *JHEP* **0607** (2006) 001, [[hep-th/0602041](#)].
- [53] J. Davey, A. Hanany, and J. Pasukonis, *On the Classification of Brane Tilings*, *JHEP* **1001** (2010) 078, [[arXiv:0909.2868](#)].
- [54] J. P. Davey, *Brane Tilings, M2-branes and Orbifolds*, [arXiv:1110.6658](#).
- [55] S. Franco and A. M. . Uranga, *Dynamical SUSY breaking at meta-stable minima from D-branes at obstructed geometries*, *JHEP* **0606** (2006) 031, [[hep-th/0604136](#)].
- [56] D. Green, Z. Komargodski, N. Seiberg, Y. Tachikawa, and B. Wecht, *Exactly Marginal Deformations and Global Symmetries*, *JHEP* **1006** (2010) 106, [[arXiv:1005.3546](#)].
- [57] K. A. Intriligator and B. Wecht, *The Exact superconformal R symmetry maximizes a*, *Nucl.Phys.* **B667** (2003) 183–200, [[hep-th/0304128](#)].
- [58] Y. Imamura, H. Isono, K. Kimura, and M. Yamazaki, *Exactly marginal deformations of quiver gauge theories as seen from brane tilings*, *Prog.Theor.Phys.* **117** (2007) 923–955, [[hep-th/0702049](#)].
- [59] F. Dolan and H. Osborn, *Applications of the Superconformal Index for Protected Operators and q-Hypergeometric Identities to N=1 Dual Theories*, *Nucl.Phys.* **B818** (2009) 137–178, [[arXiv:0801.4947](#)].
- [60] M. A. Luty, M. Schmaltz, and J. Terning, *A Sequence of duals for $Sp(2N)$ supersymmetric gauge theories with adjoint matter*, *Phys.Rev.* **D54** (1996) 7815–7824, [[hep-th/9603034](#)].
- [61] T. Sakai, *Duality in supersymmetric $SU(N)$ gauge theory with a symmetric tensor*, *Mod.Phys.Lett.* **A12** (1997) 1025–1034, [[hep-th/9701155](#)].

- [62] K. A. Intriligator and N. Seiberg, *Duality, monopoles, dyons, confinement and oblique confinement in supersymmetric $SO(N(c))$ gauge theories*, *Nucl.Phys.* **B444** (1995) 125–160, [[hep-th/9503179](#)].
- [63] C. Csaki, M. Schmaltz, and W. Skiba, *Confinement in $N=1$ SUSY gauge theories and model building tools*, *Phys.Rev.* **D55** (1997) 7840–7858, [[hep-th/9612207](#)].
- [64] C. Romelsberger, *Counting chiral primaries in $N = 1$, $d=4$ superconformal field theories*, *Nucl.Phys.* **B747** (2006) 329–353, [[hep-th/0510060](#)].
- [65] J. Kinney, J. M. Maldacena, S. Minwalla, and S. Raju, *An Index for 4 dimensional super conformal theories*, *Commun.Math.Phys.* **275** (2007) 209–254, [[hep-th/0510251](#)].
- [66] C. Romelsberger, *Calculating the Superconformal Index and Seiberg Duality*, [arXiv:0707.3702](#).
- [67] V. Spiridonov and G. Vartanov, *Elliptic Hypergeometry of Supersymmetric Dualities*, *Commun.Math.Phys.* **304** (2011) 797–874, [[arXiv:0910.5944](#)].
- [68] V. Spiridonov and G. Vartanov, *Superconformal indices of $\mathcal{N} = 4$ SYM field theories*, *Lett.Math.Phys.* **100** (2012) 97–118, [[arXiv:1005.4196](#)].
- [69] R. Blumenhagen, B. Jurke, T. Rahn, and H. Roschy, *Cohomology of Line Bundles: A Computational Algorithm*, *J.Math.Phys.* **51** (2010) 103525, [[arXiv:1003.5217](#)].
- [70] S.-Y. Jow, *Cohomology of toric line bundles via simplicial Alexander duality*, *Journal of Mathematical Physics* **52** (Mar., 2011) 033506, [[arXiv:1006.0780](#)].
- [71] T. Rahn and H. Roschy, *Cohomology of Line Bundles: Proof of the Algorithm*, *J.Math.Phys.* **51** (2010) 103520, [[arXiv:1006.2392](#)].
- [72] M. A. A. van Leeuwen, A. M. Cohen, and B. Lissner, *LiE, A Package for Lie Group Computations*, *Computer Algebra* (1992). <http://www-math.univ-poitiers.fr/~maavl/LiE>.